Computational Study of the Boron-Nitrogen Dative Bond

By

Hailiang Zhao

Thesis presented in partial fulfillment of the requirements for the degree of

Master of Science at Stellenbosch University

Department of Chemistry and Polymer Science

Supervisor: Prof J. Dillen

December 2008

Declaration

By submitting this thesis electronically, I declare that the entirety of the work contained therein is my own, original work, that I am the owner of the copyright thereof (unless to the extent explicitly otherwise stated) and that I have not previously in its entirety or in part submitted it for obtaining any qualification.

Date: 15 December 2008

Opsomming

In hierdie werk word tien geselekteerde boor-stikstof verbindings en drie boraankarboniel-komplekse bestudeer met ’n verskeidenheid van berekeningsmetodes. Dit is algemeen bekend dat die B-N datiewe binding in die vaste toestand korter is as in die gasfase. Die B-CO binding egter, vertoon die omgekeerde effek.

Die Hartree-Fock, Møller-Plesset tweede-orde en Kohn-Sham elektrondigtheidsteorie kwantummeganiese tegnieke is gebruik om die geometrieë van geïsoleerde molekule te bereken en hulle te vergelyk met dié wat gevind word in die molekulêre bondels wat gebruik is om die vaste toestand te modelleer. Daar is gevind dat die berekende molekulêre geometrieë baie sensitief is ten opsigte van die keuse van die basisstel.

Die effek van dipool-dipool interaksies is verder ondersoek deur ‘n eksterne elektriese veld met variërende grootte op geïsoleerde molekules toe te pas, asook deur die sentrale molekuul in ’n sekere bondel te vervang met ’n ander verbinding.

’n Poging is ook onderneem om die variasies in die lengtes van die datiewe bindings te korreleer met die grootte van die kristalveld wat bereken is met behulp van klassieke puntlandings. Daar is egter vasgestel dat daar groot verskille is in die atoomladings wat bekom word met die gebruiklike metodes soos Mulliken of Merz-Kollman-Singh. ’n Analise van 67 kristalstrukture geneem uit die Cambridge Kristallografiese Databank het geen korrelasie tussen die lengte van die B-N binding en die kristalveld bereken met atoomladings volgens die Qeq-ekwilibrasiemetode gewys nie.

Tenslotte is ’n valenskragveld vir H_3N-BH_3 ontwikkel. Dit is aangetoon dat ’n baie beter passing van die vibrasiespektrum bekom word indien die B-N rekvibrasie geassosieer word met die band by 603 cm^{-1} pleks van die band by 968 cm^{-1}.

Summary

In this study, ten selected boron-nitrogen compounds and three borane carbonyl complexes were investigated by a number of computational methods. It is well known that the B-N dative bond is shorter in the solid state than in the gas phase. The B-CO distance, on the other hand, displays the opposite effect.

Quantum mechanical techniques at the Hartree-Fock, Møller-Plesset second-order and Density Functional Theory level were used to calculate the geometries of the isolated molecules and to compare them with those found in molecular clusters built to model the solid state. It was found that calculated geometries were very sensitive to the choice of the basis set.

The effects of dipole-dipole interactions were further investigated by applying an external electric field with varying strength to isolated molecules, and by replacing the central molecule in a cluster with a different compound. The B-N bond was found to respond much more to the applied field than the B-CO bond.

An effort was made to correlate the lengthening or shortening of the dative bond to the strength of the crystal field, the latter being calculated classically from point charges. Unfortunately, large differences were noted between the charges calculated with common methods like Mulliken or Merz-Kollman-Singh. Furthermore, an analysis of 67 crystal structures taken from the Cambridge Structural Database did not reveal a correlation between the length of the B-N bond and the crystal field calculated with Charge Equilibration charges.

Finally, a valence force field was developed for H_3N-BH_3. It was shown that a much better fit of the vibrational spectrum can be obtained if the B-N stretching mode is assigned to the 603 cm^{-1} band rather than the peak observed at 968 cm^{-1}.

To my beloved family

Acknowledgements

My sincere gratitude to the following:

- My supervisor, Prof. J.L.M. Dillen, for his expert guidance, continued advice and fruitful suggestions to my work.

- Prof. L.J. Barbour and Dr. C. Esterhuysen, for their kindness for accepting me to attend their weekly group meeting.

- Dr. P.F.M. Verhoeven, for his professional suggestions in the infrared experiment.

- Ms. P.W. Snijman, for her handy help in the infrared experiment.

- My parents and sisters, for their encouragement and financial support.

- My colleagues in the chemistry department, for always being willing to give a few thoughts.

- My friends, for their support and words of encouragement.

- The University of Stellenbosch for their financial support.

Presentation

- A poster was presented at the Carman National Physical Chemistry Symposium, 23-27th September 2007, V&A Waterfront, Cape Town, South Africa. The poster was entitled *Computational Study of the Boron-Nitrogen Dative Bond.*

Table of Contents

NB: Addendum and the output files of the calculations are on the attached CD.

List of Tables

Chapter One

Introduction

In the early 1990's, the two most drastic examples of phase-dependent structural changes were found in complexes with boron-nitrogen bonds, HCN-BF_3[1] and CH_3CN–BF_3[2]. The difference in the B-N bond length between the gas and condensed phase is 0.84 Å for HCN-BF_3, and 0.38 Å for CH_3CN–BF_3! The N-B-F angles also change considerably, by 14^o and 10^o, respectively. This type of bond is known as a dative bond. The changes have predominantly been attributed to the dipole-dipole interactions, mostly interacting over short distances.[3] Although much work has been done to characterize the intermolecular interactions, there are still many puzzling features (e.g. how the crystal environment effects the dative bond length?) of this type of donor-acceptor complexes that are not completely understood. The overall aim of this study is to determine which specific effects in the crystalline state are responsible for the changes observed through experimental structure determination. The hypothesis adopted is that a crystal lattice is assembled by billions of charged atoms, which will generate an electric field. The positively charged atoms move along the self-generated electric field and the negatively ones move against the electric field during the crystallizing process. Several B-N and B-CO complexes will be investigated with quantum methods. Two important phases, the gas and the solid, will be involved in this study. Numerous B-N complexes have been selected from the Cambridge Structural Database (CSD)[4] to perform a statistical analysis, to investigate whether it is possible to correlate the B-N dative bond lengths with their corresponding crystal environment.

In 1973, Smith *et al.*[5] obtained the spectra of ammonia-borane, H_3B-NH_3, and two of its deuterated isotropic species D_3N-BD_3 and D_3N-BH_3, which were isolated in an argon matrix at liquid hydrogen temperature. The B-N stretching mode was assigned at 968

cm^{-1}. The argon-matrix result is in sharp contrast to the calculation done by Dillen *et al.*[6], who suggested that the B-N stretching mode should be at 539 cm^{-1}. This brings another aim of this study: experimentally and theoretically prove Dillen *et al.*'s[6] assignment.

Another type of compound, namely, borane carbonyl compounds, which are similar to non-classical metal carbonyls, are also interesting for this study, because of a similar observation. In these compounds, the B-CO bond is longer in the crystal phase than in the gas phase, which is the opposite trend to that found for the boron-nitrogen complexes. Although the differences between the B-CO bond lengths are not as much as for the boron-nitrogen complexes, analyzing these compounds may help explain the observed features of the B-N dative bond.

In the second chapter, we give a brief summary of the literature on the subject of large changes between gas phase and condensed phase structures and an introduction to boron-nitrogen and boron-carbonyl adducts. The third chapter presents an introduction to computational chemistry. The Hartree-Fock method (HF), Møller-Plesset perturbation theory (MP*n*) and Density Functional Theory (DFT) are introduced individually. Basis sets and the associated nomenclature are briefly discussed. Thereafter follows is an introduction to the information on orbital-based analysis techniques of the wave function: atoms in molecules (AIM), natural population analysis (NPA) and atomic partial charges. The last section in the third chapter delivers an introduction to another computational method — molecular mechanics.

Chapter four contains details of the gas phase calculations. These include calculations not only of the isolated molecules, but also when a varying external electric field is applied along the B-N and B-CO bonds. Different population analyses also lead to different atomic partial charges. Chapter five offers the calculations done on the various crystal clusters. The optimized geometry of a molecule placed in a spherical cluster was calculated with the HF and DFT methods. Some dimeric, trimeric, tetrameric and pentameric models were built to prove that short-range dipole-dipole interactions are responsible for the significant shortening of the bonds. Chapter six is about the valence

force field calculations for the vibrational frequencies of the H_3N-BH_3 complex. A new assignment of the experimental spectrum is proposed. Chapter seven gives a statistical analysis of a number of selected B-N complexes crystal structures, taken from the CSD, with the aim of finding a relationship between the bond lengths and their corresponding crystal environments, such as electric field, dipole moment, etc.

The final chapter contains a summary of the conclusions as well as suggestions for some future work and questions that still need attention.

Chapter Two

Background

2.1 Introduction

In this chapter, a general introduction will be given on the dative bond in section 2.2. In section 2.3, an overview of the boron-nitrogen dative bond will be presented. Section 2.4 contains a general introduction to carbonyl adducts of the boranes.

2.2 The Dative Bond

A chemical bond is formed by the attractive interactions between atoms or molecules. It is an indication of the stability of diatomic or polyatomic chemical compounds. Classically, chemical bonds are usually classified as ionic (electrostatic), covalent, or metallic.[7] When the electronegativity difference between the bonded atoms is small or non-existent, a covalent bond will form. Covalent bonding is a form of chemical bonding that is characterized by the sharing of pairs of electrons between atoms. They are normally found in organic compounds. When the electronegativity difference between the atoms is over 1.6, the bond is considered an ionic bond. These bonds are formed between metal (or polyatomic ions such as ammonium) and non-metal ions through electrostatic attractions. The metal donates one or more electrons, forming a positively charged ion or cation with a stable electron configuration. These electrons are then transferred to the non-metal, causing it to form a negatively charged ion, or anion, which also has a stable electron configuration. The electrostatic attraction between the oppositely charged ions causes them to come together and form an ionic bond. Metallic bonding is the electrostatic attraction between delocalized electrons, which are called

conduction electrons, and the metallic ions within metals. It involves the sharing of free electrons among a lattice of positively-charged metal ions. The metallic bond accounts for many physical characteristics of metals, such as strength, malleability, ductility, conduction of heat and electricity, and luster. They are found in metals like copper. Weakly bound molecules exhibit yet another type of bonding, which is characterized by van der Waals interactions.

Most bonds in chemical compounds can be identified as belonging to one of these classes. However, there is one type of chemical bonds that makes such an assignment difficult, called a coordination bond. These bonds exist in coordination complexes, especially involving metal ions, where a Lewis base donates its free electron pair to a Lewis acid. The electron donors are called ligands. Common ligands often contain oxygen, sulphur, nitrogen or halide atoms. The most common ligand is water (H_2O), and it forms coordination complexes with metal ions, e.g. $[Cu(H_2O)_6]^{2+}$.

A popular qualitative model for interpretation of donor-acceptor interactions is the theory of hard and soft acids and bases (HSAB) suggested by Pearson.[8] A quantitative evaluation and prediction of donor-acceptor interactions has been made by Drago,[9] who introduced the so-called ***E*** and ***C*** parameters in an attempt to predict the bond strength of new complexes. The ***E*** and ***C*** model has been applied to understand solvent effects and the reactivity of chemical and biological systems.

One difference between the Lewis-type donor-acceptor bond and normal covalent bonds is that the dissociation of the former yields two closed-shell fragments with an electron lone-pair donor and electron-pair acceptor, while the latter gives two open-shell fragments. Haaland[10] defines dative bonds as a new bond type on the basis of their bond rupture behavior, which is different from covalent bonds. The difference is that the bond length of a normal covalent bond is usually similar in different aggregation states, while donor-acceptor bonds frequently have larger inter-atomic distances in the gas phase than in the solid state. The bond is formed when a Lewis base (an electron donor) donates a pair of electrons to a Lewis acid (an electron acceptor) to give a so-called *adduct*. The

process of forming a dative bond is called *coordination*. The electron donor acquires a positive formal charge, while the electron acceptor acquires a negative formal charge. The most common complexes containing dative bonds are boron-nitrogen and sulphur-nitrogen adducts. Those dative bonds have been mentioned in the crystallographic literature for some time.[11] They have very low interaction energies, and in fact they become influenced by the lattice energy when crystallizing. Phase-dependent structural changes should thus occur in principle. This phenomenon was observed in perhaps its most drastic example when the microwave spectrum of HCN–BF_3 was determined in 1993.[12] The B-N distance decreases 0.835 Å from 2.473 Å in the gas phase to 1.638 Å in the solid state and the N-B-F angle increases 14.1^o from 91.5^o to 105.6^o.

Although much work has been done to characterize the intermolecular interactions undergone by these complexes in the solid state, there are still many puzzling features (e.g. how the crystal environment effects the dative bond length?) of donor-acceptor complexes that are not completely understood.

2.3 Boron-Nitrogen Adducts

BX_3 (X = F, Cl, Br) compounds are known as Lewis acids. The order of decreasing acidity of the boron trihalides is[13]

$$BBr_3 > BCl_3 \geq BF_3$$

which is the opposite of what is expected on the grounds of electronegativity and steric effects. More electronegative substituents withdraw more charge from the boron atom and this should lead to a more favorable interaction with a donor.

The order of decreasing donor strength of common nitrogen-containing compounds is[3]

$$NH_3 >> CH_3CN > HCN$$

The relative strength of the Lewis acids and bases can give a general idea of what to expect when complexes of different combinations of these donors and acceptors are compared.

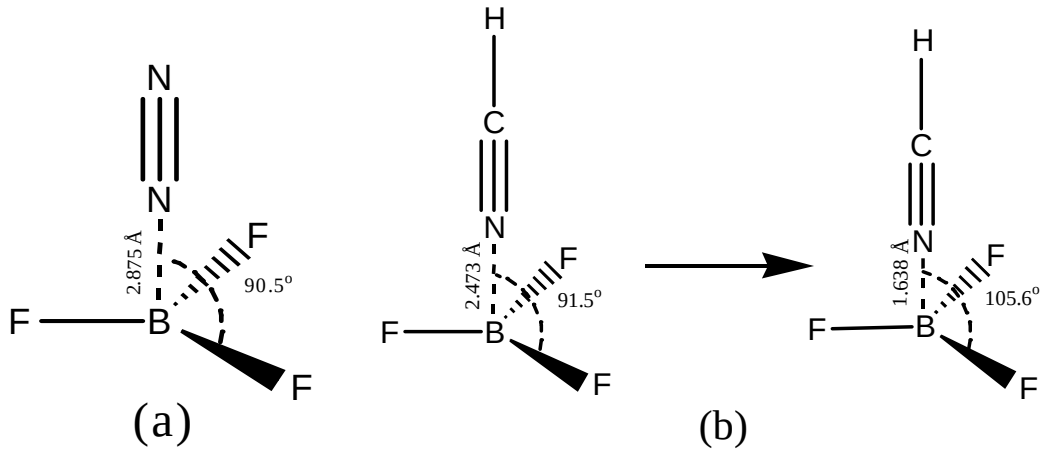

Figure **2.1**: The gas phase structures of N_2-BF_3 (a), and HCN–BF_3 (b) as it progresses from the gas phase (left) to the crystal phase (right).

In boron-nitrogen adducts, the nitrogen has a lone electron pair, which it donates to the empty *p*-orbital in boron to form a donor-acceptor complex. The common feature of these complexes is that the B-N bond is considerably shorter in the crystal than it is in the gas phase. The covalent radius for boron is 0.70 Å and 0.88 Å for nitrogen.[14] The fully-formed covalent bond between B and N is expected in the region of 1.58 Å. The sum of van der Waals radii for boron and nitrogen is estimated as 2.91 Å by Leopold.[15] A search in the Molecular Gas Phase Documentation (MOGADOC)[16] reveals 48 entries with a B-N bond distance range of 1.238 to 2.875 Å. The longest B-N bond exists in dinitrogen-trifluoroborane BF_3-N_2, 2.875(20) Å[17], where this value is very close to the sum of the van der Waals radii for boron and nitrogen. By using the ConQuest software[18] to search and visualize crystal structures in the Cambridge Structural Database (CSD)[4], the B-N bond distance range decreases to 1.230-1.978 Å. HCN-BF_3 and CH_3CN-BF_3 are the only two phase-dependent complexes with large structural changes of 0.84 Å and 0.38 Å, respectively. H_3N-BF_3, on the other hand, shows a very small structural change. The crystal structure was determined in 1951, with a B-N distance of 1.60 Å,[19] while the gas phase structure was determined in 1991 and with a B-N distance of 1.59 Å.[1] This bond is already very close to being fully formed in the gas phase, based on a comparison with the sum of the covalent bond radii of boron and nitrogen.

H_3N-BH_3 is the simplest B-N donor-acceptor t complex. In 1994, Jonas and Frenking[3] performed an *ab initio* study on the H_3N-BH_3 gas molecule. By using different basis sets and correlation methods, they suggested that the B-N distance should be 1.68±0.02 Å. This is about 0.09 Å longer than the gas phase determination. This was supported by Fujiang *et al.*[20], who redetermined the gas structure by microwave spectroscopy and found the gas phase bond to be 1.673 Å. They pointed out that the result of the first determination was due to an underestimation of the experimental principal axis coordinate, z_B. The first crystal structure determination was also incorrect, as the assignment of the boron and nitrogen atoms was reversed. This was corrected by the neutron diffraction study by Klooster *et al.*[21] Along with the change in dative bond length, the hybridization angle of the accepting moiety also changes significantly. In the free adduct the hybridization at the boron atom is sp^2, corresponding to a trigonal planar structure. Accompanying bond formation results in a change to tetrahedral sp^3 hybridization.

Several computational studies, regarding the molecular geometry, binding energy, topology of the electron density, and vibrational frequencies (only for H_3N-BH_3), have been done using *ab initio* methods.[3,22-33] The early works were focused on the investigation of medium effects. Bühl *et al.*[24] reported an *ab initio* (*Gaussian 92*) self-consistent reaction field (SCRF) study. The calculated B-N bond of this very polar species (dipole moment, 5.22 D) changed by 0.093 Å from 1.657 Å in the gas phase to 1.564 Å in the crystal. Later on, Cremer *et al.*[34] gave a more detailed examination of H_3N-BH_3 and Hofmann and Schleyer[35] did an investigation on H_2O-SO_3. They all supported that the structures of other amine borane complexes also are influenced by the medium, but to a lesser extent. Wong *et al.*[36,37] found that the N-S separation is decreased by 0.1 Å for the zwitterionic $^+H_3NSO_3^-$ form of sulfamic acid in a medium with a high dielectric constant. Jurgens and Almlöf's[38] 1991 MP2 calculation of the CH_3CN-BF_3 complex founded a B-N bond distance of 2.17 Å**.** This is much longer than the value (1.64 Å**)** in the solid state.[19,39] This discrepancy was attributed to "crystal packing effects". In contrast, the gas phase N-B distances for the weaker $NCCN$-BF_3 complex in both the MP2 calculation and the experimental work are nearly identical (2.60[39] and

2.64[25] Å, respectively). In 1994, Schleyer *et al.*[25] did several self-consistent reaction field (SCRF) calculations. They found that the B-N bond length of H_3N-BH_3 is reduced from 1.689 Å in the gas phase to 1.62 Å in a hexane solution and 1.57 Å in a water solution. They suggested that the dipolar field could be responsible for the observed shortening of the dative bond in the crystal. After a further study on HCN-BF_3, H_3CCN-BF_3, N_2-BF_3, and other similar complexes, they pointed out that the medium effects seem to be found only for complexes in which the donor molecule has a permanent dipole moment. Donors without permanent dipoles (NCCN and N_2) may have no or only small medium effects on geometries. At the same time, Frenking *et al.*[3] did quantum mechanical calculations at the MP2/TZ2P level of theory to predict geometries and bond energies of donor-acceptor complexes of the Lewis acids BH_3, BF_3, $BC1_3$, $AlC1_3$, and SO_2. In their study, simple dimeric and tetrameric models were built to simulate the solid-state structure of H_3N-BH_3. The two molecules in the dimeric model are anti-parallel to each other and in the tetrameric model three molecules are anti-parallel to the central molecule. From the results, they proposed that short-range dipole-dipole interactions between the molecules are responsible for the significant shortening of the bond. Recently, Dillen *et al.*[6] built several larger molecular clusters of H_3N-BH_3. In those models the number of molecules was progressively increased in the direction of the molecular axis. As a result, the B-N bond decreased from 1.689 Å in the gas phase to 1.609 Å for the central molecule surrounded by 20 molecules. From this study, they concluded that short-range interactions were important in shortening the B-N bond, but long-range interactions play a significant role as well. In 2004, Gillert[40] did several tests of the MP2 models and various DFT models in predicting the structures and B-N bond dissociation energies of amine-boranes $(X_3C)_mH_{3-m}B$-$N(CH_3)_nH_{3-n}$ (X = H, F; m = 0-3; n = 0-3). He showed that the B3LYP model performed poorly in predicting the structures and B-N bond dissociation energies. He pointed out that if usable, the MP2 approach gave good agreement with experiment. The MPW1K approach could be used as well if the computational demands were too large for MP2.

A DFT investigation was done by Venter[41] in order to find the effect of the surrounding molecules on the structure of selected boron-nitrogen compounds. He found that a large

structural change occurs when $HCN–BF_3$ and $CH_3CN–BF_3$ crystallize. In particular, the B-N distance shortened by 0.735 Å for $HCN–BF_3$ and 0.654 Å for $CH_3CN–BF_3$, when seven molecules were added. The N-B-F angle also showed large changes. He suggested that through delocalization of the fluorine lone pairs, the anti-bonding σ^*(B–N) orbital becomes increasingly occupied as the N-B-F angle reduces and vice versa. A further investigation was done by applying uniform electric fields of varying strength along the donor-acceptors bond axis of a series of compounds of the form X–Y (X = H_3N, HCN, CH_3CN; Y = BF_3, BH_3, SO_3). All of the compounds are found to be sensitive to the external electric field. In particular, the compounds having nitrile donors and acceptors with fluorine atoms showed large changes in geometry.

The boron-nitrogen complexes, $(CH_3)_3N\text{-}BX_3$ (X = H, F, Cl, Br, CN), $H_3N\text{-}BY_3$ (Y = H, CH_3, CF_3), $(C_2H_5)H_2N\text{-}B(CF_3)_3$ and $(C_2H_5)_2HN\text{-}B(CF_3)_3$ were selected for further study in this work. All have simple substituents bonded to B or N. The small groups imply relatively small inter-molecular interactions. Another reason for selecting them is that most of them have both gas phase and solid state experimental structures, and this is good for comparison between experimental and calculated geometries. Most of the complexes are also highly symmetrical, belonging to the C_{3v} or C_s point group. The three-fold axis or mirror plane passes through the N and B atoms and this reduces the computational cost.

2.4 Borane Carbonyls

The CO bond in borane carbonyls has a high stretching wavenumber, as it does in the main group analogues of σ-bonded transition metal carbonyl cations. In both classes, the CO bond is polarized by positively charged central atoms, resulting in a strengthening of the CO bond by electrostatic contributions. The simplest borane carbonyl, $H_3B\text{-}CO$, has been known since 1937.[42] Approximately twenty other borane carbonyl derivatives are known so far. They are synthesized primarily by addition of CO to suitable

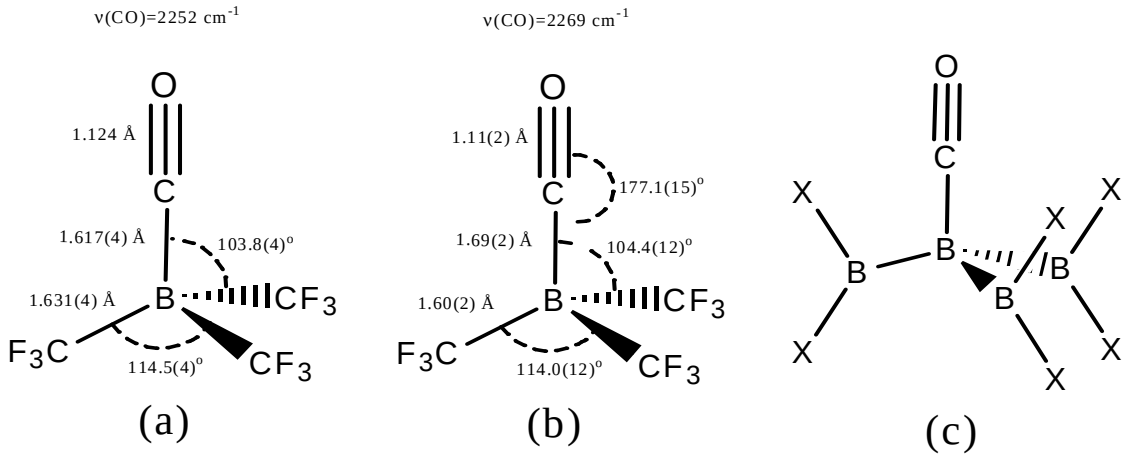

Figure **2.2**: Schematic representation of the molecular structure of $(CF_3)_3B$-CO in the gas phase (a) and in the solid state (b), and the molecular framework for $(BX_2)_3B$-CO (X = F, Cl) (c).

boranes and boron subhalides.[43] They are similar to non-classical metal carbonyls, which means the metal-to-CO π back donation is reduced.

Only a few studies have been published on B-CO complexes: Finze *et al.*[44] synthesized the $(CF_3)_3B$-CO complex and did a quantum chemical calculation of the gas molecule. The B-CO bond was found to be very sensitive to the level of theory used: HF/6-311G(2d) gives a bond length of 1.700 Å, MP2/cc-pVDZ 1.610 Å and B3LYP/6-311+G* 1.589 Å. Mackie *et al.*[45] did *ab initio* calculations on borane carbonyl compounds $(BX_2)_3B$-CO (X = F, Cl, Br and I). Two starting geometries were used: the first conformer, where the BX_2 groups lie coplanar with the C-O bond, and then the second conformer, where the BX_2 groups are twisted 90^o away from the coplanar arrangement. For Conformer B, the calculations have failed to reach energy minima on the potential energy surface. For conformer A, the change in geometry for $(BF_2)_3B$-CO was found to result from the inclusion of electron correlation and from increasing the size of the basis set. There was a change in the length of the C-B bond for $(BCl_2)_3B$-CO and increasing the basis set also had little effect on the C-B distance. For X = Br, the size of the basis set also had little effect on the geometry. For X = I, the BI_2 groups were twisted approximately 35^o away from the positions in which they were coplanar with the C-O bond. When increasing the

basis sets, the C-O bond length decreased. When increasing the level of theory from HF/6-311+G* to DFT/6-311+G*, the C-B bond length decreased by approximately 9 pm. Finally, they concluded that the halogen substituents did not alter the overall symmetry of the molecules, except for X = I, but they have important effects on the bond lengths and angles in the molecules. The twisting of the BI_2 groups is due to the strong steric interactions between the large iodine atoms.

In these two publications, all bond parameters, determined both in the gas phase and in the solid state, are within their standard deviations in fair agreement, except for inter-nuclear distances most noticeable the B-CO bond length. It is 1.69(2) Å in the solid state and 1.617(12) Å in the gas phase determined by microwave-electron diffraction analysis for $(CF_3)_3$B-CO, and 1.522 Å for the solid state, 1.502 Å in the gas phase determined by gas-phase electron diffraction for $(BF_2)_3$B-CO.

The B-CO bonds are longer in the solid state than in the gas phase. Obviously, they have the opposite trend comparing with the B-N dative bonds. The similarity with the B-N dative bonds brings some interests for the B-CO complexes. The borane carbonyls $(CF_3)_3$B-CO and $(BX_2)_3$B-CO (X = F, Cl), were selected for further study in this work. The three adducts possess C_{3v} symmetry. The three-fold axis passes through the B and CO ligand, thus reducing the computational cost.

Chapter Three

Introduction to Computational Chemistry

3.1 Introduction

In this chapter a general discussion will be given on the basic concepts underlying some computational methods. Section 3.2 contains a detailed discussion of the Schrödinger equation. The Born-Oppenheimer approximation is described in section 3.3. Sections 3.4 and 3.5 contain discussions of the *ab initio* quantum mechanical methods which are used in this study, namely, Hartree-Fock (HF) and Møller-Plesset second-order (MP2). Density Functional Theory (DFT) is a different type theory to HF and MP2 and will be discussed in section 3.6. Basis sets are introduced in section 3.7. Population analysis (calculation of atomic partial charges) plays an important role in understanding molecular bonding. This is described in section 3.8, whereas the purely topological approach, which is called *Atoms In Molecules* (AIM), is presented in section 3.9. The method of using Newtonian mechanics to model a molecular system is called molecular mechanics (MM), and is described in section 3.10.

This summary was compiled from material taken from the following excellent textbooks: *Quantum Chemistry* by Levine,[46] *Modern Quantum Chemistry: Introduction to Advanced Electronic Structure Theory* by Szabo and Ostlund,[47] *Introduction to Computational Chemistry* by Jensen,[48] *Essentials of Computational Chemistry* by Cramer,[49] *Understanding Chemistry with Theoretical Molecular Models: An introduction to some classical and quantum techniques of molecular modelling* by Dillen,[50] and *Encyclopedia of Computational Chemistry* by Schleyer *et al*.[51]

3.2 The Schrödinger Equation

In 1926, the Austrian physicist Erwin Schrödinger proposed a famous equation based on the wave equations of classical mechanics. It describes the space- and time-dependence of quantum mechanical systems. The equation also gives an explanation for the emission spectrum of the hydrogen atom. It can only be solved exactly for a limited number of model systems and for the one-electron hydrogen atom.

For a particle with mass *m* traveling in space, the time-independent Schrödinger equation can be expressed as:

$$\frac{-\hbar^2}{2m}\nabla^2\psi(\vec{r}) + V(\vec{r})\psi(\vec{r}) = E\psi(\vec{r})$$

or in short

$$\hat{H}\psi = E\psi \tag{3.1}$$

where $\hbar$ is Planck's constant divided by 2π, $\vec{r}$ is the position of the particle in space, $\psi(\vec{r})$ is the wave function describing the state of the particle, $V(\vec{r})$ is the potential energy, E is the total energy of the particle, and $\hat{H}$ is the Hamiltonian operator.

The Hamiltonian for a system containing *N* electrons and *M* nuclei is:

$$\hat{H} = \hat{T}_n + \hat{T}_e + \hat{V}_{ne} + \hat{V}_{ee} + \hat{V}_{nn} \tag{3.2}$$

$\hat{T}_n$ is the kinetic energy operator for the nuclei:

$$\hat{T}_n = -\sum_{k=1}^{M}\frac{\hbar^2}{2M_k}\nabla^2_{\vec{R}_k} = -\sum_{k=1}^{M}\frac{\hbar^2}{2M_k}\left(\frac{\partial^2}{\partial X_k^2} + \frac{\partial^2}{\partial Y_k^2} + \frac{\partial^2}{\partial Z_k^2}\right) \tag{3.3}$$

where M_k is the mass of nucleus *k*, $\vec{R}_k$ is its position, X_k, Y_k and Z_k are the coordinates of the nucleus *k* and ∇^2 is the Laplace operator.

$\hat{T}_e$ represents the kinetic energy operator for the electrons:

$$\hat{T}_e = -\sum_{i=1}^{N} \frac{\hbar^2}{2m_i} \nabla_{\vec{r}_i}^2 \tag{3.4}$$

$\hat{V}_{ne}$ defines the interactions between the nuclei and the electrons:

$$\hat{V}_{ne} = -\frac{1}{4\pi\varepsilon_0} \sum_{i=1}^{N} \sum_{k=1}^{M} \frac{e(Z_k e)}{\left|\vec{R}_k - \vec{r}_i\right|} \tag{3.5}$$

where ε_0 is the permittivity of free space, e is the electron charge, $\vec{R}_k$ is the position of the nucleus *k*, $\vec{r}_i$ is the position of the electron *i* and Z_k is the atomic number.

$\hat{V}_{ee}$ describes the repulsive interactions between the individual electrons:

$$\hat{V}_{ee} = \frac{1}{4\pi\varepsilon_0} \sum_{i=1}^{N} \sum_{j=i+1}^{N} \frac{e^2}{\left|\vec{r}_j - \vec{r}_i\right|} \tag{3.6}$$

$\hat{V}_{nn}$ characterizes the repulsive interactions between the individual nuclei:

$$\hat{V}_{nn} = \frac{1}{4\pi\varepsilon_0} \sum_{k=1}^{M} \sum_{l=k+1}^{M} \frac{(Z_k e)(Z_l e)}{\left|\vec{R}_l - \vec{R}_k\right|} \tag{3.7}$$

3.3 The Born-Oppenheimer Approximation

The Hamiltonian operator contains terms for both electrons and nuclei. In the Born-Oppenheimer approximation, the situation is simplified by fixing the positions of the nuclei. The electronic wave function then becomes dependent only on the positions of the electrons relative to each other, and on the positions of the electrons relative to the nuclei. The Hamilton operator is split into an electronic part $\hat{H}_e$ and a nuclear part $\hat{H}_n$:

$$\hat{H}_e = \hat{T}_e + \hat{V}_{ne} + \hat{V}_{ee} \tag{3.8}$$

and

$$\hat{H}_n = \hat{T}_n + \hat{V}_{nn} \tag{3.9}$$

The electronic part can be rewritten as:

$$\hat{H}_e = \sum_i^N \hat{h}_i + \sum_i^N \sum_{j>i}^N \hat{g}_{ij} + \hat{V}_{nn} \tag{3.10}$$

$\hat{h}_i$ is an operator describing the motion of electron *i* in the field of all the nuclei:

$$\hat{h}_i = -\frac{\hbar^2}{2m_i}\nabla^2_{\vec{r}_i} - \frac{1}{4\pi\varepsilon_0}\sum_k^M \frac{Z_k e^2}{\vec{r}_{ik}} \tag{3.11}$$

$\hat{g}_{ij}$ describes the two-electron operator representing electron-electron repulsion:

$$\hat{g}_{ij} = \frac{1}{4\pi\varepsilon_0}\frac{e^2}{\vec{r}_{ij}} \tag{3.12}$$

Note that the electronic Hamiltonian also depends on $\hat{V}_{nn}$, i.e. the *relative* positions of the nuclei.

3.4 The Hartree-Fock Approximation

Ab initio methods are computational chemistry methods. The phrase *ab initio* is a Latin term for "from the beginning" or "from first principles". These calculations are based on fundamental physical constants (e.g. Planck's constant, mass and charge of elementary particles, speed of light, etc.) without referring to any experimental data. Hartree-Fock (HF) and Møller-Plesset perturbation theory (MP*n*) are the most popular *ab initio* electronic structure calculation methods.

The Hartree-Fock (HF) method is an approximate method to determine the ground-state wavefunction and the ground-state energy of a many-body system. The exact, N-body wavefunction of a system is approximated by a single Slater determinant. The solution of the resulting equations yields a HF wavefunction and the energy of the system. Details of the HF approximation will be addressed in this section.

3.4.1 Atomic Units

Atomic units (a.u.) are very common in quantum mechanics. They can simplify most of the mathematical equations dramatically. In this system the numerical values of some key properties are chosen as one, for instance, electron mass $m_e = 1$, electron charge $e = 1$, angular momentum $\hbar = 1$, etc.

For example, the Bohr radius, in SI units, can be expressed as:

$$a_0 = \frac{4\pi\varepsilon_0\hbar^2}{m_e e^2} = 0.529177 \text{ Å}$$

In atomic units, this becomes 1 and is used as the atomic unit of length. Table 3.1 lists some common atomic units and shows the conversion factors to SI units.

Table 3.1: Some atomic units and the conversion factors to SI units.[52]

Physical quantity	Conversion factor to SI units
Electron mass	0.910938×10^{-30} kg
Proton mass	1836.1527 electron mass
Atomic mass unit (amu)	1822.8880 electron mass
Electron volt (eV)	23.06055 kcal mol^{-1}
Hartree	627.5095 kcal mol^{-1} (27.2114 eV)
Bohr-electron	2.541746 Debye
$Debye^2$-$angstrom^{-2}$-amu^{-1}	42.2561 km mol^{-1}
Electric field	5.142206×10^{11} V m^{-1}
Electric polarizability	1.648777×10^{-41} C^2 m^2 J^{-1}
Dipole moment	8.478352×10^{-30} C m^2

3.4.2 Dirac Bracket Notation

The Dirac bracket notation is used in quantum mechanics as a short notation to represent integrals and functions. A vector $\vec{a}$ in N dimensions with N basis vectors, $\{i_N\}$ is written in this notation as the *ket* vector:

$$\left|a\right\rangle = \sum_{i=1}^{N} i_N a_i$$

The matrix notation of this vector, in basis $\{i_N\}$, is

$$a = \begin{pmatrix} a_1 \\ a_2 \\ \vdots \\ a_N \end{pmatrix}$$

Similarly, the *bra* vector in its basis $\{i_N\}$ is given by:

$$\langle a| = \sum_{i=1}^{N} a_i^* i_N$$

and in matrix notation as the transpose of the matrix containing the complex conjugates, which is called the adjoint.

$$\mathrm{a}^\dagger = (a_1^*, a_2^*, \cdots, a_N^*)$$

The scalar product between a bra $\langle a|$ and a ket $|b\rangle$ is defined as:

$$\langle a||b\rangle \equiv \langle a|b\rangle = (a_1^*, a_2^*, \cdots, a_N^*)\begin{pmatrix} b_1 \\ b_2 \\ \vdots \\ b_N \end{pmatrix} = \sum_{i=1}^{N} a_i^* b_i \qquad (3.13)$$

A further use of this notation is the extension to functions. To make the analogy it is convenient to introduce the notation:

$$a(x) \equiv |a\rangle \qquad a^*(x) \equiv \langle a|$$

The product of two functions is then written as:

$$\langle a|b\rangle = \int a^*(x) b(x) dx \qquad (3.14)$$

Finally, an operator $\hat{O}$ acting on a function $a(x)$ to yield the function $f(x)$,

$$\hat{O}a(x) = f(x)$$

is described in Dirac bracket notation as:

$$\hat{O}|a\rangle = |f\rangle$$

As for Eq. (3.13), the above is then written as:

$$\langle a|\hat{O}|b\rangle = \int a^*(x)\hat{O}b(x)dx = \int a^*(x)f(x)dx \tag{3.15}$$

3.4.3 The Many-Electron Wavefunction

Every electron has a spin quantum number of ½. Electrons can align themselves either along or opposite to an external magnetic field. The two possible alignments are related to two corresponding spin states and they are denoted as α and β. The spatial orbital, $\varphi(\vec{r})$, is a function of the position $(\vec{r})$ of the particle only. The total wavefunction of an electron is the product of the spatial orbital with either α or β. The total one-electron wavefunction is known as a spin orbital, $\phi(\vec{r},\sigma)$. It is a function of the spatial coordinates of the electron, $\vec{r}$, and also the spin coordinate σ. For an electron *i* with an α-spin, the spin orbital can be expressed as:

$$\phi(\vec{r}_i,\sigma_i) = \varphi(\vec{r}_i)\alpha(\sigma_i) = \varphi(\vec{r}_i)\alpha(i) \tag{3.16}$$

For an electron *j* with a β-spin, the spin orbital can be expressed as:

$$\phi(\vec{r}_j,\sigma_j) = \varphi(\vec{r}_j)\beta(\sigma_j) = \varphi(\vec{r}_j)\beta(j) \tag{3.17}$$

For convenience, a shorter notation (x_i) is used instead of $(\vec{r}_i,\sigma_i)$. Eq. (3.16) and (3.17) can be rewritten as:

$$\phi(\vec{r}_i,\sigma_i) = \phi(x_i)$$

The spin orbitals are orthonornal, i.e.

$$\left\langle \phi_i(x) \middle| \phi_j(x) \right\rangle = \delta_{ij} = \begin{cases} 1 & (i = j) \\ 0 & (i \neq j) \end{cases} \tag{3.18}$$

The total electronic wavefunction of a many-electron system is $\Psi(x_1, x_2, \cdots, x_N)$. The Pauli principle states that the total electronic wavefunction of a system must be anti-symmetric with respect to the exchange of two electrons:

$$\Psi(x_1, x_2, \cdots, x_i, x_j, \cdots, x_N) = -\Psi(x_1, x_2, \cdots, x_j, x_i, \cdots, x_N) \tag{3.19}$$

The wavefunction can be constructed from a Slater determinant. If the system is an N-electron system, the Slater determinant is

$$\Phi_0 = \frac{1}{\sqrt{N!}} \begin{vmatrix} \phi_1(x_1) & \phi_2(x_1) & \cdots & \phi_N(x_1) \\ \phi_1(x_2) & \phi_2(x_2) & \cdots & \phi_N(x_2) \\ \vdots & \vdots & & \vdots \\ \phi_1(x_N) & \phi_2(x_N) & \cdots & \phi_N(x_N) \end{vmatrix} \tag{3.20}$$

where $\frac{1}{\sqrt{N!}}$ is a normalization constant. The single Slater determinant is an approximation of the total electronic wave function of a many-electron system. Interchange of any two rows in the Slater determinant changes the sign of the determinant, hereby satisfying the anti-symmetry condition.

3.4.4 Hartree-Fock Self Consistent Field

The electronic energy of the system can be expressed as:

$$E = \left\langle \Phi_0 \middle| \hat{H} \middle| \Phi_0 \right\rangle \tag{3.21}$$

After several mathematical substitutions, the energy of a closed shell system (see page 24) can be rewritten as:

$$E = 2\sum_{i}^{N/2} h_i + \sum_{i}^{N/2}\sum_{j}^{N/2}(2J_{ij} - K_{ij}) \tag{3.22}$$

The term h_i is a one-electron contribution and it is known as a *core* integral:

$$h_i = \left\langle \varphi_i(\vec{r}_1) \middle| \hat{h}_1 \middle| \varphi_i(\vec{r}_1) \right\rangle \tag{3.23}$$

where $\vec{r}_1$ are the coordinates of electron "one".

The term J_{ij} is a *Coulomb* integral:

$$J_{ij} = \left\langle \varphi_i(\vec{r}_1)\varphi_j(\vec{r}_2) \middle| \hat{g}_{12} \middle| \varphi_i(\vec{r}_1)\varphi_j(\vec{r}_2) \right\rangle \tag{3.24}$$

where $\vec{r}_2$ are the coordinates of electron "two".

The term K_{ij} is an *exchange* integral:

$$K_{ij} = \left\langle \varphi_i(\vec{r}_1)\varphi_j(\vec{r}_2) \middle| \hat{g}_{12} \middle| \varphi_i(\vec{r}_2)\varphi_j(\vec{r}_1) \right\rangle \tag{3.25}$$

3.4.5 The Hartree-Fock Equations

For convenience, a new operator, the *Fock* operator $\hat{F}$, is introduced and it is defined as:

$$\hat{F}_1 = \hat{h}_1 + \sum_{j}^{N/2}(2\hat{J}_j - \hat{K}_j) \tag{3.26}$$

The term $\hat{J}_j$ is called a *Coulomb* operator and is defined as:

$$\hat{J}_j = \left\langle \varphi_j(\vec{r}_2) \middle| \hat{g}_{12} \middle| \varphi_j(\vec{r}_2) \right\rangle \tag{3.27}$$

The term $\hat{K}_j$ is called an *Exchange* operator and is defined as:

$$\hat{K}_j = \left\langle \varphi_j(\vec{r}_2) \middle| \hat{g}_{12} \middle| \varphi_i(\vec{r}_2) \right\rangle \tag{3.28}$$

The *Fock* operator is an effective one-electron operator. It describes the kinetic energy of an electron, the attraction to all the nuclei, and the repulsion to all other electrons. After applying this operator, a set of pseudo-eigenvalue equations is obtained:

$$\hat{F}_1 \varphi_i(\vec{r}_1) = \varepsilon_i \varphi_i(\vec{r}_1) \tag{3.29}$$

where ε_i has the dimension of energy.

This set of equations is also known as the *Hartree-Fock* equations. The Fock operator is dependent on the values of the orbitals φ_j. Thus solving the HF equation is an iterative approach by using φ_j to find φ_i.

3.4.6 The Basis Set Approximation

Historically, the quantum calculations for molecules were performed as LCAO MO, i.e. *Linear Combination of Atomic Orbitals – Molecular Orbitals*. This means that molecular orbitals are formed as a linear combination of atomic orbitals:

$$\varphi_i = \sum_j^M c_{ji} \chi_j \tag{3.30}$$

where χ_j is an atomic orbital and c_{ji} is a coefficient.

The set of functions in Eq. (3.30) is known as the basis set. Substitution of the new MO into the Hartree-Fock equations gives:

$$\hat{F}_1 \sum_j^M c_{ji}\chi_j = \varepsilon_i \sum_j^M c_{ji}\chi_j$$

Roothaan and Hall rewrote the Hartree-Fock equations again:

$$\sum_j^M c_{ji} \langle \chi_k | \hat{F}_1 | \chi_j \rangle = \varepsilon_i \sum_j^M c_{ji} \langle \chi_k | \chi_j \rangle$$

or in matrix form:

$$\mathbf{FC} = \mathbf{SCE} \tag{3.31}$$

where $\boldsymbol{C}$ is the matrix of coefficients, $\boldsymbol{E}$ is a diagonal matrix with elements ε_i, $\boldsymbol{S}$ is the *overlap matrix* with elements $S_{rs} = \langle \chi_r | \chi_s \rangle$, and $\boldsymbol{F}$ is the Fock matrix with elements $F_{rs} = \langle \chi_r | \hat{F}_1 | \chi_s \rangle$.

3.4.7 Classification of Hartree-Fock

Each molecular orbital can be occupied by two electrons. Electrons in the same spatial orbital have opposite spin, forming a pair. This is known as a closed shell system. The valence shell is completely filled. An open shell system is a system whose valence shell is not completely filled with electrons or that has not donated all of its valence electrons through chemical bonds with other atoms or molecules during a chemical reaction. So far, only closed shell systems were considered in the previous sections. There are several

other ways for the electrons to occupy the orbitals. HF calculations can be classified into three types. (i) If the electrons share spatial orbitals in pairs, the method is called the Restricted Hartree-Fock (RHF). (ii) If the number of electrons is odd and all electrons but one share spatial orbitals in pairs, it is called Restricted Open Hartree-Fock method (ROHF). (iii) If all electrons are allowed to occupy different spatial orbitals, the method is called Unrestricted Hartree-Fock (UHF). Open shell molecules have to be handled by either the ROHF method or the UHF method.

3.5 Møller-Plesset Perturbation Theory

In 1934, Møller and Plesset[47] suggested using the HF wavefunction and HF energy as the zeroth-order approximation to the exact wavefunction and energy. The theory is called Møller-Plesset Perturbation Theory (MP*n*) and it is one of the post-Hartree-Fock *ab initio* methods. It improves the Hartree-Fock method by adding electron correlation effects by means of the Rayleigh-Schrödinger perturbation theory (RS-PT), usually to second (MP2), third (MP3), or fourth (MP4) order.

3.5.1 Rayleigh-Schrödinger Perturbation Theory

The major difference between the operators in HF and MPn is that Rayleigh-Schrödinger perturbation theory (RS-PT) adds a small perturbation operator $\hat{V}$ to the normal unperturbed Hamiltonian operator $\hat{H}_0$:

$$\hat{H} = \hat{H}_0 + \lambda\hat{V} \tag{3.32}$$

where λ is an arbitrary real parameter.

The perturbed wave function and perturbed energy are expressed in the form of a Taylor series in λ:

$$E = \lambda^0 W_0 + \lambda^1 W_1 + \lambda^2 W_2 + \cdots + \lambda^n W_n \tag{3.33}$$

$$\Psi = \lambda^0 \Psi_0 + \lambda^1 \Psi_1 + \lambda^2 \Psi_2 + \cdots + \lambda^n \Psi_n \tag{3.34}$$

or in short

$$E = \lim_{n\to\infty} \sum_{i=0}^{n} \lambda^i W_i \text{ and } \Psi = \lim_{n\to\infty} \sum_{i=0}^{n} \lambda^i \Psi_i$$

where $W_0, W_1, W_2, \cdots, W_n$ and $\Psi_0, \Psi_1, \Psi_2, \cdots, \Psi_n$ are unperturbed , first, second,…, *n*th order energy and wavefunction corrections.

Substitution of these series into the time-independent Schrödinger equation (Eq. (3.1)) gives a new equation:

$$(\hat{H}_0 + \lambda \hat{V})(\sum_{i=0}^{n} \lambda^i \Psi_i) = (\sum_{i=0}^{n} \lambda^i W_i)(\sum_{i=0}^{n} \lambda^i \Psi_i) \tag{3.35}$$

where λ^i in this equation gives an *i*th-order perturbation equation, where i = 0,1,2,...,n.

It is convenient to choose the perturbed wave function to be intermediately normalized, i.e. the overlap with the unperturbed wave function should be 1. This has the consequence that all correction terms are orthogonal to the reference wave function.

$$\langle \Psi | \Phi_0 \rangle = 1$$

which results in

$$\langle \Psi_0 + \lambda \Psi_1 + \lambda^2 \Psi_2 + \cdots | \Phi_0 \rangle = 1$$

then

$$\langle \Psi_0 | \Phi_0 \rangle + \lambda \langle \Psi_1 | \Phi_0 \rangle + \lambda^2 \langle \Psi_2 | \Phi_0 \rangle + \cdots = 1$$

finally,

$$\langle \Psi_{i\neq 0} | \Phi_0 \rangle = 0 \tag{3.36}$$

All the terms in Eq. (3.35) are linearly independent, so the equation must be satisfied for each order *n*.

Collecting all the terms with the same power of λ gives:

$$\begin{aligned}
&\text{order 0: } \hat{H}_0\Psi_0 = W_0\Psi_0 \\
&\text{order 1: } \hat{H}_0\Psi_1 + \hat{H}'\Psi_0 = W_0\Psi_1 + W_1\Psi_0 \\
&\text{order 2: } \hat{H}_0\Psi_2 + \hat{H}'\Psi_0 = W_0\Psi_2 + W_1\Psi_1 + W_2\Psi_0 \\
&\quad\vdots \\
&\text{order } n\text{: } \hat{H}_0\Psi_n + \hat{H}'\Psi_{n-1} = \sum_{i=0}^{n} W_i\Psi_{n-i}
\end{aligned} \tag{3.37}$$

These are the zero-, first, second,…, *n*th-order perturbation equations. The zero-order equation is just the unperturbed Schrödinger equation. The first-order equation contains two unknowns. The first unknown is the first-order correction to the energy, W_1. The second one is the first-order correction to the wavefunction, Ψ_1. The *n*th-order correction can be calculated by multiplying from the left by Φ_0 and integrating:

$$\langle\Phi_0|\hat{H}_0|\Psi_n\rangle + \langle\Phi_0|\hat{H}'|\Psi_{n-1}\rangle = \sum_{i=0}^{n} W_i\langle\Phi_0|\Psi_{n-i}\rangle \tag{3.38}$$

The rightmost term in Eq. (3.38) is zero except for $n - i = 0$ or $i = n$, where it becomes W_n. The Hamiltonian is a Hermitian operator:

$$\langle\Phi_0|\hat{H}_0|\Psi_n\rangle = \langle\Psi_n|\hat{H}|\Phi_0\rangle = E_0\langle\Psi_n|\Phi_0\rangle = 0 \qquad (n \neq 0) \tag{3.39}$$

Finally, the *n*th order correction to the energy can be calculated:

$$W_n = \langle\Phi_0|\hat{H}'|\Psi_{n-1}\rangle \qquad (n \neq 0) \tag{3.40}$$

3.5.2 Møller-Plesset Perturbation Theory

In order to apply perturbation theory to the calculation of correlation energy, the unperturbed Hamilton operator must be selected. The most common choice is to take this as a sum over Fock operators, leading to Møller-Plesset perturbation theory (MP*n*).

$$\hat{H}_0 = \sum_{i=1}^{N} \hat{F}_i = \sum_{i=1}^{N} \hat{h}_i + \sum_{i}^{N}\sum_{j}^{N} (\hat{J}_j - \hat{K}_j) = \sum_{i=1}^{N} \hat{h}_i + \sum_{i}^{N}\sum_{j}^{N} \hat{g}_{ij} \tag{3.41}$$

Then the perturbation Hamiltonian becomes:

$$\hat{H}' = \hat{H} - \hat{H}_0 = \frac{1}{2}\sum_{i}^{N}\sum_{j}^{N} \hat{g}_{ij} - \sum_{i}^{N}\sum_{j}^{N} \hat{g}_{ij} = -\frac{1}{2}\sum_{i}^{N}\sum_{j}^{N} \hat{g}_{ij} \tag{3.42}$$

The zero-order wave function is the HF determinant, and the zero-order energy is just a sum of MO energies. The first order correction becomes:

$$W_1 = \left\langle \Phi_0 \middle| \hat{H}' \middle| \Phi_0 \right\rangle = -V_{ee} \tag{3.43}$$

Then, the following relation is found:

$$E_{MP1} = E_{MP0} + W_1 = E_{HF} \tag{3.44}$$

Thus, 1st order Møller-Plesset perturbation theory simply gives the Hartree-Fock energy, and real corrections only start with MP2.

3.6 Density Functional Theory

A functional is a prescription for producing a number from a function, which in turn depends on variables. Density functional theory (DFT) uses functionals to perform

calculations and it is a quantum mechanical method used in physics and chemistry to investigate the electronic structure of many-body systems, in particular molecules and condensed phases. Unlike traditional methods, such as HF, which is based on the complicated many-electron wavefunction, DFT uses electron density as the basic quantity.

3.6.1 Early Approximations

Thomas and Fermi[53,54] did the earliest *a priori* attempt at evaluating the molecular energy based only on the electron density. Their model treats the kinetic energy with a quantum statistical model while the electron-electron and electron-nuclear contributions are treated classically. The potential energy for the attraction between the density and the nuclei is:

$$V_{ne}[\rho(\vec{r})] = \sum_{k}^{nuclei} \int \frac{Z_k}{|\vec{r} - \vec{r}_K|} \rho(\vec{r}) d\vec{r} \tag{3.45}$$

and for the self-repulsion of a classical charge distribution:

$$V_{ee}[\rho(\vec{r})] = \frac{1}{2} \int\int \frac{\rho(\vec{r}_1)\rho(\vec{r}_2)}{|\vec{r}_1 - \vec{r}_2|} d\vec{r}_1 d\vec{r}_2 \tag{3.46}$$

where $\vec{r}_1$ and $\vec{r}_2$ are dummy integration variables running over all space.

The kinetic energy is derived by using fermion statistical mechanics:

$$T_{ueg}[\rho(\vec{r})] = \frac{3}{10}(3\pi^2)^{2/3} \int \rho^{5/3}(\vec{r}) d\vec{r} \tag{3.47}$$

In 1951 J. C. Slater[55] proposed an expression for the exchange energy of a system based

on the electron density.

$$E_x[\rho(\vec{r})] = -\frac{9\alpha}{8}\left(\frac{3}{\pi}\right)^{1/3}\int \rho^{4/3}(\vec{r})d\vec{r} \qquad (3.48)$$

Earlier, Bloch and Dirac[56,57] had derived a similar expression in which α had the value of 2/3 and combined with the Thomas-Fermi expression gave the Thomas-Dirac-Fermi model.

3.6.2 The Hohenberg-Kohn Theorems

After the early approximations described in the previous section (section 3.6.1) were widespread, fairly large errors and the failure of the theories were rigorously found in molecular calculations. In 1964, Hohenberg and Kohn[58] proved two theorems critical to establishing DFT as a legitimate quantum chemical methodology:

(a) *The Hohenberg-Kohn Existence Theorem*
The external potential is determined, within a trivial additive constant, by the electron density.

If one assumes that the existence of two external potentials which differ by more than a constant and lead to the same ground state density, this implies the existence of two different Hamiltonians with respective differing wavefunctions that both correspond to the same ground state density. When interchanging these wavefunctions it is easily shown that the assumption of two differing potentials leading to the same density is not correct. As the density determines all properties of the ground state, the total ground state energy, the ground state kinetic energy, the energy of the electrons in the external potential and the electron-electron interaction energies are all functionals of the density.
The first Hohenberg-Kohn theorem thus gives the existence of a total energy functional, but it does not provide the means to solve the many-body problem.

(b) *The Hohenberg-Kohn Variational Theorem*

The variational theorem, as in molecular orbital theory, applies in the case of an electron density functional. Thus the energy of a trial electron density will always be an upper bound to the true ground state energy.

$$E[\tilde{\rho}(\vec{r})] \geq E_0[\rho_0(\vec{r})] \tag{3.49}$$

3.6.3 The Kohn-Sham Approach

In 1965, Kohn and Sham[59] solved the energy function $E[\rho(\vec{r})]$ by applying the Lagrangian method of undetermined multipliers. In their approach, the Hamiltonian is expressed as a sum of one-electron operators, and has eigenfunctions that are Slater determinants of the individual one-electron eigenfunctions, and has eigenvalues that are simply the sum of the one-electron eigenvalues.

Firstly, the energy functional is divided into specific components to facilitate further analysis:

$$E[\rho(\vec{r})] = T_{ni}[\rho(\vec{r})] + V_{ne}[\rho(\vec{r})] + V_{ee}[\rho(\vec{r})] + \Delta T[\rho(\vec{r})] + \Delta V_{ee}[\rho(\vec{r})] \tag{3.50}$$

where the terms in the above equation refer, respectively, to the kinetic energy of the non-interacting electrons, the nuclear-electron interaction (Eq. (3.45)), the classical electron-electron repulsion (Eq. (3.46)), the correction to the kinetic energy deriving from the interacting nature of the electrons, and all non-classical corrections to the electron-electron repulsion.

Within an orbital expression for the density, Eq. (3.50) may then be rewritten as:

$$E[\rho(\vec{r})] = \left(\langle \chi_i | -\frac{1}{2}\nabla_i^2 | \chi_i \rangle - \langle \chi_i | \sum_k^{nuclei} \frac{Z_k}{|\vec{r}_i - \vec{r}_k|} | \chi_i \rangle \right) + \sum_i^N \langle \chi_i | \frac{1}{2} \int \frac{\rho'(\vec{r})}{|\vec{r}_i - \vec{r}'|} d\vec{r}' | \chi_i \rangle + E_{xc}[\rho(\vec{r})] \tag{3.51}$$

where the terms ΔT and ΔV_{ee} have been put together in a term E_{xc} (exchange-correlation energy). In order to find the orbitals χ by minimizing E in Eq. (3.51), we find that they satisfy the pseudoeigenvalue equations:

$$h_i^{KS} \chi_i = \varepsilon_i \chi_i \tag{3.52}$$

where the Kohn-Sham (KS) one-electron operator is defined as:

$$h_i^{KS} = -\frac{1}{2}\nabla_i^2 - \sum_k^{nuclei} \frac{Z_k}{|\vec{r}_i - \vec{r}_k|} + \int \frac{\rho(\vec{r}')}{|\vec{r}_i - \vec{r}'|} d\vec{r}' + V_{xc} \tag{3.53}$$

and

$$V_{xc} = \frac{\delta E_{xc}}{\delta \rho} \tag{3.54}$$

3.6.4 Exchange-Correlation Functionals

In principle, E_{xc} not only accounts for the difference between the classical and quantum mechanical electron-electron repulsion, but it also includes the difference in kinetic energy between the fictitious non-interacting system and the real system. In practice, the functional dependence of E_{xc} on the electron density is expressed as an interaction between the electron density and an "energy density" ε_{xc} that is dependent on the

electron density:

$$E_{xc}[\rho(\vec{r})] = \int \rho(\vec{r})\varepsilon_{xc}[\rho(\vec{r})]d\vec{r} \tag{3.55}$$

The energy density ε_{xc} is a per particle density and always treated as a sum of individual exchange and correlations. In Eq. (3.48), the energy density is

$$\varepsilon_{xc}[\rho(\vec{r})] = -\frac{9\alpha}{8}(\frac{3}{\pi})^{1/3}\rho^{1/3}(\vec{r}) \tag{3.56}$$

Exchange energy only involves electrons of similar spin. Since correlation between opposite spin electrons involves both inter- and intra-orbital contributions it will always be larger than correlation between similar spin electrons. Exchange energy can thus be given as the sum of both α and β contributions, whereas correlation energy is given in terms of its $\alpha \leftrightarrow \alpha$, $\beta \leftrightarrow \beta$ and $\alpha \leftrightarrow \beta$ components:

$$\begin{aligned} E_x[\rho(\vec{r})] &= E_x^{\alpha}[\rho^{\alpha}(\vec{r})] + E_x^{\beta}[\rho^{\beta}(\vec{r})] \\ E_c[\rho(\vec{r})] &= E_c^{\alpha\alpha}[\rho^{\alpha}(\vec{r})] + E_c^{\beta\beta}[\rho^{\beta}(\vec{r})] + E_c^{\alpha\beta}[\rho^{\alpha}(\vec{r}), \rho^{\beta}(\vec{r})] \end{aligned} \tag{3.57}$$

This leads to the definition spin polarization:

$$\zeta(\vec{r}) = \frac{\rho^{\alpha}(\vec{r}) - \rho^{\beta}(\vec{r})}{\rho(\vec{r})} \tag{3.58}$$

so that the α spin density is simply one-half the product of the total ρ and $(\zeta + 1)$, and the β spin density is the difference between that value and the total ρ.

3.6.5 Local-Density Approximation

The problem with DFT is that the exact exchange and correlation functionals are not known, hence the Local-Density Approximation (LDA) was introduced. Here it is assumed that the density can be treated locally as a uniform electron gas, or equivalently that the density is a slowly varying function. In the LDA the functional depends only on the density at the coordinate where the functional is evaluated. The exchange energy for a uniform electron gas is given as:

$$E_x^{LDA}[\rho(\vec{r})] = -C_x \int \rho^{4/3}(\vec{r})d\vec{r}$$
$$\varepsilon_x^{LDA}[\rho(\vec{r})] = -C_x \rho^{1/3}(\vec{r}) \tag{3.59}$$

where ε_x describes the energy per particle.

Generally, the electrons with α-spin and β-spin have different densities. The *Local Spin Density Approximation* (LSDA) was used to replace the LDA. It raises the individual densities to the 4/3 power:

$$E_x^{LSDA}[\rho(\vec{r})] = -2^{1/3} C_x \int [\rho_\alpha^{4/3}(\vec{r}) + \rho_\beta^{4/3}(\vec{r})]d\vec{r}$$
$$\varepsilon_x^{LSDA}[\rho(\vec{r})] = -2^{1/3} C_x [\rho_\alpha^{1/3}(\vec{r}) + \rho_\beta^{1/3}(\vec{r})] \tag{3.60}$$

3.6.6 Generalized Gradient Approximation

The Generalized Gradient Approximation (GGA) is a better approach to improve on LSDA. It expresses electron density as a non-uniform gas. The exchange and correlation energies calculated by GGA depend on the electron density as well as the derivative of the density.

$$E_{xc}^{GGA}[\rho_\alpha, \rho_\beta] = \int f(\rho_\alpha, \rho_\beta, \vec{\nabla}\rho_\alpha, \vec{\nabla}\rho_\beta)d\vec{r} \tag{3.61}$$

The gradient-corrected functionals provide a much better prediction for the geometries, vibrational spectra, and energetics of hydrogen-bonded systems.

3.6.7 HF/DFT Hybrid Functionals

Although the main error of the LDA method (an improper description of the exchange interactions) is improved by GGA, Becke gave a new approach for improving LDA by mixing "exact" HF exchange with DFT exchange and correlation energies. These are popular types of exchange functionals. One is Becke's half-and-half (BHH) which uses one half of HF and Becke's exchange. Another is Becke's three parameter mixing of exchange (B3).[60] There are four choices of correlation functionals are most common: the local Vosko-Wilk-Nusair (VWN),[61] gradient-corrected Perdew (P86),[62] Perdew and Wang (PW91),[63] and Lee-Yang-Parr (LYP)[64] functionals. The most popular functional is B3LYP. It can be defined as:[65]

$$E_{xc}^{B3} = 0.2E_x^{HF} + 0.8E_x^{LDA} + 0.72E_x^{B} + 1.0E_c^{LDA} + 0.81E_c^{NL} \tag{3.62}$$

3.7 Basis Set Terminology

A basis set is a set of functions used to create the molecular orbitals, which are expanded as a linear combination of such functions with the weights or coefficients to be determined. Normally, the functions are atomic orbitals and they are centered on atoms. Sometimes, the functions centered on bonds or lone pairs are also used. In this section, a few different functions will be explained.

3.7.1 Slater Type Orbitals

Initially, the Slater Type Orbitals (STOs) were used as basis functions due to their similarity to atomic orbitals of the hydrogen atom. They are expressed as:

$$\chi_{\zeta,n,l,m}(r,\ \theta,\ \phi) = Nr^{n-1}e^{-\zeta r}Y_{l,m}(\theta,\ \phi) \tag{3.63}$$

where N is a normalization constant and ζ is called the orbital exponent. r, θ and ϕ are spherical coordinates, and $Y_{l,m}$ is the angular momentum part (the function describing the "shape" of the orbital). n, l and m are quantum numbers: principal, angular momentum and magnetic, respectively.

3.7.2 Gaussian Type Orbitals

However, STOs are not suitable for fast calculations of the two-electron integrals. They were therefore replaced by Gaussian Type Orbitals (GTOs). GTO functions are described as follows:

$$\chi_{\alpha,l,m,n}(x,\ y,\ z) = Ne^{-\alpha r^2}x^l y^m z^n \tag{3.64}$$

where N is a normalization constant and α is called the exponent. x, y and z are Cartesian coordinates. l, m and n are integral exponents of the Cartesian coordinates. The summation of l, m and n is called L, which is used to determine the type of orbital. For instance, s-type (L=0), p-type (L=1), d-type (L=2), f-type (L=3), etc. $\chi_{\alpha,l,m,n}$ are not orbitals and are called Gaussian primitives.

Unfortunately, there is a problem with d-type and higher functions. There are six possible Cartesian Gaussians, namely, x^2, y^2, z^2, xy, xz and yz, but there are only five linearly independent and orthogonal d orbitals, namely, xy, xz, yz, x^2-y^2 and $3z^2-r^2$.

Similarly, *f*-type functions show ten possible Cartesian gaussians, but there are only seven linearly independent *f*-type functions.

Together with the fact that Gaussian functions are differentiable at the nucleus ($r = 0$) they also show radial decay exponential in r^2, where hydrogenic real atomic orbitals decay exponentially in r. Therefore, in practice, linear combinations of GTOs have to be made to better approximate the true shape of atomic orbitals. These combinations are called *contractions* and the individual Gaussians are called *primitives*. Furthermore, there are two ways of making the contractions, segmented or general contractions. In segmented contractions, each primitive is only used once. In general contractions, all primitives are used in each contraction. GTOs are thus defined by their contractions coefficients and the orbital exponents of each primitive.

3.7.3 Notation

In a minimal basis set only one basis function (contraction) per Slater atomic orbital is used. The term for this set is called *single zeta (SZ). Double zeta (DZ)* sets have two basis functions per orbital; *triple zeta (TZ)* sets have three; etc. There are more basis functions assigned to describe valence orbitals. This is because valence orbitals of atoms are more affected by forming a bond than the inner (core) orbitals. The improved basis sets are called *split-valence (SV).* Pople and his co-workers adopted a new convention. In this convention, the basis set structure is given for the whole molecule, rather than a particular atom. Symbols like *n-ijG or n-ijkG* are used. *n* is the number of primitives for the inner shells; *ij* or *ijk* are the number of primitives for the contractions in the valence shell. For example, 6-311G means that 6 primitives gaussians are used for the core electrons and 3+1+1 primitives for the valence electrons.

These basis sets can include polarization functions. The notation for *d* type polarization functions on heavy atoms is *n-ijG** or *n-ijkG** (sometimes also *n-ijG(d) or n-ijkG(d)* is used). The polarization functions are important for reproducing chemical bonding. For

polarization functions on all atoms with *p*-functions on hydrogens, the notation changes to *n-ijG*** or *n-ijkG*** (sometimes *n-ijG(d,p) or n-ijkG(d,p)* is also used).

Diffuse functions are usually necessary for improving the description of anions and weak bonds (e.g. hydrogen bonds) and are frequently used for calculations of properties such as dipole moments, polarizabilities, etc. When one set of diffuse *s*-type and *p*-type Gaussian are added to heavy atoms, an *n-ij+G* or *n-ijk+G* notation is used. If one diffuse *s*-type and *p*-type is placed on heavy atoms and one diffuse *s*-type gaussian on hydrogens, an *n-ij++G* or *n-ijk++G* notation is used.

Table **3.2**: Availability of polarization and diffuse functions and the range of applicability for selected built-in basis set in *Gaussian 98* and *03*.[52]

Basis set	Applies to	Polarization functions	Diffuse functions
3-21G	H-Xe	*	+
6-21G	H-Cl	(d)	
6-31G	H-Kr	(3df, 3pd)	++
6-311G	H-Kr	(3df, 3pd)	++
CEP-31G	H-Rn	* *(Li-Ar only)*	
CEP-121G	H-Rn	* *(Li-Ar only)*	
LanL2DZ	H, Li-Ba, La-Bi		
cc-pV6Z	H, B-Ne	*included in definition*	*added via* **AUG-** *prefix*
SV	H-Kr		
SVP	H-Kr	*included in definition*	
TZV and TZVP	H-Kr	*included in definition*	

3.7.4 Effective Core Potentials

Systems involving third row atoms or heavier elements contain a large number of chemically unimportant but energetically important core electrons. Calculations can be

sped up significantly if the core electrons are replaced by analytical functions that approximate the core electron interactions. These are called *effective core potentials* (ECPs) or *pseudopotentials*. Another advantage is that relativistic effects, which become significant for heavy elements, can be introduced implicitly through ECPs.

3.8 Population Analysis

A partial charge is a charge with an absolute value of less or more than one elementary charge unit. This is because of the asymmetric distribution of electrons in chemical bonds. Section 3.8.1 will give an introduction to population analysis based on basis functions. Section 3.8.2 contains an introduction to population analysis based on the electrostatic potential. In section 3.8.3, an overview of population analysis based on natural orbitals will be presented.

3.8.1 Mulliken Population Analysis

Mulliken population analysis[66] is based on the linear combination of atomic orbital molecular orbitals method (utilizing basis functions). It uses the **PS** matrix for distributing the electrons into atomic contributions.

$$q_i = Z_i - \sum_{\mu \in i} (\mathrm{PS})_{\mu\mu} \tag{3.65}$$

in which the summation is carried out over all atomic orbitals $\left|\varphi_\mu(r)\right\rangle$, centered on atom *i* with nuclear charge Z_i. ***P*** and ***S*** are the density matrix and the overlap matrix, respectively. $P_{\mu\nu} = 2\sum_k c^*_{\mu k} c_{\nu k}$, $S_{\mu\nu} = \left\langle \varphi_\mu \middle| \varphi_\nu \right\rangle$ where $c^*_{\mu k}$ and $c_{\nu k}$ are the coefficients of the wavefunction.

There are some arguments against this type of population analysis: (i) the charge due to overlap is distributed evenly between the atoms, (ii) the multipole moments of higher orders in the overlap regions are not included, (iii) the moments obtained by transferring the charge onto the atoms due to the overlap are neglected, and, (iv) it is not compatible with diffuse functions. As will be discussed later on, the charges calculated by this method are found to be inadequate for the description of electrostatic properties, as well as pure Coulomb interactions.

3.8.2 Potential Derived Charges

Cox and Williams[67] proposed a different method to derive the atomic charges. The electrostatic potential is calculated over a predefined grid of N_{pnt} points.

$$V(\vec{r}) = \sum_A Z_A T(\vec{r}, \vec{r}_A) - \sum_\mu \sum_\nu P_{\mu\nu} \times \int \varphi_\mu^*(\vec{r}^{\,\prime}) \varphi_\nu(\vec{r}^{\,\prime}) T(\vec{r}, \vec{r}^{\,\prime}) d\vec{r}^{\,\prime} \qquad (3.66)$$

where $T(\vec{r}, \vec{r}^{\,\prime}) = \left| \vec{r} - \vec{r}^{\,\prime} \right|^{-1}$.

The charges $\{q_i\}$ are calculated by minimizing the functional:

$$f(\{|q_i|\}) = \sum_k^{N_{pnt}} \left[V(\vec{r}_k) - \sum_i^{N_{atom}} q_i T(\vec{r}_k, \vec{r}_i) \right]^2 \qquad (3.67)$$

Chirlian and Francl[68] proposed a non-iterative method. They introduce a constraint on the sum of charges, and an associated Lagrangian multiplier, allowing an exact reproduction of the total molecular charge. Later on, Singh and Kollman[69,70] improved the approach of Cox and Williams by modifying the original electrostatic potential (ESP). The predefined points are defined on a van der Waals envelope. The charges calculated with this method are called MKS due to the process of fitting the electrostatic potential at points selected according to the Merz-Singh-Kollman scheme. CHelpG[71] is another

method for obtaining a potential derived charge. The charge is produced by fitting the electrostatic potential at points selected according to the CHelpG scheme.

3.8.3 Natural Orbital Analysis

Natural orbital analysis was devised by Löwdin.[72] Later on, Weinhold[73] developed the theory further. They use the one-electron density matrix for defining the shape of the atomic orbitals in the molecular environment, and to derive molecular bonds from electron density between the atoms. *Natural Atomic Orbitals* (NAOs) describe the natural orbital of an atom in a molecule. They consist of *core* orbitals (cor), *valence* orbitals (val), and *virtual* or *Rydberg* orbitals (Ryd). The occupancy of each NAO is referred to as the *natural population* of that orbital. *Natural Population Analysis* (NPA)[74,75] refers to the distribution of electrons (atomic charge) in a molecule. The method can describe the N-electron wavefunction *ψ(1, 2, …, N)* in terms of localized orbitals or configurations that are closely tied to chemical bonding concepts. The density operator $\hat{\Gamma}$ is defined as:

$$\hat{\Gamma} = N\int \psi(1,2,\cdots,N)\psi^{*}(1',2,\cdots,N)d\tau_2\cdots d\tau_N \tag{3.68}$$

The charge *q* is obtained as:

$$q_\phi = \langle \phi | \hat{\Gamma} | \phi \rangle \tag{3.69}$$

Natural Bond Orbitals (NBOs) are then used to describe the *Natural Hybrid Orbitals* (NHOs) in a molecule. A NHO on atom A can be obtained as:

$$h_A = \sum_k a_k \Lambda_k^{(A)} \tag{3.70}$$

where $\Lambda_k^{(A)}$ is defined as a maximum occupancy orbital.

Two-centre bonding NBOs are formed using a normalized, linear combination of two NHOs.

$$\sigma_{AB} = a_A h_A + a_B h_B \tag{3.71}$$

where the coefficients a_A and a_B are normalized by $a_A^2 + a_B^2 = 1$.

The corresponding anti-bonding NBO is

$$\sigma_{AB}^* = a_A h_A - a_B h_B \tag{3.72}$$

3.9 Atoms in Molecules

Bader proposed a purely topological approach to the analysis of the electron density which is called *Atoms In Molecules* (AIM).[76,77] The density is obtained either experimentally or from theoretical electronic structure calculations. In this approach, a molecular volume is divided into atomic subspaces. The electron density is calculated by squaring the wavefunction integrated over *N-1* coordinates.

$$\rho(\vec{r}_1) = \int \left|\Psi(\vec{r}_2, \vec{r}_3, \cdots, \vec{r}_N)\right|^2 d\vec{r}_2 d\vec{r}_3 \cdots d\vec{r}_N \tag{3.73}$$

It is found that the maxima in the electron density always occur at or near the nuclei. This makes sense, because they are the only sources of positive charge. These maxima are called *attractors* of the electron density. Between two attractors, there is a line of maximum electron density which is called the *bond path.* The point of minimum electron density along the bond path is called the *bond critical point* (BCP). The *ring critical point* (RCP) has minimum electron density in the plane of a ring, but maximum electron

density perpendicular to the plane. The *cage critical point* (CCP) has a minimum electron density in all spatial directions. The four points are related by the *Poincaré-Hopf* equation.

Table 3.3: Summary of the four types of critical points.[50]

Critical point	Signature (r, s)
Nuclear attractor	(3, -3)
Bond critical point	(3, -1)
Ring critical point	(3, +1)
Cage critical point	(3, +3)

The *Poincaré-Hopf* relation relates the number of non-degenerate critical points for non-periodic systems as follows:

$$n - b + r - c = 1 \tag{3.74}$$

where n is the number of nuclear attractors, b is the number of bond critical points, r is the number of ring critical points and c is the number of cage critical points.

Critical points are normally represented by two numbers given in parentheses (r, s) where r is the rank or dimension of the critical point and s is the sum of the signs of the eigenvalues or local curvatures of the electron density. (r, s) is also called a *signature*.

The atomic and bond properties may also be calculated using AIM. Atomic charge, q, is obtained as:

$$q_\Omega = Z - N_\Omega = Z - \int_\Omega \rho(\vec{r})d\vec{r} \tag{3.75}$$

where Ω is the atomic basin and N_Ω is the *electron population.*

The atomic dipole, *M,* is a measure of the displacement of the electron density from the nucleus. It is obtained as:

$$M_\Omega = \int_\Omega \rho(\vec{r})\vec{r}_\Omega d\vec{r} \tag{3.76}$$

where $\vec{r}_\Omega$ is a vector centered on the nucleus of the atom.

The Laplacian of the electron density is the derivative of the gradient vector field of the electron density, and is defined as:

$$\nabla^2\rho(\vec{r}) = \frac{\partial^2\rho(\vec{r})}{\partial x^2} + \frac{\partial^2\rho(\vec{r})}{\partial y^2} + \frac{\partial^2\rho(\vec{r})}{\partial z^2} \tag{3.77}$$

For convenience, a new function $L(\vec{r})$ is defined as $L(\vec{r}) = -\nabla^2\rho(\vec{r})$. This function is positive for a local charge concentration and negative for a local charge depletion. If $L(\vec{r})$ >0 at the bond critical point, the bond is defined as a *sharing interaction*. If $L(\vec{r})$ <0, the bond is defined as a *closed-shell interaction.* If $L(\vec{r})$ ≈0, the bond is defined as a *van der Waals interaction.*

3.10 Molecular Mechanics Methods

The method of using Newtonian mechanics to model molecular systems is called molecular mechanics (MM). The potential energy of the systems is calculated by using force fields. There are three assumptions underlying molecular mechanics. One is that each atom is treated as a single particle. The second is that each particle is assigned a radius (normally van der Waals radius), polarizability, and a net charge. The third is that the interactions between bonded particles are treated as a spring with an equilibrium

distance equal to the experimental or calculated bond length and a stiffness described by a force constant.

The potential energy of a molecular system is the summation of individual energy terms:

$$E = E_{covalent} + E_{noncovalent} \tag{3.78}$$

where as:

$$E_{covalent} = E_{bond} + E_{angle} + E_{dihedral} \tag{3.79}$$

and

$$E_{noncovalent} = E_{electrostatic} + E_{vanderWaals} \tag{3.80}$$

The advantage of molecular mechanics is short calculation times, even for large, complex systems. The disadvantages are (i) bond breaking and formation are difficult to model; (ii) force field parameters must be known, and (iii) development of force fields can be long and labor-intensive.

3.10.1 Force Field

Force fields are an integral part of molecular mechanics. In the force field, several functional forms and parameter sets are used to calculate the potential energy of a system of particles. The typical parameter set includes values for atomic mass, van der Waals radius, and partial charge for individual atoms, and equilibrium values of bond lengths, bond angles, and dihedral angles for pairs, triplets, and quadruplets of bonded atoms, and values corresponding to the effective force constant for each potential. Because the functional forms of the potential terms vary extensively between even closely related force fields (or successive versions of the same force field), the parameters from one force field should never be used in conjunction with the potential from another.

3.10.2 Electrostatic Interactions

Since, as was pointed out in the previous chapter, electrostatic interaction is considered to be the driving force behind the shortening of the dative bond in the condensed state, a classical description of these interactions will be given in some detail.

Schleyer *et al.*[29] define the electric dipole as

$$\vec{\mu} = q\vec{l} \tag{3.81}$$

where $\vec{l}$ is the distance vector directed from the centre of gravity of the electron density to the centre of gravity of the positive electric charge, the absolute magnitude of each charge being *q*. The dipole moment of a complex molecule can be represented approximately in the form of the vectorial sum of the individual bond moments.

The electrostatic interaction between two charges, q_1 and q_2, is also called the *Coulomb Potential* and is given as:

$$U_q = \frac{1}{4\pi\varepsilon_0}\frac{q_1 q_2}{r} \tag{3.82}$$

The electrostatic interactions within a molecule or between molecules can also be expressed in terms of the effective dipole moment, $\bar{\mu}$, of the bonds in the molecule. The energy is dependent on both the magnitude and the orientation of the dipoles.

$$U_\mu = \frac{1}{4\pi\varepsilon_0}\left[\frac{\bar{\mu}_a\bar{\mu}_b}{r^3} - 3\frac{(\bar{\mu}_a\cdot\bar{r})(\bar{\mu}_b\cdot\bar{r})}{r^5}\right] \tag{3.83}$$

where *r* is the distance between the centers of the two dipoles ($\bar{\mu}_a$ and $\bar{\mu}_b$).

From this definition, the effect of the relative orientations of the two dipoles on the potential energy, is easily calculated.

Table **3.4**: Four general dipole-dipole interaction patterns.[50]

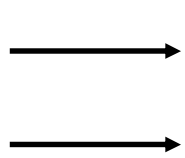	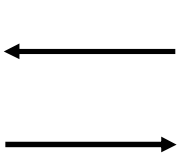	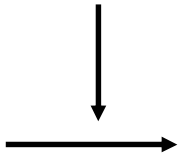	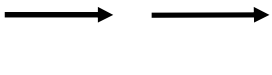
$E = \frac{1}{4\pi\varepsilon_0}\frac{\mu_a\mu_b}{r^3}$	$E = \frac{-1}{4\pi\varepsilon_0}\frac{\mu_a\mu_b}{r^3}$	$E = 0$	$E = \frac{-2}{4\pi\varepsilon_0}\frac{\mu_a\mu_b}{r^3}$

3.10.3 Other Useful Electrostatic Properties

The electrical force between q_1 and q_2 can be calculated from Coulomb's Law:

$$\vec{F} = \frac{1}{4\pi\varepsilon_0}\frac{q_1 q_2}{r^3}\vec{r} \tag{3.84}$$

where *r* is the distance between the two charges. A positive force means the two charges attract each other and a negative one means the two charges repel each other.

The electric field *E* at a point *P* caused by a single point charge *q* at a distance *r* from *P* can be calculated as:

$$E = \frac{1}{4\pi\varepsilon_0}\frac{q}{r^3}\vec{r} \tag{3.85}$$

So the total electric field at *P* is the vector sum of the fields E_1, E_2, and so on.

$$E = E_1 + E_2 + \cdots = \frac{1}{4\pi\varepsilon_0}\frac{q_1}{r_1^3}\vec{r}_1 + \frac{1}{4\pi\varepsilon_0}\frac{q_2}{r_2^3}\vec{r}_2 + \cdots \tag{3.86}$$

The potential energy at *P* for a charged particle (q') is obtained as:

$$U = \frac{q'}{4\pi\varepsilon_0}\sum\frac{q_i}{r_i} \tag{3.87}$$

Then, the electrical potential at *P* is calculated as:

$$V = \frac{U}{q'} = \frac{1}{4\pi\varepsilon_0}\sum\frac{q_i}{r_i} \tag{3.88}$$

Chapter Four

Gas Phase Calculations

4.1 Introduction

Gas phase calculations are important for this study since a single gas molecule is not influenced by its surroundings and experiences only results of intra-molecular interactions (e.g. van der Waals repulsion, etc.). In section 4.2, the isolated gas molecules studied with HF, DFT and MP2 levels of theories are described. Various diffuse and polarization functions were also added to the basis sets. Section 4.3 reports the rotational analysis for the selected molecules. The aim of section 4.4 is to determine the relationship between the X-B-N and Y-N-B angles and the B-N bond length. This was done using constraints on the B-N distance to find out how the angles change as the B-N bond distance changes. In the gas phase calculations, four different types of charges were also calculated. They are listed and discussed in section 4.5. One of the purposes of this study was to find out in detail what the effect of an electric field is on the geometry of gas molecule. This was done by simulating an external electrical field during the calculations for isolated molecules. This gives a good comparison with the molecule in the solid state. The results are presented in section 4.6. In section 4.7, all the atoms except boron and nitrogen were fixed during the optimization in various external electrical fields. The results obtained here are quite different to the results given in section 4.6. The detailed results are shown in addendum A (attached CD).

4.2 Gas Phase Calculations

The monomers of $(CH_3)_3N\text{-}BX_3$ (X = H, F, Cl, Br, CN), $H_3N\text{-}BY_3$ (Y = H, CH_3, CF_3), $(C_2H_5)H_2N\text{-}B(CF_3)_3$ and $(C_2H_5)_2HN\text{-}B(CF_3)_3$ complexes were built with the *Cerius*[2]

software[78]. The geometries of Me_3N-BCl_3, Me_3N-BF_3, $(CF_3)_3B$-CO and $(BCl_2)_3B$-CO were optimized either with the *Gaussian 98*[79] or *Gaussian 03*[80] programs. The calculations were done at the HF, DFT (B3LYP), and MP2 levels of theory. Various diffuse and polarization functions were also added to the basis sets: 6-31G, 6-31G(d), 6-31G(d,p), 6-31+G, 6-31++G, 6-31++G(d,p), 6-311G, 6-311G(d), 6-311G(d,p), 6-311+G, 6-311++G, and 6-311++G(d,p). The purpose was to check how the levels of theory and basis sets affect the calculated lengths of the B-N dative bond and the B-CO bond.

Table 4.1: B-N distances (Å) for Me_3N-BF_3 and Me_3N-BCl_3 in the gas phase at different levels of theory with several basis sets.

	Me_3N-BF_3			Me_3N-BCl_3		
Basis Set	HF	DFT	MP2	HF	DFT	MP2
6-31G	1.6365	1.6586	1.6628	1.6311	1.6535	1.6546
6-31G(d)	1.6777	1.6987	1.6658	1.6626	1.6781	1.6653
6-31G(d,p)	1.6744	1.6946	1.6655	1.6556	1.6724	1.6583
6-31+G	1.6301	1.6487	1.6527	1.6281	1.6498	1.6545
6-31++G	1.6299	1.6485	1.6530	1.6278	1.6469	1.6546
6-31++G(d,p)	1.6647	1.6821	1.6574	1.6527	1.6748	1.6703
6-311G	1.6293	1.6510	1.6415	1.6280	1.6462	1.6406
6-311G(d)	1.6693	1.6907	1.6668	1.6583	1.6762	1.6589
6-311G(d,p)	1.6662	1.6844	1.6670	1.6556	1.6724	1.6583
6-311+G	1.6265	1.6435	1.6370	1.6233	1.6415	1.6381
6-311++G	1.6365	1.6433	1.6372	1.6227	1.6408	1.6375
6-311++G(d,p)	1.6597	1.6758	1.6608	1.6527	1.6705	1.6612
Average	1.6501	1.6683	1.6556	1.6415	1.6603	1.6544
Standard Deviation	0.0201	0.0214	0.0114	0.0157	0.0149	0.0105
Experimental	1.636(4)[81], 1.674(4)[82]			1.652(9)[83]		

Comparing the results obtained in Table 4.1, the HF calculations mostly underestimate the B-N dative bonds, the DFT calculations overestimate them and the MP2 calculations lie in between the HF and DFT calculations and closer to the HF calculations. The MP2 calculations have the smallest standard deviation. The HF and DFT calculations have nearly the same standard deviation. Me_3N-BF_3 has deviations (differences between the longest and shortest bond length) of 0.0512 Å, 0.0554 Å and 0.0300 Å for HF, DFT and MP2, respectively. The corresponding deviations for Me_3N-BCl_3 are 0.0399 Å, 0.0373 Å and 0.0328 Å. This implies that the B-N dative bond in the two selected complexes is basis set sensitive. For the three methods, it is noticed that the diffuse functions make the bond shorter and the polarization functions lengthen the bond. There is only a small B-N bond length change of about 0.01 Å when adding polarization functions or diffuse functions either on heavy atoms or on all atoms. Increasing the size of the basis set results in a decrease in B-N bond lengths. Increasing the level of theory from HF to MP2, for the calculations without any additional functions, the B-N bond lengths increase about 0.02 Å; for most calculations with polarization functions, the B-N bond lengths increase less than 0.003 Å; for calculations with diffuse functions, the B-N bond lengths undergo only a small change of about 0.002 Å; for calculations with addition of both diffuse and polarization functions, the B-N bond lengths increase about 0.01 Å. This means that the results with the additional diffuse or polarization functions are not sensitive to the electron correlation effects.

Me_3N-BF_3 has two experimental values, 1.636(4) Å was obtained utilizing microwave spectroscopy and 1.674(4) Å using gas-phase electron diffraction. For both Me_3N-BF_3 and Me_3N-BCl_3 complexes, the results obtained with HF/6-31G(d) and HF/6-31G(d,p) are quite close to the experimental value. Due to the lower computational cost, HF/6-31G(d) is chosen as the standard method for the future calculations.

Table 4.2: B-CO distances (Å) for complexes $(BCl_2)_3B$-CO and $(CF_3)_3B$-CO in the gas phase at different levels of theory with several basis sets.

	$(BCl_2)_3B$-CO			$(CF_3)_3B$-CO		
Basis Set	HF	DFT	MP2	HF	DFT	MP2
6-31G	1.5993	1.5200	1.5479	1.6810	1.5827	1.6294
6-31G(d)	1.6073	1.5214	1.5162	1.7089	1.5810	1.6027
6-31G(d,p)	1.6073	1.5214	1.5162	1.7089	1.5810	1.6027
6-31+G	1.6016	1.5206	1.5500	1.6803	1.5961	1.6344
6-31++G	1.6016	1.5206	1.5500	1.6803	1.5961	1.6344
6-31++G(d,p)	1.6077	1.5209	1.5479	1.7101	1.5961	1.6027
6-311G	1.5971	1.5187	1.5415	1.6797	1.5917	1.6266
6-311G(d)	1.6016	1.5185	1.5164	1.7026	1.5840	1.6028
6-311G(d,p)	1.6016	1.5185	1.5164	1.7026	1.5840	1.6028
6-311+G	1.5972	1.5183	1.5409	1.6804	1.5958	1.6267
6-311++G	1.5972	1.5183	1.5409	1.6804	1.5958	1.6267
6-311++G(d,p)	1.6012	1.5171	1.5157	1.7021	1.5885	1.6039
Average	1.6017	1.5195	1.5333	1.6931	1.5894	1.6163
Standard Deviation	0.0039	0.0015	0.0155	0.0136	0.0065	0.0142
Experimental		n.r.[a]			1.617(4)[44]	

[a]Not reported.

Data for the optimized $(BCl_2)_3B$-CO and $(CF_3)_3B$-CO gas molecules are shown in Table 4.2. DFT calculations give the smallest standard deviation; MP2 has the largest standard deviation. $(BCl_2)_3B$-CO has deviations (differences between the longest and shortest bond length) of 0.0106 Å, 0.0043 Å, and 0.0343 Å for HF, DFT, and MP2, respectively, and $(CF_3)_3B$-CO has corresponding deviations of 0.0304 Å, 0.0151 Å, and 0.0317 Å. This implies that the B-CO bond is also basis set sensitive. For $(CF_3)_3B$-CO, the optimized B-CO bond distances calculated by MP2 are close the experimental values, and the HF and DFT calculations disagree with the experimental value. Increasing the size of the basis set results in a decreased B-CO bond length. When increasing the level of

theory from HF to MP2, the B-CO bond distance decreases over 0.05 Å. Because there were no hydrogen atoms in the selected compounds, the basis sets with "+" and "++" are equal to each other and basis sets with "d" and "d,p" are equal as well. Although the DFT method is better for B-CO calculations, in order to be consistent with the B-N complexes, HF/6-31G(d) was chosen as the standard method for future B-CO calculations as well.

Table 4.3 shows the experimental and optimized B-N and B-CO distance for all the selected molecules. Some of the gas molecules have two different experimental bond lengths. This is due to the two different methods of study: microwave spectroscopy (MW) and gas-phase electron diffraction (GD). The two experimental methods lead to different experimental bond lengths. MW gives a shorter bond distance. GD studies provide a bond length that is closer to the calculated value. The optimized B-N distances for the selected B-N gas molecules agree with the experimental values. The optimized B-CO distances for the selected B-CO complexes disagree with each other, and only the MP2 calculations agree with the experimental values.

Table 4.3: Comparison of calculated B-N, B-CO distances (Å) and experimental values for the gas phase. The calculations were carried out using different models and the standard 6-31G(d) basis set.

Complex	Name	Expt.	HF	DFT	MP2
Me_3N-BH_3	Trimethylamine – borane	1.638(10)[84], 1.656(3)[85]	1.6776	1.6623	1.6485
Me_3N-BF_3	Trimethylamine – trifluoroborane	1.636(4)[81], 1.674(4)[82]	1.6777	1.6986	1.6658
Me_3N-BCl_3	Trimethylamine – trichloroborane	1.652(9)[83]	1.6626	1.6811	1.6623
Me_3N-BBr_3	Trimethylamine – tribromoborane	1.663(13)[83]	1.6473	1.6642	1.6485
Me_3N-$B(CN)_3$	Trimethylammonio – tricyanoborate	n.r.[a]	1.6404	1.6628	1.6428
H_3N-BH_3	Ammonia – borane	1.6722(5)[86]	1.6887	1.6686	1.6636
H_3N-$B(CF_3)_3$	Tris(Trifluoromethyl)borane – ammine	n.r.[a]	1.6247	1.6215	1.6057
$(C_2H_5)H_2N$-$B(CF_3)_3$	Tris(Trifluoromethyl)borane – ethylamine	n.r.[a]	1.6232	1.6202	1.6036
$(C_2H_5)_2HN$-$B(CF_3)_3$	Tris(Trifluoromethyl)borane – diethylamine	n.r.[a]	1.6447	1.6412	1.6214
H_3N-BMe_3	Aminetrimethyl – borane	n.r.[a]	1.7384	1.7096	1.6804
$(BF_2)_3B$-CO	Carbonyltris(difluoroboryl)boron	1.502(5)[45]	1.5688	1.4970	1.5014
$(BCl_2)_3B$-CO	Carbonyltris(dicoboryl)boron	n.r.[a]	1.6073	1.5214	1.5162
$(CF_3)_3B$-CO	Carbonyltris(trifluoromethyl)boron	1.617(4)[44]	1.7089	1.5808	1.6027

[a]Not reported.

4.3 Rotational Analysis along the B-N Bond

The B-N complexes, $(CH_3)_3N\text{-}BX_3$ (X = F, Cl, Br, CN), were selected to perform a rotational analysis. The substituents along the B-N bond were rotated from 0º, which is the eclipsed conformation  , to 60º which is the staggered one  in increments of 10º. The substituents have local C_{3v} symmetry, so the full rotational conformation map can be reproduced by symmetry. The complexes were optimized with HF/6-31G(d).

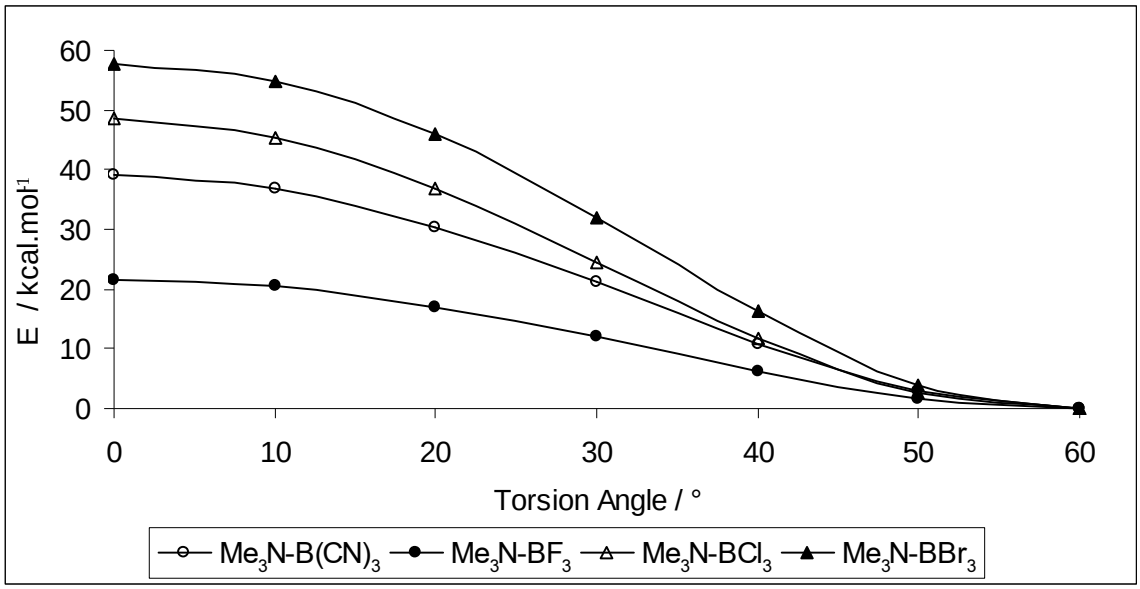

Figure 4.1: The optimized relative Hartree-Fock energy in a selection of B–N complexes, as a function of the torsion angle. The energies are relative to the most stable conformation.

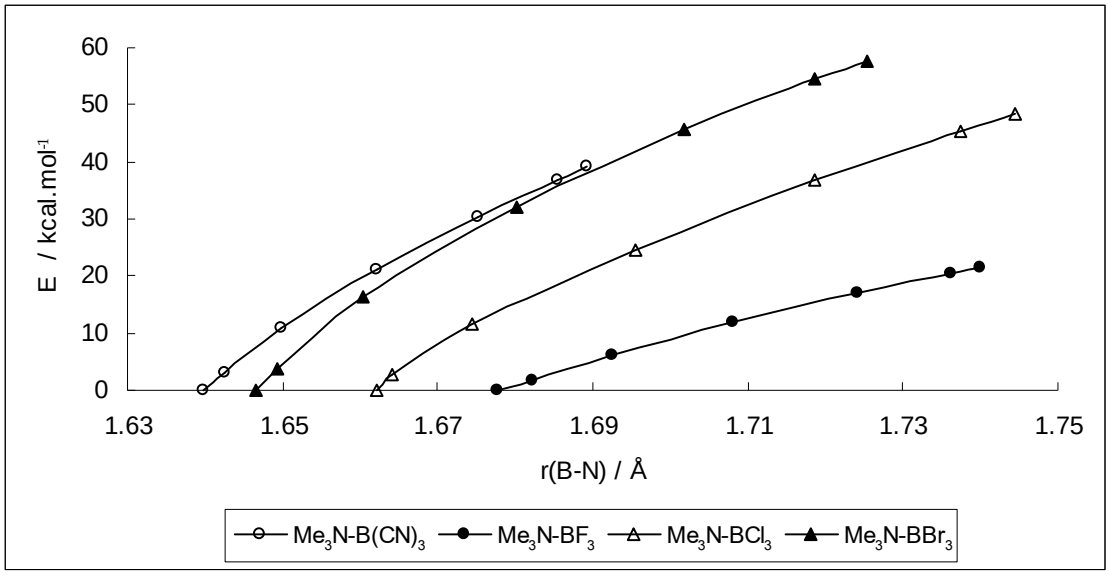

Figure 4.2: The optimized relative Hartree-Fock energies in a selection of B–N complexes, as a function of the optimized B-N bond length. The energies are relative to the most stable conformation.

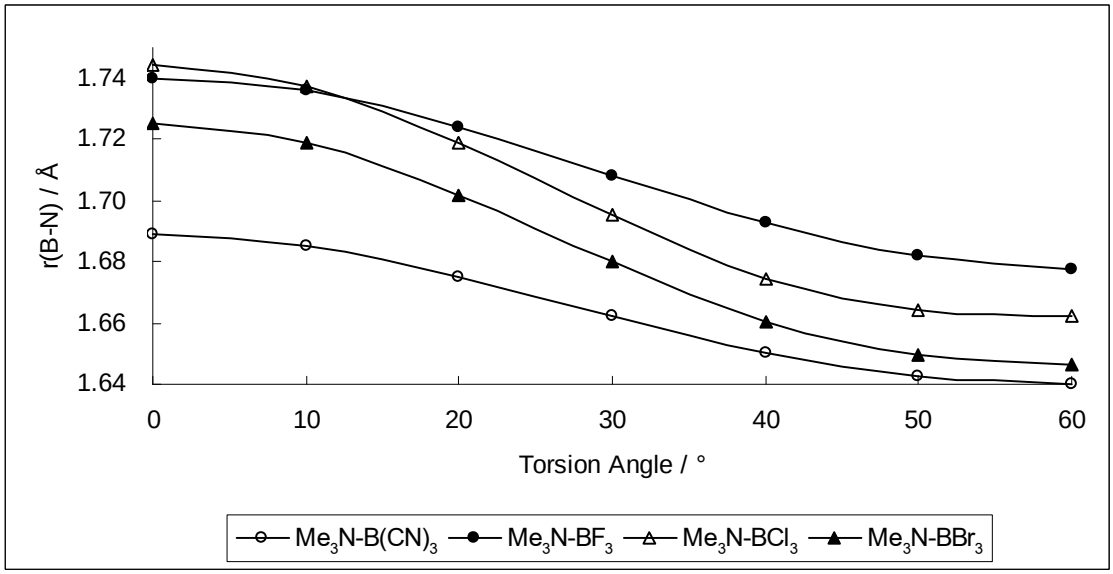

Figure 4.3: The optimized B-N bond length in a selection of B–N complexes, as a function of the torsion angle.

The rotational analysis along the B-N bond shows that when going from the eclipsed conformation to the staggered one, the molecule becomes more stable and the B-N bond length decreases. In the selected B-N complexes, the lowest rotational energy is as high as about 20 kcal/mol. By comparing the distance of the closest substituents on B and N with the sum of van der Waals radii for those atoms, we conclude that the van der Waals repulsion force has also decreased from the eclipsed conformation to the staggered one. Normally, van der Waals repulsion forces are very small, but in this case the small force changes the geometries of the selected B-N complexes substantially, with the B-N bond changing by almost 0.1 Å. This may due to the weakness of the B-N dative bond. The question here is that if the intra-molecular interactions affect the B-N bond length a lot in the gas phase, will they affect the bond length in the crystal as well?

4.4 Relationship between the B-N Bond and the C-N-B, X-B-N Angles

From the previous section 4.3, we can see that the van der Waals repulsion force is the determinant of the B-N bond length. It is known that increasing the distance results in decreasing the van der Waals repulsion force. The substituents also move away from each other and this results in changing the angles between the substituents and the bond. In this section, calculations are described where the B-N dative bond distance in Me_3N-BX_3 (X = H, F, Cl, Br) was increased from 1.5 Å to 1.8 Å by an increment of 0.03 Å. In each step, the B-N bond distance was constrained during the geometry optimization.

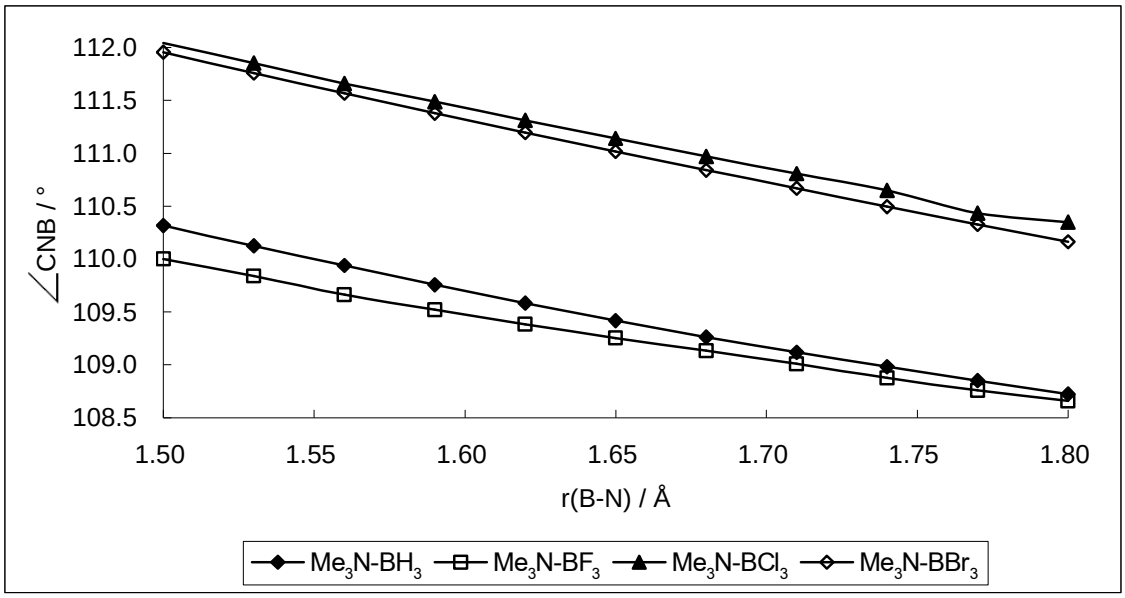

Figure 4.4: The optimized C-N-B angle in a selection of B–N complexes, as a function of the B-N bond length.

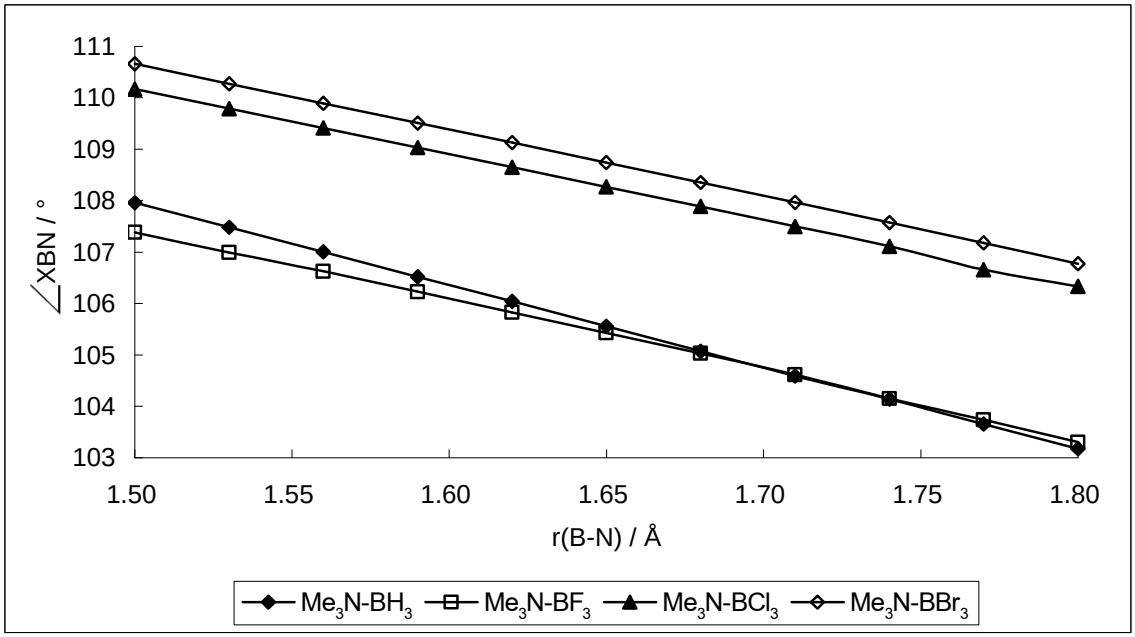

Figure 4.5: The optimized X-B-N (X = H, F, Cl, Br) angle in a selection of B–N complexes, as a function of the B-N bond length.

From Figures 4.4 and 4.5, a trend can be seen: the longer the B-N bond distance, the smaller the C-N-B and X-B-N (X = H, F, Cl, Br) angles. There is a ~2° angle change for the C-N-B angle, but the X-B-N angle changes about 5° from ~110° to ~105° when the B-N bond changes from 1.5 to 1.8 Å. This implies that the orbital hybridization type changes from sp^3 to sp^2 character and that the BX_3 part tends to change to a planar geometry. In the solid state, the B-N bond lengths decrease by about 0.05 Å in the selected complexes. From the study in this section, the X-B-N angle is expected to increase ~1° and the C-N-B angle should change ~0.5° in the crystal phase.

4.5 Charge Comparison

This section deals with the atomic charges in the gas phase. Four different types of partial charge were calculated, namely, NPA[76], CHelpG[75], MKS[73,74], and Mulliken[70]. The charges for the selected B-N complexes were mainly obtained with HF/6-31G(d) and for the B-CO complexes they were derived using both HF/6-31G(d) (as main method) and B3LYP/6-31G(d) (comparison).

Table **4.4**: Comparison of the atomic charges (e) on B and N in a selection of B-N adducts.

	NPA		CHelpG		MKS		Mulliken	
	Q(N)	Q(B)	Q(N)	Q(B)	Q(N)	Q(B)	Q(N)	Q(B)
Me_3N-BH_3	-0.511	-0.033	0.341	0.211	0.302	0.096	-0.566	0.154
Me_3N-BF_3	-0.584	1.556	0.155	0.818	0.093	0.833	-0.652	1.096
Me_3N-BCl_3	-0.595	0.477	0.060	0.260	-0.035	0.143	-0.630	0.350
Me_3N-BBr_3	-0.603	0.233	----	----	-0.104	-0.262	-0.649	0.635
H_3N-BH_3	-0.962	-0.036	-0.395	0.339	-0.376	0.253	-0.936	0.106
H_3N-$B(CF_3)_3$	-0.984	0.332	-0.854	-0.296	-0.955	-0.277	-1.069	0.306
H_3N-BMe_3	-0.976	0.733	-0.737	0.752	-0.775	0.849	-1.011	0.691

Table **4.5**: Comparison of the atomic charges (e) on B and C in a selection of B-CO adducts.

		NPA		CHelpG		MKS		Mulliken	
		Q(B)	Q(C)	Q(B)	Q(C)	Q(B)	Q(C)	Q(B)	Q(C)
$(BF_2)_3B$-CO	HF	-0.989	0.690	-1.299	0.978	-0.961	0.634	-0.742	0.539
	DFT	-1.259	0.802	-0.762	0.525	-0.723	0.484	-0.505	0.425
$(BCl_2)_3B$-CO	HF	-1.020	0.981	-0.197	0.425	0.588	0.083	-0.027	0.490
	DFT	-1.010	0.819	-0.031	0.282	0.650	-0.013	0.202	0.360
$(CF_3)_3B$-CO	HF	0.052	0.930	-0.526	0.681	-0.607	0.707	0.118	0.457
	DFT	-0.122	0.818	-0.478	0.631	-0.503	0.614	-0.002	0.404

The charges were calculated according to the four different schemes. The values obtained are quite different from each other. For the selected B-N complexes, the charges for the N atoms calculated by NPA are all negative and most of the charges for B are positive except for Me_3N-BH_3 and H_3N-BH_3. Since CHelpG and MKS are similar methods using the electrostatic potential (ESP) to derive atomic charges, it is not surprising to see that the charges calculated by them are similar. The charges for N and B calculated by these methods are irregular. On the other hand, the charges calculated by Mulliken are very regular. The charges for N are all negative and all positive for B. For the selected B-CO complexes, two different theories, namely, HF and DFT, were used for the calculating of atomic charges. The charges for B calculated with NPA are negative (except for the HF model of $(CF_3)_3B$-CO) and positive for C. Despite their similarity, the CHelpG and MKS methods give surprisingly different charges. The charges for B calculated by CHelpG are all negative and all positive for C. The charges for B calculated by both MKS and Mulliken are irregular and all positive for C. The HF and DFT models give different optimized geometries, and charges calculated in the two models are also quite different.

4.6 Effects of a Varying External Electric Field

The selected complexes have C_{3v} symmetry. The B-N or B-CO bond is the three-fold axis. Aligning the B-N or B-CO bond to the Z-axis, an external electric dipole field was applied along the bond. The molecular symmetry was switched off to prevent the rotation of the molecule from the input orientation to the standard orientation, since the finite field will not lead to correct numerical derivatives, if the selected field breaks the molecular symmetry. The input geometry is either in traditional Z-matrix coordinates or symbolic Cartesian coordinates.

The range of the strength of the external applied electric field was chosen based on those values which could change the B-N or B-CO bond distance to the value close to the one in the crystal. Therefore, the B-N complexes were optimized in electric fields from -0.30 a.u. to +0.20 a.u. with HF/6-31G(d), and for the B-CO complexes were chosen from -0.10 a.u. to +0.10 a.u. with HF/6-31G(d) and B3LYP/6-31G(d) method. The direction of the field was positive from B to N, or B to CO. The atomic unit of electric field is equal to $5.1423\times10^{11}\ V.m^{-1}$ in SI units (cf. Table 3.1).

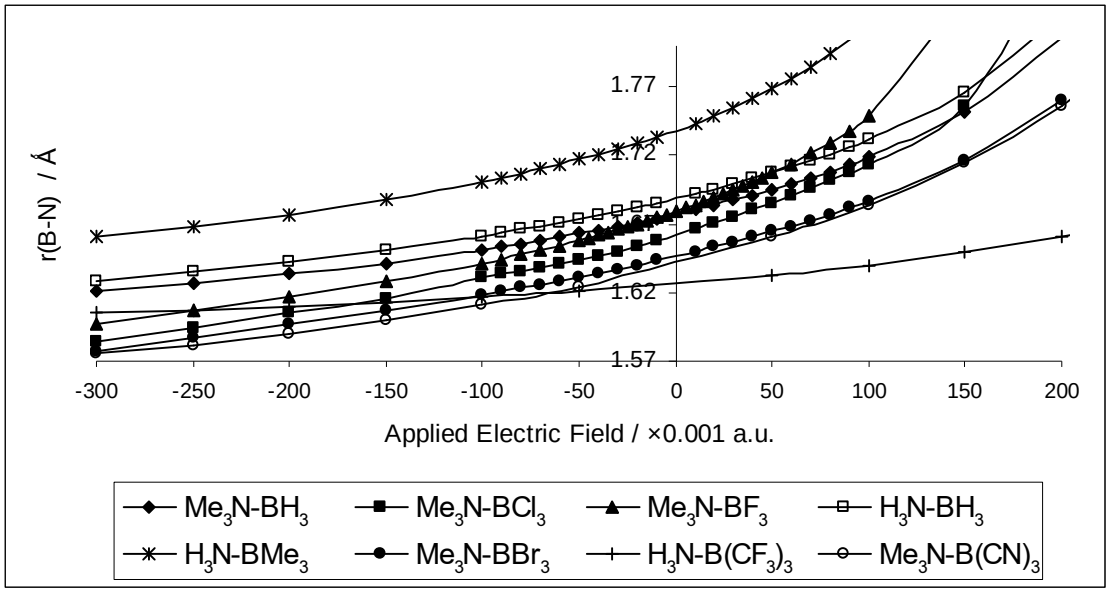

Figure 4.6: The optimized dative bond length, as a function of the applied external electric field for the selected B-N complexes. The negative electric field stabilizes the bond and is orientated against the molecular dipole moment, the positive electric field destabilizes the bond and is orientated opposite to the dipole moment.

Table **4.6**: The percentage decreases in the B-N bond length (Å) at different applied external electric fields (a.u.).

Complex	r(B-N) E at 0	r(B-N) E at -100	%decrease in r[a]	r(B-N) E at -200	%decrease in r[a]
Me_3N-BF_3	1.6777	1.6415	2.16	1.6164	3.65
H_3N-BMe_3	1.7385	1.7007	2.17	1.6768	3.55
Me_3N-BCl_3	1.6626	1.6306	1.93	1.6051	3.46
Me_3N-$B(CN)_3$	1.6404	1.6108	1.80	1.5896	3.10
Me_3N-BBr_3	1.6473	1.6184	1.76	1.5973	3.04
H_3N-BH_3	1.6887	1.6613	1.62	1.6422	2.75
Me_3N-BH_3	1.6776	1.6613	0.97	1.6339	2.60
H_3N-$B(CF_3)_3$	1.6247	1.6162	0.52	1.6097	0.92

[a] The percentage decrease is calculated basing on the B -N bond distance at 0 a.u. applied electric field.

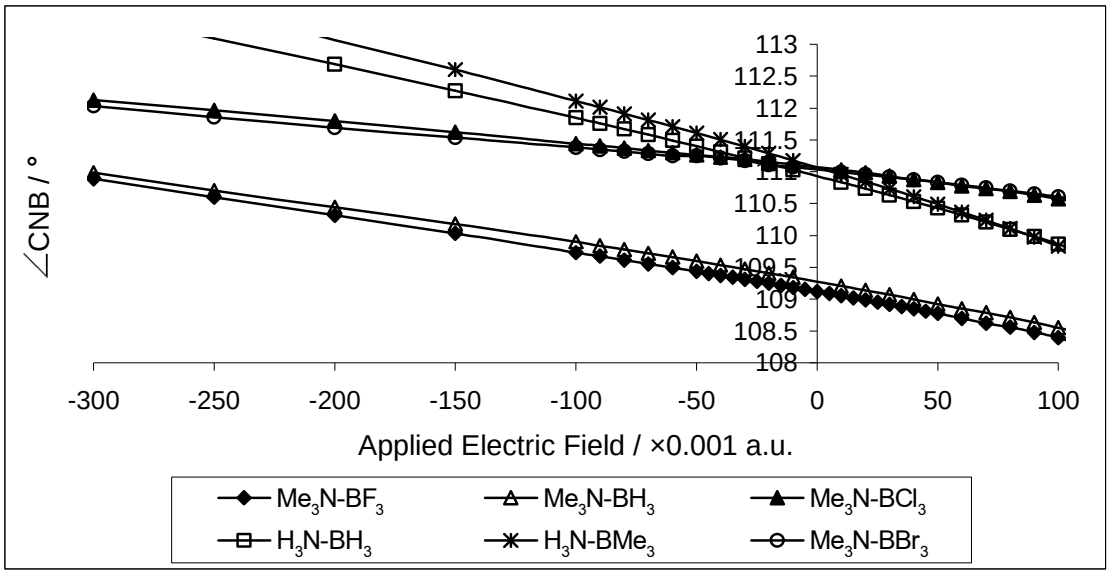

Figure 4.7: The optimized C-N-B angle in a selection of B–N complexes, as a function of the applied external electric field. The negative electric field is orientated against the molecular dipole moment and makes the C-N-B angle larger.

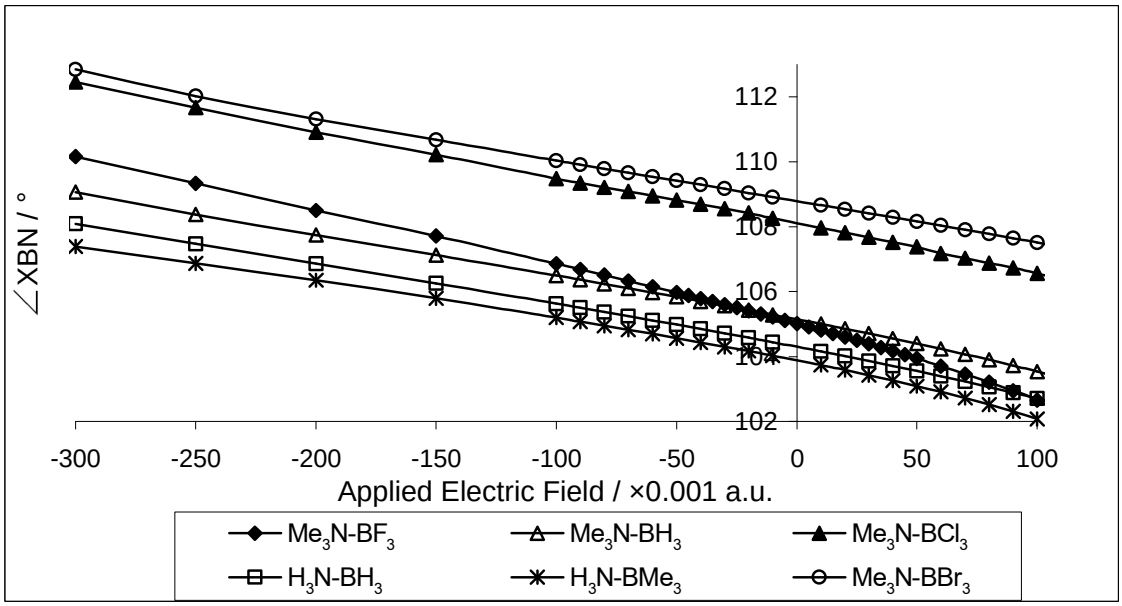

Figure 4.8: The optimized X-B-N angle in a selection of B–N complexes, as a function of the applied external electric field. The negative electric field is orientated against the molecular dipole moment and makes the X-B-N angle larger.

In Figure 4.6, the optimized dative bond in the selected B–N complexes increases as the applied external electric field increases. In the selected electric field range, the B-N bond length of H_3N-BH_3 changes the most with 0.1922 Å, and the B-N bond in H_3N-$B(CF_3)_3$ only increases slightly by 0.0543 Å. From the percentage decreases in the B-N bond length (cf. Table 4.6), Me_3N-BF_3 appears on top with a 3.65% B-N bond length decrease at -0.20 a.u. applied electric field. Because all of the B-N complexes display a similar trend in the applied electric fields, the charges for each B should have the same sign, and the same applies to N. The negative electric field stabilizes the bond and is orientated against the molecular dipole moment, the positive electric field destabilizes the bond and is orientated opposite to the dipole moment. The charges calculated by the Mulliken method (cf. Table 4.4) for nitrogen are all negative and for boron they are all positive. According the criteria, they are the most suitable ones to explain the bond shortening.

Each complex could be divided into two parts: N part (i.e. C-N-B angle) and B part (i.e. X-B-N angle). From Figure 4.7, the C-N-B angles decrease by ~2^o. The B-N dative bonds in H_3N-BH_3 and H_3N-BMe_3 are the two most decreased ones. If we look at the Mulliken charges for the isolated molecules (cf. Table 4.4), the charges for N are -0.936 e, -1.011 e for H_3N-BH_3 and H_3N-BMe_3, respectively. For the remaining four B-N complexes in Figure 4.7, the charges for N are all around -0.6 e. This could explain the less steep decrease, and also indicates the importance of the charges. In Figure 4.8, the X-B-N angles change ~5^o in the selected range. If we look at the Mulliken charges for B (cf. Table 4.4), they range from +0.106 e to +1.096 e. This implies that the B atom is more sensitive than the N atom, and the B atom should be the major factor causing the B-N bond shortening in the crystal. Most of the curves in Figure 4.8 are more or less parallel to each other.

The bond shortening in the applied electric field can be explained as follows (Figure 4.9). Me_3N-BCl_3 is used as an example. In the external electric field, the positively charged B atom and methyl groups move along the direction of the electric field, and the negatively charged N and Cl atoms (cf. Mulliken charges in Table 4.4) move in the opposite direction. The distance between B and N decreases and the Cl-B-N and C-N-B angles

increases. From section 4.4, it is known that the shortening of the bond will increase the van der Waals repulsion force between the substituents and this also apply in the presence of the electric field. The shorter B-N bond makes the Cl-B-N and C-N-B angles become larger as well. The charges and shortening of the B-N bond play a same role for enlarging the angles and the influences of them overlap each other.

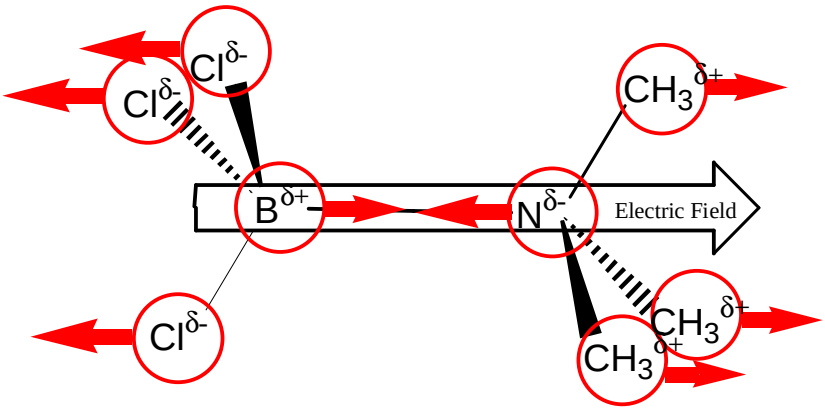

Figure **4.9**: Illustration of the movements of all the atoms in molecules in an applied external electric field.

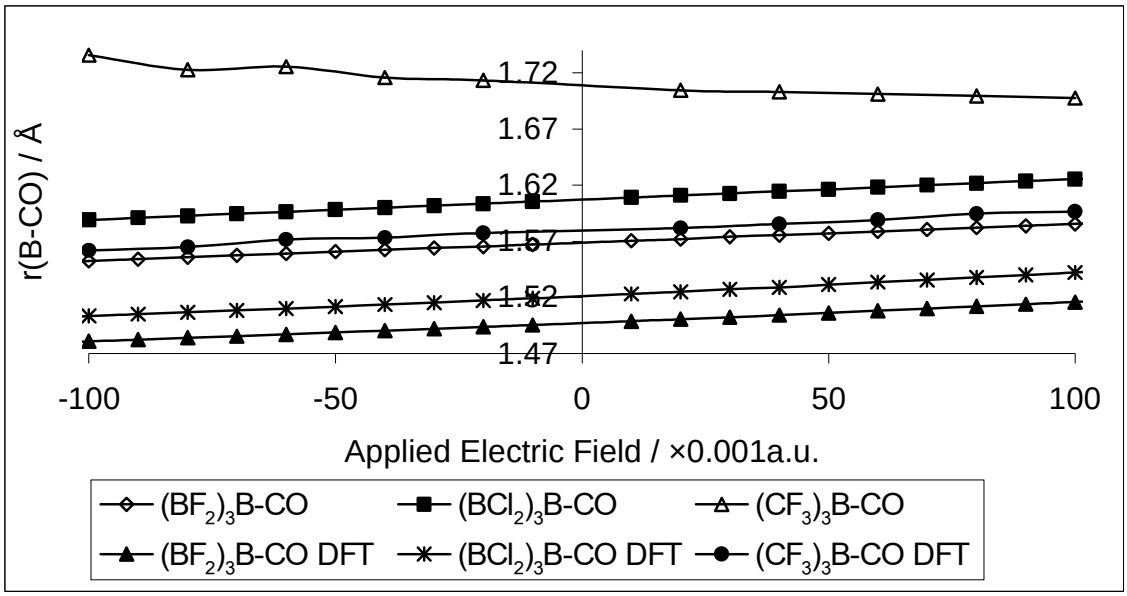

Figure 4.10: The optimized dative bond length in a selection of B–CO complexes, as a function of the applied external electric field. The negative electric field stabilizes the bond and is orientated against the molecular dipole moment, the positive electric field destabilizes the bond and is orientated opposite the dipole moment.

Figure 4.10 shows similar trends to Figure 4.6. Except for the HF model of $(CF_3)_3B$-CO, the optimized B-CO bond length decreases in the negative electric field. The negative electric field stabilizes the bond and is orientated against the molecular dipole moment, the positive electric field destabilizes the bond and is orientated opposite the dipole moment. This implies that except for the HF model of $(CF_3)_3B$-CO, the charges for C should be positive and for B should be negative. The boron and carbon atoms then could move closer to each other in the negative electric field. For the HF model of $(CF_3)_3B$-CO, the charges for B should be positive. So the boron and carbon atoms could move to the same direction in the negative electric field, and this makes the B-CO bond became longer in the negative electric field. If we look at the charges in Table 4.4, the values calculated with NPA are the best ones to explain the figure. The B-CO bond length only changes about 0.03 Å in the applied electric fields from -0.10 a.u. to +0.10 a.u. Most of the B-N complexes change over 0.07 Å in the same region.

4.7 Fixing the Substituents in the Applied External Electric Fields

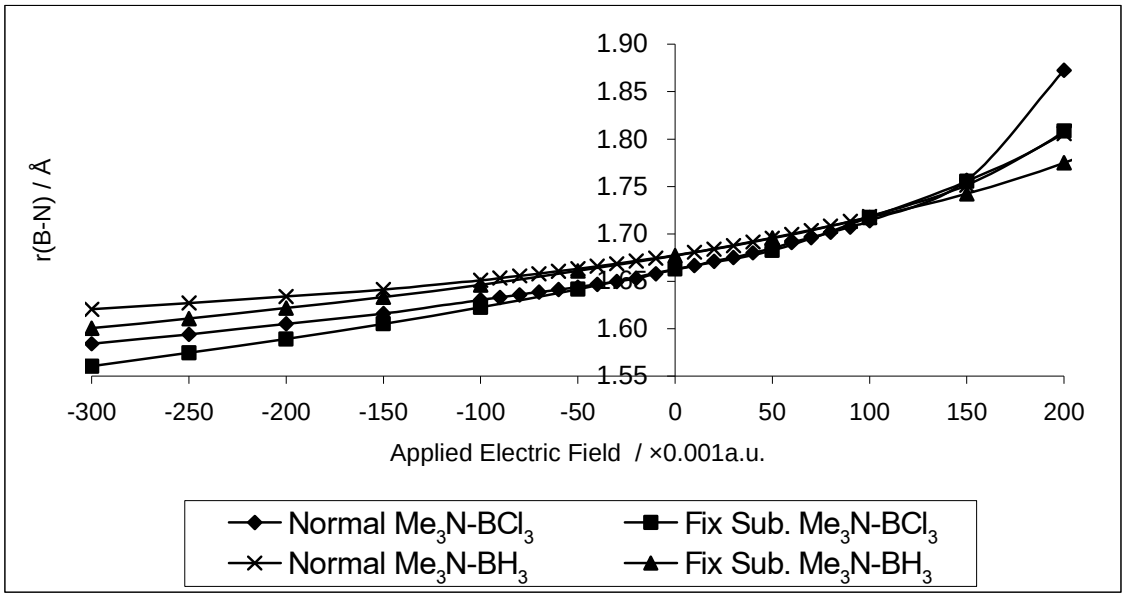

Figure **4.11**: The optimized dative bond length in Me_3N-BH_3 and Me_3N-BCl_3 complexes, as a function of the applied external electric field. There are two kinds of calculations here: one is the normal calculation as previously described, the other is the calculation done by fixing all atoms except B and N. The negative electric field stabilizes the bond and is orientated against the molecular dipole moment, the positive electric field destabilizes the bond and is orientated opposite the dipole moment.

In complexes Me_3N-BCl_3 and Me_3N-BH_3, all the atoms except B and N were fixed to the optimized positions. These complexes were put in a varying external electric field as in the previous section. The B-N bond was optimized in the electric field in a range from -0.30 a.u. to +0.20 a.u. in increments of 0.05 a.u. The changes in valence angles are only due to the movements of the boron and nitrogen atoms.

Comparing the data obtained by both calculations (normal and fixing the substituents) in the negative electric field part of Figure 4.11, it is noticed that when fixing the substituents the B-N bond length is shorter than those corresponding calculations where all atoms are allowed to move. This may be explained by assuming that in the normal

calculations there are electric forces acting on the substituents of B and N. Those forces have vector components in the B-N direction. The vector components resist the B-N moving, so under normal conditions the B-N bond length is longer. In the positive electric field part, the curves for the normal calculation and for the calculation when the surrounding atoms are fixed overlap each other. This can be explained by noting that when the B-N bond becomes longer, the bonds between B or N and the corresponding substituents become shorter and the resisting force disappears.

4.8 Effects of the External Electric Field on Atomic Charges

The molecular geometries and the electron density in external electric fields are different compared to the isolated molecule, and so could affect the atomic partial charges. In the earlier section 4.6, charges calculated by the Mulliken method were considered as being the best to explain the B-N bond shortening in an electric field. As seen in Table 4.7, the charges for B and N for the two selected complexes Me_3N-BCl_3 and H_3N-BH_3 change with the strength of the applied external electric field. The boron charge is more sensitive to the applied field. When decreasing the electric field to -0.30 a.u., the boron charge increases 42% compared to the charge at 0 a.u. and the nitrogen charge only decreases 3% for Me_3N-BCl_3. For H_3N-BH_3, the situation is similar, but the boron charge increases 79%, changing much more than the boron in Me_3N-BCl_3.

The charge on each atom allows them to move in the electric field, and the movement or electric field influences the charges. In conclusion, it can be said that the change in geometries in an external electric field is due to the charges and the charges change when the geometries change. Thus, they change simultaneously.

Table **4.7**: The boron and nitrogen Mulliken charges (e) at different electric fields (a.u.) and the increase percentage in the boron charge.

	Me_3N-BCl_3			H_3N-BH_3		
E-Field	Q(B)	Q(N)	%increase Q(B)	Q(B)	Q(N)	%increase Q(B)
0.00	0.350	-0.630	0	0.106	-0.936	0
-0.05	0.368	-0.632	5	0.114	-0.933	8
-0.10	0.389	-0.638	11	0.125	-0.932	19
-0.15	0.412	-0.638	18	0.138	-0.931	31
-0.20	0.437	-0.642	25	0.153	-0.931	45
-0.25	0.465	-0.646	33	0.170	-0.932	61
-0.30	0.496	-0.650	42	0.189	-0.934	79

Chapter Five

Solid State Calculations

5.1 Introduction

The molecules in the solid state were modeled as being confined in their own cavities in an otherwise fixed crystal lattice. It was consumed that inter-molecular interactions would exert the major influence on the molecular geometries. Intra-molecular interactions should still exist but play a minor role for the geometries. In section 5.2, various HF and DFT models are presented. The crystal environment was simulated by building spherical clusters. Dimeric, trimeric, tetrameric and pentameric models were built to simulate the short-range interactions. In section 5.3, the crystal field is investigated in detail. In section 5.4, the central molecule in the crystal clusters was replaced by other B-N complexes. Additional simulations were performed in section 5.5.

5.2 Crystal Structures Selected for the Solid State Calculations

The Cambridge Structural Database (CSD)[4] is a database of mainly organic and organometallic compounds whose structures have been determined by X-ray diffraction. We used the search and retrieve facilities to search the database for suitable compounds for computational investigation.

There are a total of 576 entries in the CSD for compounds that contain a B-N bond. Most of them have bulky or disordered groups attached, and do not contain a dative bond. The 10 crystal structures selected for the lattice calculations are shown in Table 5.1.

Table 5.1: The CSD identifier and space group for the selected B-N and B-CO complexes.

Chemical formula	CSD identifier	Space group	R-factor (%)
$(CH_3)_3N\text{-}BH_3$	ZZZVPE01	*R*3m	3.5
$(CH_3)_3N\text{-}BF_3$	TMAMBF10	*R*3m	23.0
$(CH_3)_3N\text{-}BCl_3$	TAMBCL (TAMBCL01)	$P2_1/m$	6.6 (5.5)
$(CH_3)_3N\text{-}BBr_3$	TMABBR	$P2_1/m$	8.7
$(CH_3)_3N\text{-}B(CN)_3$	ABEMEZ	*P*nma	3.6
$H_3N\text{-}BH_3$	FUYVUQ01 (FUYVUQ02)	$Pmn2_1$	n.r.[a] (10.9)
$H_3N\text{-}B(CH_3)_3$	RIJHIB	$Pna2_1$	4.3
$H_3N\text{-}B(CF_3)_3$	YAMSAG	*P*nma	7.0
$(C_2H_5)H_2N\text{-}B(CF_3)_3$	VELYAM	$P2_1/c$	6.7
$(C_2H_5)_2HN\text{-}B(CF_3)_3$	VELXUF	*P*nma	12.1
$(CF_3)_3B\text{-}CO$	LULYUM	$P2_1/c$	n.r.[a]
$(BF_2)_3B\text{-}CO$	XAYYEB	$P2_1/n$	4.2
$(BCl_2)_3B\text{-}CO$	XAYYIF	*R*3m	3.9

[a]Not reported.

5.3 Solid State Calculations

In the solid state, molecules experience dipole-dipole interactions. As stated earlier, those short- and long-range interactions make the B-N bond shorter. Section 5.3.1 reports the calculations on the crystal clusters of the selected B-N and B-CO complexes. Several additional simple clusters are discussed in section 5.3.2, in order to check how short-range interactions affect the B-N or B-CO lengths.

5.3.1 Crystal Clusters

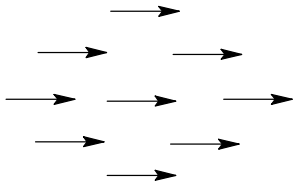

Figure 5.1: Side view of the C_{3v} symmetry clusters.

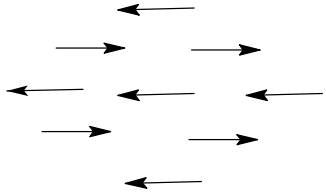

Figure 5.2: Side view of the C_s symmetry clusters.

The positions of H atoms are not determined properly by X-ray diffraction. Therefore, the positions of the H atoms were optimized with the *Cerius*^{2} software[78] using the Universal Force Field (UFF) whilst keeping all other atoms fixed. Then the unit cell was rebuilt and the size of the crystal lattice was increased to 5×5×5. Following this, all molecules within a 7 Å sphere of an arbitrary chosen molecule were selected. The coordinates of the molecules in the sphere were transformed to an input format compatible with the *Gaussian 03* program. In order to distinguish from clusters considered later and the previously discussed molecular clusters, the clusters built here are called crystal clusters.

The crystal clusters can be classified into three groups according to their point groups, namely, C_1, C_s and C_{3v}. Figure 5.1 shows the side view of the C_{3v} symmetry clusters and Figure 5.2 represents the side view of the C_s symmetry clusters. The arrows indicate the direction of the dipoles of the molecules. The crystal cluster of $(C_2H_5)_2HN\text{-}B(CF_3)_3$ has a C_1 symmetry, and the molecules are randomly aligned. The $Me_3N\text{-}BH_3$ and $Me_3N\text{-}BF_3$ clusters have C_{3v} symmetry. The dipoles of the surrounding molecules are all parallel to the central molecule. The other clusters have C_s symmetry. In the calculations with *Gaussian 03*, only the atoms in the central molecule were allowed to adjust their positions during the energy minimization, while the coordinates of all the atoms of the surrounding molecules were fixed to the experimental values. The central molecules were constrained

to lie on the crystallographic mirror plane, if any. The calculations were carried out using DFT (B3LYP) and HF theories and with the standard 6-31G(d) basis set.

As seen from Table 5.2, the calculated bond lengths with HF theory are quite close to the experimental values for Me_3N-BX_3 (X = Cl, Br, CN), $(CF_3)_3B$-CO and H_3N-$B(CF_3)_3$. Most of the values obtained with DFT (B3LYP) theory are similar to the ones with HF, except for the borane carbonyls, the B-CO bond lengths calculated with DFT are much larger than the values calculated by HF. For the some crystal models, the calculations disagree with the experimental values. For example, for Me_3N-BH_3, there is a 0.0657 Å difference for the HF model and the difference is 0.0646 Å for the DFT model. This may indicate that the current crystal models are not suitable for those molecules. However, it is also worthwhile to point out that there are some large differences between two X-ray studies of the same compounds, e.g. 0.037 Å for Me_3N-BCl_3.

Table 5.2: The experimental and optimized B-N and B-CO bond lengths (Å).

Complex	Expt.	HF/6-31G(d)	B3LYP/6-31G(d)
Me_3N-BH_3	1.586[87]	1.6517	1.6506
Me_3N-BF_3	1.616[98]	1.6573	1.6825
Me_3N-BCl_3	1.574[89] (1.611[90])	1.6068 (1.6073)	1.6235 (1.6241)
Me_3N-BBr_3	1.603[90]	1.6020	1.6188
Me_3N-$B(CN)_3$	1.597[91]	1.5809	1.6020
H_3N-BH_3	1.601[87] (1.585[92])	n.c.[a] (1.6359)	n.c.[a] (1.6191)
H_3N-BMe_3	1.648[87]	1.6858	1.6777
H_3N-$B(CF_3)_3$	1.596[93]	1.6023	1.6091
$(C_2H_5)H_2N$-$B(CF_3)_3$	1.589[94]	1.6015	1.6082
$(C_2H_5)_2HN$-$B(CF_3)_3$	1.597[93]	1.6164	1.6308
$(CF_3)_3B$-CO	1.694[44]	1.6973	1.5999
$(BF_2)_3B$-CO	1.522[45]	1.5807	1.5100
$(BCl_2)_3B$-CO	1.545[45]	1.5940	1.5162

[a]Not calculated.

5.3.2 Simple Molecular Clusters

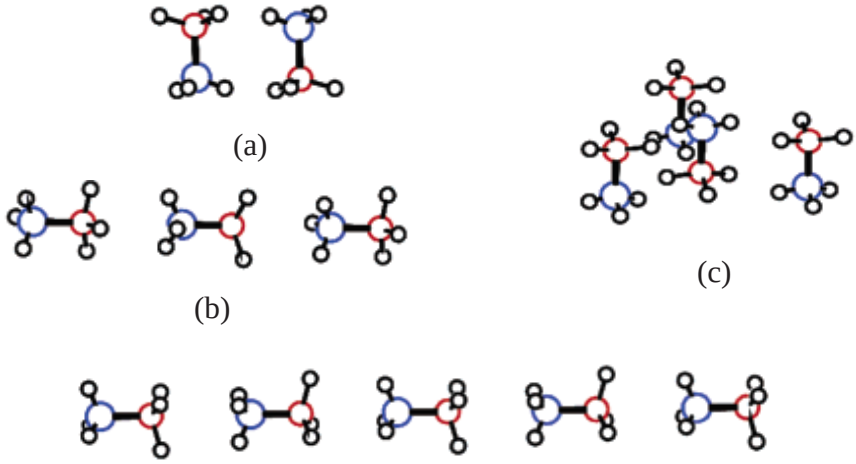

Figure 5.3: Schematic representation of the simple crystal clusters using a molecular dimer (a), trimer (b), tetramer (c) and pentamer (d).

In 1993, Frenking *et al.*[3] used simple dimeric and tetrameric models (cf. Figure 5.3) to simulate the solid-state structure of H_3N-BH_3. The two molecules in the dimeric model are anti-parallel to each other and in the tetrameric model three molecules are anti-parallel to the central molecule. From their results, they proposed that short-range dipole-dipole interactions between the molecules are responsible for the significant shortening of the bond. In our study, similar models for Me_3N-BH_3, Me_3N-BF_3 were also built, and two additional molecular clusters, a trimeric and a pentameric, were built as well. The molecules in the trimeric and pentameric models are aligned head to tail along a straight line. Only dimeric models were built for the three borane carbonyls.

Dimeric Clusters:

Table 5.3: The optimized dative bond (Å) in Me_3N-BH_3 and Me_3N-BF_3 dimeric crystal clusters with various basis sets and HF method.

Complex	6-31G(d)	6-31G(d,p)	6-31++G(d)	6-311G(d)
Monomer Me_3N-BH_3	1.6774	1.6673	1.6729	1.6705
Dimer Me_3N-BH_3	1.6691	1.6601	1.6647	1.6627
Monomer Me_3N-BF_3	1.6777	1.6744	1.6668	1.6693
Dimer Me_3N-BF_3	1.6606	1.6661	1.6524	1.6520

Table 5.4: The optimized B-CO and C-O bonds (Å) in B-CO dimeric clusters.

Crystal Cluster	HF/6-31G(d)		B3LYP/6-31G(d)	
	r(B-CO)	r(C-O)	r(B-CO)	r(C-O)
Monomer $(CF_3)_3B$-CO	1.7089	1.0992	1.5808	1.1300
Dimer $(CF_3)_3B$-CO	1.7047	1.0980	1.5894	1.1278
Monomer $(BF_2)_3B$-CO	1.5688	1.1079	1.4970	1.1416
Dimer $(BF_2)_3B$-CO	1.5730	1.1070	1.5007	1.1412
Monomer $(BCl_2)_3B$-CO	1.6073	1.1051	1.5214	1.1383
Dimer $(BCl_2)_3B$-CO	1.6078	1.1049	1.5219	1.1381

Trimeric, Tetrameric and Pentameric Clusters:

Table 5.5: The optimized dative bonds (Å) in the central molecule of the Me_3N-BH_3 and Me_3N-BF_3 trimeric, tetrameric and pentameric clusters.

Crystal Cluster	HF/6-31G(d)	B3LYP/6-31G(d)
Monomer Me_3N-BH_3	1.6776	1.6623
Trimer Me_3N-BH_3	1.6548	1.6424
Tetramer Me_3N-BH_3	1.6540	1.6407
Pentamer Me_3N-BH_3	1.6501	1.6383
Monomer Me_3N-BF_3	1.6777	1.6986
Trimer Me_3N-BF_3	1.6429	1.6585
Tetramer Me_3N-BF_3	1.6333	1.6455
Pentamer Me_3N-BF_3	1.6359	1.6493

Comparing the B-N dative bond lengths in the gas molecule with the ones in molecular clusters, it is seen that the B-N bond lengths are shorter in the central molecules. The bond difference between monomers and dimers is about 0.01 Å. For the tetramers the difference is much larger, over 0.02 Å for Me_3N-BH_3 and over 0.04 Å for Me_3N-BF_3. The dative bonds in the central molecule of the trimers and tetramers also decrease by about 0.02 Å.

For the B-CO complexes, the larger clusters were unstable. Hence, only dimeric models were considered. The B-CO bond lengths in the dimers show the opposite trend to the B-N complexes: the B-CO bonds increase but not much. Hence, the short-range dipole-dipole interactions do not affect the B-CO bond.

5.4 The Classical Electric Field

Table 5.6: The NPA, CHelpG, MKS and Mulliken charges (e) in the selected B-N complexes for the B and N atoms in the gas phase and the central molecule in the crystal clusters.

Complex	NPA		CHelpG		MKS		Mulliken	
	Q(N)	Q(B)	Q(N)	Q(B)	Q(N)	Q(B)	Q(N)	Q(B)
Me_3N-BBr_3(g)	-0.603	0.233	---	---	-0.104	-0.262	-0.649	0.635
Me_3N-BBr_3(s)	-0.626	0.279	---	---	-0.080	---	-0.661	0.674
Me_3N-BCl_3(g)	-0.595	0.477	0.060	0.260	-0.035	0.143	-0.630	0.350
Me_3N-BCl_3(s)	-0.616	0.514	-0.487	0.542	-1.338	0.971	-0.635	0.360
Me_3N-BF_3(g)	-0.584	1.556	0.155	0.818	0.093	0.833	-0.652	1.096
Me_3N-BF_3(s)	-0.583	1.554	0.307	0.968	1.803	1.504	-0.655	1.166
Me_3N-BH_3(g)	-0.511	-0.033	0.341	0.211	0.302	0.096	-0.566	0.154
Me_3N-BH_3(s)	-0.503	-0.046	0.107	0.321	-0.280	0.451	-0.574	0.158
H_3N-$B(CF_3)_3$(g)	-0.984	0.332	-0.854	-0.296	-0.955	-0.277	-1.069	0.306
H_3N-$B(CF_3)_3$(s)	-1.001	0.327	-0.313	-0.169	-0.123	0.012	-1.109	0.337
H_3N-BH_3(g)	-0.962	-0.036	-0.395	0.339	-0.376	0.253	-0.936	0.106
H_3N-BH_3(s)	-0.948	-0.061	-0.570	0.227	-0.181	-0.301	-1.015	0.072
H_3N-BMe_3(g)	-0.976	0.733	-0.737	0.752	-0.775	0.849	-1.011	0.691
H_3N-BMe_3(s)	-0.972	0.718	-0.358	0.425	-0.333	0.444	-1.068	0.721

The NPA, CHelpG, MKS, and Mulliken charges for both B and N atoms of the central molecule in the crystal clusters were calculated with HF/6-31G(d). The MKS charges are sensitive, so the ones obtained by a single point calculation may differ from those obtained during the energy minimization. The NPA and Mulliken charges are regular. Most of the charges of B increase from the gas phase to the solid state and those of N decrease. For MKS and CHelpG, some of the charges surprisingly have different signs in the two phases. Furthermore, the Br radius is not listed in the CHelpG scheme and MKS charges on the Br atom in the solid state are calculated incorrectly at -12 e.

The magnitude of the electric field at *the central point of the B-N bond, the B atom,* and *the N atom* in the central molecule were calculated using Eq. (3.86). The electric field obtained is called a *"classical"* electric field. It is a summation of the contributions of the individual charges in the crystal cluster. Every atom in the crystal clusters is treated as a point charge. However, all atoms in a 1.5 Å sphere with the selected point (*the central point of the B-N bond, the B atom,* or *the N atom*) as a centre are excluded when calculating electrostatic potential properties. This is because the atoms within the 1.5 Å are too close to be treated as point charges. In addition, the individual charges of the atoms in the central molecule of the cluster were also excluded from the summation. The direction from the B atom to the N atom is defined as being positive. The *angle* between the electric field and the B-N bond is also indicated. The classical electric field relies strongly on types of charges. Only MKS and Mulliken charges were used to calculate the electric field. The entries labeled *"predicted"* in Table 5.8 refer to Figure 4.6, and they indicate what the value of the external electric field should be to cause the same bond shortening in an isolated molecule compared to the HF crystal calculation. Because the latter are external electric fields, they align along the B-N axis. This means the angle between the electric field and the B-N bond is 0^{o}.

Table 5.7: The classical and predicted electric fields ($\times 10^{10}$ N/C) for Me_3N-BH_3.

		B-N centre		B atom		N atom	
		E	Angle	E	Angle	E	Angle
HF	Mulliken	0.0317	179.9°	0.0857	179.9°	0.0285	179.9°
(r=1.6517 Å)	MKS	0.0606	17.0°	0.0434	45.6°	0.0572	9.9°
DFT	Mulliken	0.1508	180.0°	0.1877	180.0°	0.1440	180.0°
(r=1.6506 Å)	MKS	0.0292	26.3°	0.0294	33.1°	0.0293	23.3°
HF	Predicted			0.102 a.u (5.245)			

Table 5.8: The classical and predicted electric fields ($\times 10^{10}$ N/C) for Me_3N-BF_3.

		B-N centre		B atom		N atom	
		E	Angle	E	Angle	E	Angle
HF	Mulliken	0.1356	179.9°	0.2096	179.9°	0.1438	179.9°
(r= 1.6573 Å)	MKS	0.2829	20.0°	0.3318	17.2°	0.2077	18.0°
DFT	Mulliken	0.1645	180.0°	0.2254	180.0°	0.1714	180.0°
(r=1.6825 Å)	MKS	0.2007	31.5°	0.2527	23.5°	0.1306	39.6°
HF	Predicted			0.059 a.u (3.054)			

Table 5.9: The classical and predicted electric fields ($\times 10^{10}$ N/C) for Me_3N-BBr_3.

		B-N centre		B atom		N atom	
		E	Angle	E	Angle	E	Angle
HF	Mulliken	0.5831	10.6°	0.5944	11.9°	0.5491	9.1°
(r=1.6020 Å)	MKS	16.41	177.0°	21.79	175.4°	13.62	178.9°
DFT	Mulliken	0.5013	9.5°	0.5075	11.0°	0.4766	8.0°
(r=1.6188 Å)	MKS	19.86	171.3°	26.72	171.8°	16.36	171.8°
HF	Predicted			0.188 a.u (9.642)			

Table 5.10: The classical and predicted electric fields ($\times 10^{10}$ N/C) for H_3N-BH_3.

		B-N centre		B atom		N atom	
		E	Angle	E	Angle	E	Angle
HF	Mulliken	0.3491	38.0^o	0.3864	67.7^o	0.2320	43.1^o
(r=1.6359 Å)	MKS	0.5434	33.5^o	0.5568	46.6^o	0.4397	44.1^o
DFT	Mulliken	0.4565	13.2^o	0.3942	35.8^o	0.3637	2.8^o
(r=1.6191 Å)	MKS	0.7951	10.2^o	0.7617	25.0^o	0.6089	4.7^o
HF	Predicted			0.289 a.u (14.861)			

Table 5.11: The classical and predicted electric fields ($\times 10^{10}$ N/C) for H_3N-BMe_3.

		B-N centre		B atom		N atom	
		E	Angle	E	Angle	E	Angle
HF	Mulliken	0.3635	26.4^o	0.3255	36.0^o	0.3446	28.5^o
(r=1.6858 Å)	MKS	0.3554	33.3^o	0.3333	45.1^o	0.3331	31.0^o
DFT	Mulliken	0.3314	28.1^o	0.2985	37.9^o	0.3192	30.3^o
(r=1.6777Å)	MKS	0.3166	32.2^o	0.3007	45.3^o	0.2950	28.6^o
HF	Predicted			0.172 a.u (8.845)			

Table 5.12: The classical and predicted electric fields ($\times 10^{10}$ N/C) for H_3N-$B(CF_3)_3$.

		B-N centre		B atom		N atom	
		E	Angle	E	Angle	E	Angle
HF	Mulliken	0.7271	8.4^o	0.6784	12.9^o	0.6395	10.6^o
(r=1.6023 Å)	MKS	0.6535	10.8^o	0.6271	17.8^o	0.6056	9.9^o
DFT	Mulliken	0.5752	1.3^o	0.5463	6.9^o	0.5150	2.7^o
(r=1.6091 Å)	MKS	0.5444	1.5^o	0.4880	3.1^o	0.5419	0.6^o
HF	Predicted			0.407 a.u (20.929)			

For Me_3N-BH_3, the HF and DFT calculations give similar results for the B-N bond length. However, the classical electric fields are totally different not only in magnitude but also the direction. The classical electric field calculated by Mulliken charges in the HF model is 2~5 times smaller than the one in the DFT model, but the electric field derived by MKS charges in the HF model is 1.5~2 times larger than the one in the DFT model. The electric fields calculated with Mulliken charges in both models have the same direction, but those using MKS also have roughly the same direction. One puzzling problem is that the electric fields using Mulliken and MKS charges have totally opposite directions. For Me_3N-BBr_3, the MKS method assigns a charge of -12 e to the Br atom. This value is not realistic and results in a larger electric field. Except for Me_3N-BF_3, the electric fields in the remaining complexes calculated with HF agree fairly well with the ones calculated with DFT.

The classical electric field for a same complex is varied at the three points (see page 78-80), this implies that the field is heterogeneous, but only with a small deviation. Compared to the predicted electric fields, the classical values are about 20 times smaller. We were unable to find an explanation for this discrepancy. If the classical electric fields were reliable, two questions would arise: (i) why is a much larger electric field needed to reduce the B-N bond length for the isolated molecules; (ii) is the inter-molecular interaction still the main source of reducing the B-N dative bond in the crystal phase?

Additional, there are two entries for Me_3N-BCl_3 in the CSD. The experimental B-N bond lengths are quite different from each other. Table 5.13 summarizes the crystallographic data for the two entries. They have similar cell parameters. The B-N bond length disagrees by 0.037 Å. Comparing this difference with the calculated gas-solid difference of 0.0516 Å, it is over the tolerance.

Comparing the calculated geometrical data for the two entries in Table 5.14, it is seen that they are very close to each other. The classical electric fields are also close. The difference in experimental values remains puzzling.

Table 5.13: Crystallographic data of Me_3N-BCl_3.

CSD Identifier	TAMBCL	TAMBCL01
Year	1969	1971
Measurement	Photographic/Densitometer	Diffractometer
Cell parameter	a=6.492(15) Å α=90.00°	a=6.677(12) Å α=90.00°
	b=10.216(20) Å β=116.00(30)°	b=10.247(3) Å β=116.18(10)°
	c=6.649(15) Å γ=90.00°	c=6.502(6) Å γ=90.00°
	volume=396.347 $Å^3$	volume=399.224 $Å^3$
B-N bond length	1.574 Å	1.611 Å

Table 5.14: The optimized geometries of the central molecules in the Me_3N-BCl_3 crystal clusters based on the two entries in the CSD.

	TAMBCL	TAMBCL01
	HF/6-31G(d)	HF/6-31G(d)
R(B-N)	1.6068 Å	1.6073 Å
∠ClBN	110.278°, 110.278°, 108.984°	110.254°, 110.254°, 108.997°
∠CNB	111.367°, 111.367°, 110.977°	111.351°, 111.351°, 111.009°
Mulliken Q(B)	0.360 e	0.361 e
Mulliken Q(N)	-0.635 e	-0.635 e
	B3LYP/6-31G(d)	B3LYP/6-31G(d)
R(B-N)	1.6235 Å	1.6241 Å
∠ClBN	109.787°, 109.787°, 108.665°	109.743°, 109.743°, 108.665°
∠CNB	111.261°, 111.261°, 110.923°	111.233°, 111.233°, 110.951°
Mulliken Q(B)	0.174 e	0.174 e
Mulliken Q(N)	-0.401 e	-0.401 e

Table 5.15: The classical and predicted electric fields ($\times 10^{10}$ N/C) for Me_3N-BCl_3.

		B-N centre		B atom		N atom	
		E	Angle[a]	E	Angle[a]	E	Angle[a]
TAMBCL	Mulliken	0.6074	9.2	0.6092	10.8	0.5818	7.7
HF	MKS	0.5482	17.1	0.4592	11.6	0.5914	19.4
TAMBCL01	Mulliken	0.5982	9.2	0.6023	10.8	0.5722	7.9
HF	MKS	0.3997	68.5	0.3326	95.3	0.4430	60.5
TAMBCL	Mulliken	0.5251	7.9	0.5269	9.6	0.5047	6.8
DFT	MKS	0.4895	11.0	0.4086	3.5	0.5375	14.0
TAMBCL01	Mulliken	0.5312	7.9	0.5314	9.6	0.5116	6.6
DFT	MKS	0.3258	62.6	0.2420	90.5	0.3700	55.9
HF	Predicted	10.849 (0.211 a.u.)					

[a] The unit for angle is ^{o}.

5.5 Replacing the Central Molecule in the Crystal Clusters

In the previous section, it is mentioned that there are three groups of crystal clusters in the selected B-N complexes if classified by the symmetry point group of the whole cluster. C_{3v} and C_s are the most important and common point groups in the selected clusters. Here we chose Me_3N-BF_3 and Me_3N-BCl_3 as the representatives for C_{3v} and C_s, respectively. In these two selected clusters, the central molecule was replaced by Me_3N-BBr_3 and Me_3N-BH_3 for the Me_3N-BCl_3 cluster, and by Me_3N-BCl_3 and Me_3N-BH_3 for the Me_3N-BF_3 cluster. There are two reasons for doing this: (i) Different crystal generates a different electric field. The same molecule in a different self-generated electric field could prove the direction of the electric field. (ii) Through changes in the B-N bond length, the relative strength of the electric fields can be ranked. All models were optimized with HF/6-31G(d).

Table 5.16: The optimized B-N dative bond length (Å), angles (°) and charges (e) of B and N for Me_3N-BBr_3 and Me_3N-BH_3 which replace the central molecule in the Me_3N-BCl_3 cluster.

Complex	r(B-N)	∠CNB	∠XBN	Q(B)	Q(N)
Me_3N-BBr_3	1.5965	111.224 111.224 110.889	111.315 111.315 109.569	0.681	-0.663
Me_3N-BCl_3	1.6073	111.351 111.351 111.009	110.254 110.254 108.997	0.360	-0.635
Me_3N-BH_3	1.6369	110.101 110.101 109.580	106.736 106.736 107.029	0.171	-0.576

Table 5.17: The optimized B-N dative bond length (Å), angles (°) and charges (e) of B and N for Me_3N-BCl_3 and Me_3N-BH_3 which replace the central molecule in Me_3N-BF_3 cluster.

Complex	r(B-N)	∠CNB	∠XBN	Q(B)	Q(N)
Me_3N-BCl_3	1.6140	109.579 109.590 109.569	108.221 108.209 108.203	0.322	-0.634
Me_3N-BF_3	1.6573	109.204 109.202 109.206	105.323 105.320 105.325	1.166	-0.655
Me_3N-BH_3	1.6623	109.288 109.291 109.287	105.213 105.210 105.212	0.160	-0.568

The calculated B-N bond lengths for the isolated Me_3N-BH_3, Me_3N-BF_3, Me_3N-BCl_3, and Me_3N-BBr_3 are 1.6776 Å, 1.6777 Å, 1.6626 Å and 1.6473 Å, respectively (cf. Table 4.3) and the corresponding values in the solid state are 1.6517 Å, 1.6573 Å, 1.6068 Å and 1.6020 Å, respectively (cf. Table 5.2). For Me_3N-BH_3, the bond length decreases by 0.0259 Å in its own crystal, and by 0.0153 Å and 0.0407 Å in the Me_3N-BF_3 and Me_3N-

BCl_3 crystal clusters, respectively. This implies that the order of increasing electric field strength of the three B-N complexes is:

$$Me_3N\text{-}BF_3 < Me_3N\text{-}BH_3 < Me_3N\text{-}BCl_3$$

For Me_3N-BCl_3, the bond length decreases by 0.0558 Å in its own crystal, by 0.0486 Å in the crystal with surrounding Me_3N-BF_3 molecules. This confirms the above order of the electric field strength. From the Me_3N-BBr_3 simulation, the order is

$$Me_3N\text{-}BBr_3 < Me_3N\text{-}BCl_3$$

There may be some problems in these simulations. The cavity for Me_3N-BBr_3 in the modified Me_3N-BCl_3 cluster, and that for Me_3N-BCl_3 in the Me_3N-BF_3 modified cluster, could be too small. The inter-molecular interaction plays an important role and the molecules were compressed in the relative small cavities. For Me_3N-BH_3, it should be the other way around with the smaller H atoms replacing the larger halides.

5.6 Additional Simulations

The molecules in the crystal are not only influenced by the self-generated electric field but also by the inter-molecular interactions (i.e. repulsion and attraction by the surrounding molecules). It would be interesting to know how the surrounding molecules influence the angles and bond lengths. In order to do this, several additional simulations were done. One was to optimize an isolated molecule, whose B-N bond was fixed to its calculated value in the crystal phase. Another was to put isolated molecules into an external electric field whose strength was equal to the predicted electric field given in section 5.3.

Me_3N-BCl_3 was chosen as a representative compound in those simulation schemes. In the *first* simulation (Figure 5.5), the B-N distance for the isolated molecule was fixed at 1.6073 Å, which is equal to the calculated value in the standard cluster. The Cl-B-N angle increased by 0.7º from 108.1º to 108.8º and the C-N-B angle increased by 0.3º from 111.1º to 111.4º. This is due to the larger van der Waals repulsion force. In the *second*

simulation (Figure 5.6), an external electric field with strength of -0.211 a.u. was applied along the B-N bond. In that field, the B-N bond distance decreased to the same value calculated for the crystal cluster. Comparing the angles in the first simulation, the Cl-B-N angle changed 2.3º to 111.1º and the C-N-B angle increased by 0.4º to 111.8º. The only difference for the two situations was the external electric field. According to the charge calculations, Cl is negatively charged and the methyl group is positively charged. As shown in Figure 5.6, the two substituents moved away from each other in the applied electric field. Figure 5.7 shows the *third* simulation, the optimized geometry was taken from the central molecule in the 7 Å sphere crystal cluster in section 5.3.1. The crystal electric field shortens the B-N bond to 1.6073 Å, exactly the same bond length as in the two previous situations. The average value for the Cl-B-N angle is 109.8º and for the C-N-B angle is 111.2º. Although the electric field is heterogeneous (section 5.4), the average angles are found to be more or less the same as the angles in the *first* simulation (108.8º for Cl-B-N, 111.4º for C-N-B). The difference between the *second* and *third* simulation is the electric field, an external electric field for the former and a crystal self-generated electric field for the latter. Both of the electric fields kept the B-N bond length at 1.6073 Å, but the magnitude of the same angle is different especially for the Cl-B-N angle. This could be explained as that in the *third* simulation, the inter-molecular interactions (by the surrounded molecules) cancel the effect of the electric field!

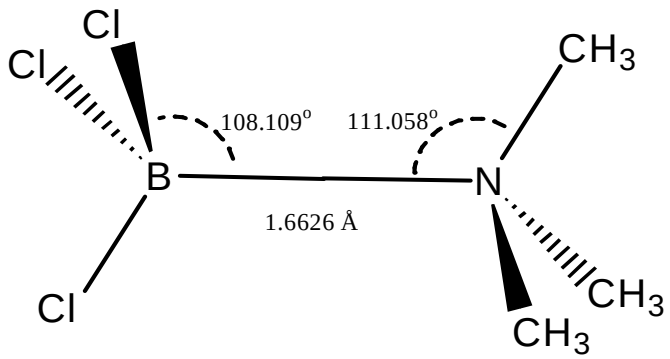

Figure 5.4: The optimized geometry of isolated Me_3N-BCl_3.

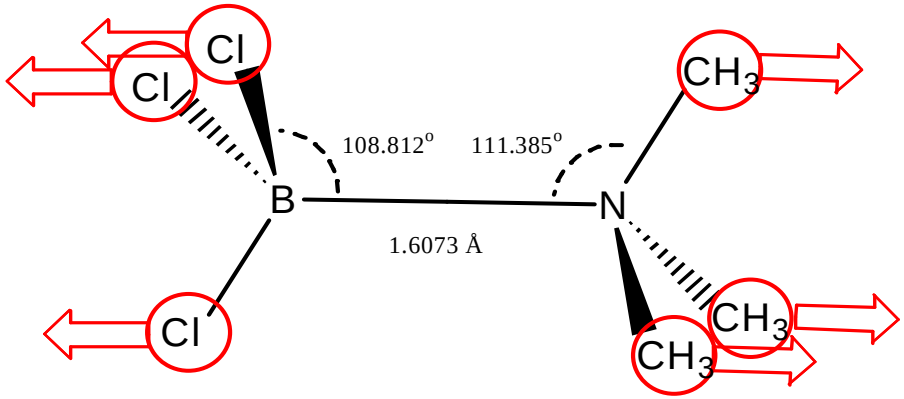

Figure 5.5: The optimized geometry of Me_3N-BCl_3 when fixing the r(B-N) length to the value calculated in the crystal cluster.

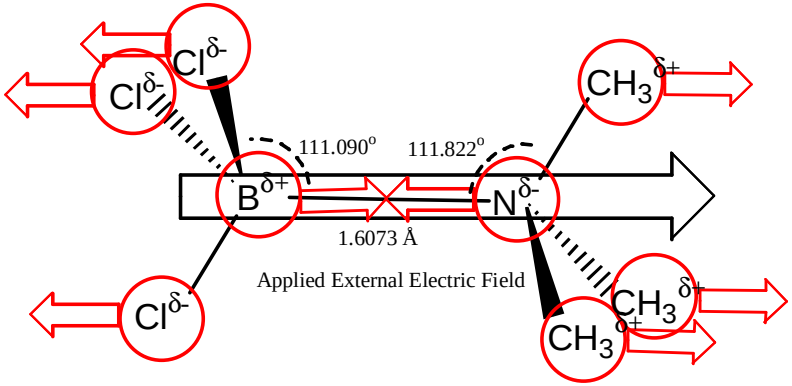

Figure 5.6: The optimized geometry of Me_3N-BCl_3 with an external electric field of strength to make r(B-N) equal to the value in the crystal cluster.

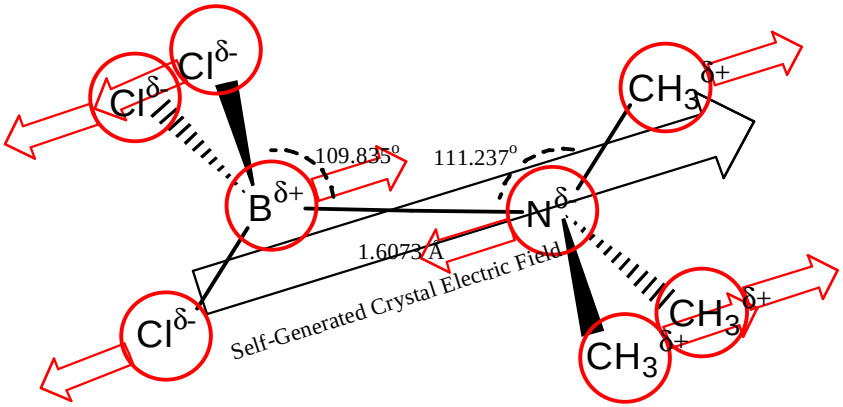

Figure 5.7: The optimized geometry of the central Me_3N-BCl_3 in the standard Me_3N-BCl_3 crystal cluster. The C_{3v} symmetry is broken and the angles are the average values.

Table 5.18: The optimized geometries (B-N distance (Å) and angles (^{o})) of the selected B-N complexes in various conditions.

	Isolated[a]				Constrained[b]		Applied Electric Field[c]		Standard Crystal Cluster[d]	
Complex	r(B-N)[e]	∠XBN	∠CNB	r(B-N)[f]	∠XBN	∠CNB	∠XBN	∠CNB	∠XBN	∠CNB
		105.048	109.136		105.328	109.224	106.135	109.494	105.323	109.204
Me_3N-BF_3	1.6777	105.048	109.136	1.6574	105.328	109.224	106.135	109.494	105.320	109.202
		105.048	109.136		105.328	109.224	106.135	109.494	105.325	109.206
		105.129	109.280		105.408	109.371	106.101	109.721	105.322	109.136
Me_3N-BH_3	1.6776	105.129	109.280	1.6590	105.408	109.371	106.101	109.721	105.322	109.136
		105.129	109.280		105.408	109.371	106.101	109.721	105.322	109.136
		108.109	111.058		108.812	111.385	111.090	111.822	110.254	111.351
Me_3N-BCl_3	1.6626	108.109	111.058	1.6073	108.812	111.385	111.090	111.822	110.254	111.351
		108.109	111.058		108.812	111.385	111.090	111.822	108.997	111.009
		108.774	111.016		109.355	111.304	111.197	111.663	111.151	111.080
Me_3N-BBr_3	1.6473	108.774	111.016	1.6022	109.355	111.304	111.197	111.663	111.151	111.080
		108.774	111.016		109.355	111.304	111.197	111.663	109.526	111.262
		107.889	110.370		108.919	110.466	115.635	111.254	111.901	110.680
Me_3N-$B(CN)_3$	1.6404	107.907	110.363	1.5809	108.903	110.541	115.635	111.254	111.901	110.680
		107.907	110.370		108.903	110.541	115.635	111.254	111.297	110.441
		105.086	111.040		105.370	111.149	111.232	115.073	107.580	112.376
H_3N-$B(CF_3)_3$	1.6247	105.086	111.040	1.6023	105.370	111.149	111.232	115.073	107.580	112.376
		105.092	111.033		105.377	111.144	111.232	115.073	107.614	112.377
		104.290	110.984		105.128	111.148	107.956	113.393	105.538	110.232
H_3N-BH_3	1.6887	104.290	110.984	1.6359	105.128	111.148	107.956	113.393	105.538	110.232
		104.290	110.984		105.157	111.051	107.956	113.393	104.841	110.164
		103.880	111.075		104.500	111.175	106.045	112.794	105.062	111.760

H_3N-BMe_3	1.7385	103.880	111.073	1.6858	104.519	111.175	106.045	112.794	104.628	111.182
		103.897	111.040		104.521	111.208	106.045	112.794	105.360	111.553

[a] The isolated molecular geometries were optimized with HF/6-31G(d). [b] The geometries were optimized by HF/6-31G(d). During the optimization, the B-N bond length was fixed to its corresponding value calculated in the crystal cluster. [c] The geometries were optimized with HF/6-31G(d). During the optimization, the external applied electric field was switched on and the strength was adjusted to make the B-N bond length just equal to the length which was calculated for the crystal cluster. [d] A sphere with radius 7 Å was selected in each crystal lattice. The geometries were optimized with HF/6-31G(d). The central molecule was allowed to adjust its position during the energy minimization and the coordinates of all the atoms of the surrounding molecules were fixed to the experimental values. [e] The B-N bond distance is for the optimized gas molecule with HF/6-31G(d). [f] The B-N bond distance is for the central molecule in the optimized standard crystal cluster with HF/6-31G(d).

Chapter Six

Valence Force Field Calculations

6.1 Introduction

This chapter describes the valence force field calculations performed on ammonia-borane, H_3B-NH_3. Section 6.2 reviews the infrared calculations on H_3B-NH_3. The assignment of the vibritional modes by Smith *et al.*[5] on the isolated gas H_3B-NH_3 is properly incorrect. Valence force field calculations were performed on ammonia-borane, H_3B-NH_3, and two of its deuterated isotopic species D_3N-BD_3 and D_3N-BH_3. A new assignment of the infrared spectrum is proposed. These results are shown in section 6.3.

6.2 Review of Previous Work on Ammonia-Borane

The IR and Raman spectra of H_3N-BH_3 and several isotope-substituted species in liquid ammonia and dimethyl ether were reported by Taylor *et al.*[95-97] in 1964. They mentioned that the B-N stretching frequency was at 787 cm^{-1}. Later, Sawodny *et al.*[98] obtained the vibrational spectra of several compounds of the form X_3N-BR_3, including H_3N-BH_3, and confirmed the B-N stretching frequency to be in the same region at 776/790 cm^{-1}. The spectra of ammonia-borane, H_3B-NH_3, and two of its deuterated isotopic species, D_3N-BD_3 and D_3N-BH_3, isolated in an argon matrix at liquid hydrogen temperature were measured by Smith *et al.*[5] The molecules in such conditions are assumed to resemble the gas state. The experimental B-N stretching band was assigned at 968/987 cm^{-1}, which is about 200 cm^{-1} higher than the corresponding value in the solid state. This assignment is controversial: the B-N bond is longer in the gas phase, so the B-N stretching frequency is expected to be lower than in the solid state.

From a computational point of view, several *ab initio* studies have focused on the vibrational frequencies of H_3B-NH_3.[5-6,27,98] Most of them quote 968 cm^{-1} as the experimental B-N stretching value. Generally, it is concluded that the discrepancy between experimental and calculated values is because the electron correlation cannot account for properties for this molecule. Vijay *et al.*[27] did a comprehensive study by employing large basis sets and high levels of theory, and they confirmed the B-N stretching frequency in solid state and predicted the frequency in gas phase should be 604 cm^{-1}. Indeed, very often, the calculated frequencies are multiplied by an empirical scale factor. The recommended scale factor for a HF/6-31G(d) calculation is 0.8929. This factor reduces Vijay *et al.*'s[27] frequency to 538 cm^{-1}. Recently, Dillen *et al.*[6] performed a computational study on H_3N-BH_3 both in the gas phase and the solid state. They concluded that the calculated frequency in the isolated molecule should be only 539 cm^{-1} which agrees with Vijay *et al.*[27] The calculated spectra for crystalline H_3N-BH_3 are in good agreement with the assignments by Sawodny *et al.*[98], whose spectra were measured using KBr pellets and Nujol samples. For the isolated molecule, the major discrepancy between the assignments of Dillen *et al.*[6] and that of Smith *et al.*[5] is that the peaks at 968/987 cm^{-1} should be the BH_3 rocking mode, rather than the B-N stretching mode and that the latter should be assigned a value of 603 cm^{-1}.

6.3 Valence Force Field Calculations

The program PEFF (A Program for the Development of Empirical Force Fields)[99] was used to calculate the vibrational modes of H_3N-BH_3 using a valence force field. The program is designed to calculate and minimize the steric energy of a molecule within the molecular mechanics or valence force field context. The crude force field is optimized by a least squares procedure. In this work, 14 interactions were introduced in the calculation: three stretch interactions (B-N, N-H, B-H), four bend interactions (H-B-H, H-N-H, H-B-N, H-N-B), one torsional interaction (H-B-N-H), four stretch-bend interactions (H-B/H-B-N, H-N/H-N-B, N-B/N-B-H, B-N/B-N-H), two bend-bend interactions (B-N-H/B-N-H, N-B-H/N-B-H), and one bend-torsion-bend interaction (H-B-N/H-B-N-H/B-N-H). These

interactions are presented in Figure 6.1. The torsional mode is neither IR nor Raman active. It was also introduced to keep the C_{3v} symmetry during the minimization. The frequencies are proportional to the second derivative of the energy. This means they are only proportional to the force constants. The valence angles were chosen as the standard sp^3 angle 109.47^o and the bond lengths B-N, B-H, and N-H were chosen at 1.60 Å, 1.19 Å and 1.02 Å, respectively, the same values as used by Smith *et al.*[5]

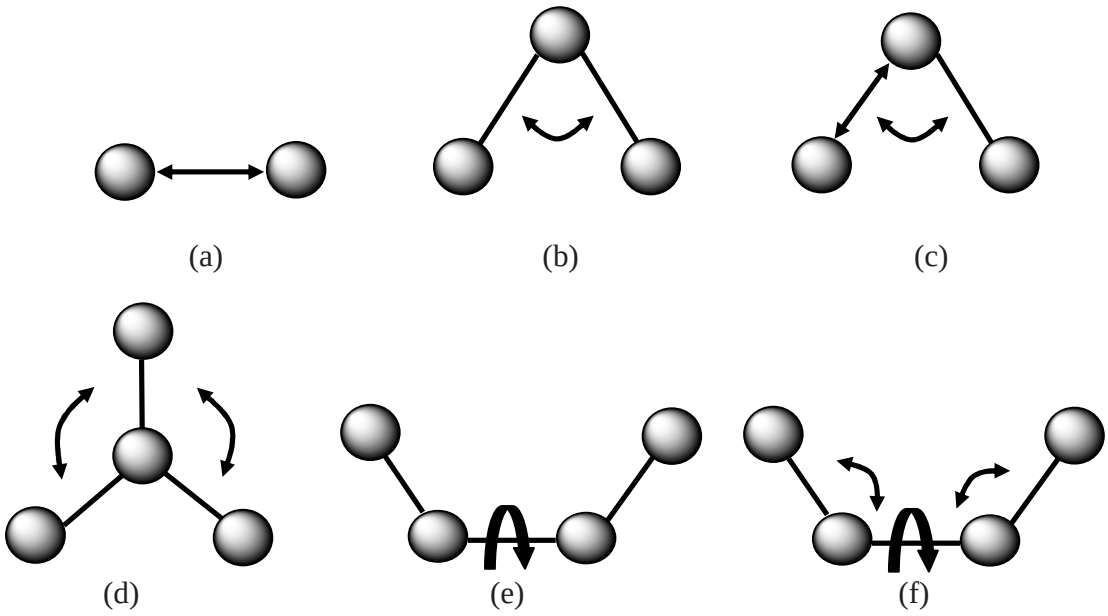

Figure 6.1: Schematic representation of the vibrational modes: stretch interaction (a), bend interaction (b), stretch-bend interaction (c), bend-bend interaction (d), torsional interaction (e) and bend-torsion-bend interaction (f).

In PEFF[99], the following formulas were used in the calculations.

$$\text{Stretch interactions} = 0.5k_s(\Delta r)^2 \tag{6.1}$$

$$\text{Bend interaction} = 0.5k_b(\Delta\theta)^2 \tag{6.2}$$

$$\text{Torsional interaction} = 0.5V_t(1+\cos 3\omega) \tag{6.3}$$

$$\text{Stretch-bend interaction} = k_{sb}\Delta r\Delta\theta \tag{6.4}$$

$$\text{Bend-bend interaction} = k_{bb}\Delta\theta\Delta\theta' \tag{6.5}$$

$$\text{Bend-torsion-bend interaction} = k_{btb}\Delta r\Delta r' \cos\omega \tag{6.6}$$

In this work, two sets of calculations were carried out. The first calculation was done by using the 14 force constants mentioned earlier and the same assignment as Smith *et al.*[5] The second calculation was done by optimizing the same 14 parameters but with a new assignment. The majority of the new assignments were guided by the paper published by Dillen *et al.*[6] and checked after each optimization by using the *VIBRAM* visual program[100]**.** During the optimization of the force field, the energies of the 14 interactions were minimized.

Table 6.1: The calculated vibrational frequencies (cm^{-1}) for the gas H_3N-BH_3 molecule compared to the existing experimental and calculated data.

	H_3N-$^{11}BH_3$			H_3N-$^{10}BH_3$		
Mode[a]	Exp.[b]	1st Cal.[c]	Smith's Cal.[d]	Exp.[b]	1st Cal.[c]	Smith's Cal.[d]
			A_1 Symmetry			
B-N str	968	987	981	987	1002	1002
BH_3 def	1052	1063	1064	1060	1072	1073
NH_3 def	1343	1342	1352	1343	1349	1352
B-H str	2340	2332	2345	2340	2338	2345
N-H str	3337	3336	3340	3337	3336	3340
			E Symmetry			
BH_3 rock	603	633	613	603	636	613
NH_3 rock	1301	1317	1318	1301	1319	1318
BH_3 def	1186	1198	1203	1186	1202	1203
NH_3 def	1608	1606	1620	1608	1610	1620
B-H str	2415	2412	2416	2415	2426	2431
N-H str	3386	3406	3391	3386	3406	3391

[a] str = stretch; def = deformation. [b] Experimental values in reference 5. [c] The first valence force calculation was performed by using PEFF and the frequency assignment in reference 5. [d] Calculated values in reference 5.

Table 6.2: The calculated and experimental vibrational frequencies (cm^{-1}) of two isotopomers of H_3N-BH_3 in the gas phase.

D_3N-$^{11}BD_3$/D_3N-$^{10}BD_3$				D_3N-$^{11}BH_3$/D_3N-$^{10}BH_3$			
Mode[a]	Exp.[b]	1st Cal.[c]	Smith's Cal.[d]	Mode[a]	Exp.[b]	1st Cal.[c]	Smith's Cal.[d]
			A_1 Symmetry				
B-N str	931/956	968/970	907/931	B-N str	945/960	912/914	908/918
BD_3 def	818	735/737	801	BH_3 def	1031/1040	1071/1086	980/995
ND_3 def	1038	1028/1052	1025	ND_3 def	1100	1046/1061	1158
B-D str	1682	1700/1712	1674	B-H str	2339	2332/2337	2344
N-D str	2406	2409	2400	N-D str	2397	2410/2409	2400
			E Symmetry				
BD_3 rock	466	463/466	1031/1040	BH_3 rock	610	582/583	600
ND_3 rock	1006	993/994	1100	ND_3 rock	1001	999	940
BD_3 def	898	866/869	2339	BH_3 def	1187	1197/1201	1157
ND_3 def	1179	1192/1197	2397	ND_3 def	1271	1258/1265	1298
B-D str	1817/1837	1810/1831	1815/1836	B-H str	2414/2426	2410/2423	2416/2430
N-D str	2528	2505	2520	N-D str	2528	2506	2521

[a] str = stretch; def = deformation. [b] Experimental values in reference 5. [c] The first valence force calculation was performed by using PEFF and the frequency assignment in reference 5. [d] Calculated values in reference 5.

Table 6.3: The calculated vibrational frequencies (cm^{-1}) for the gas H_3N-BH_3 molecule by using the new assignment.

Mode[a]	H_3N-$^{11}BH_3$			H_3N-$^{10}BH_3$		
	Org.[b]	New[c]	2nd Cal.[d]	Org.[b]	New[c]	2nd Cal.[d]
			A_1 Symmetry			
B-N str	968	603	610	987	603	612
BH_3 def	1052		1034	1060		1060
NH_3 def	1343	1301	1323	1343		1324
B-H str	2340		2334	2340		2339
N-H str	3337		3333	3337		3333
			E Symmetry			
BH_3 rock	603	968	988	603	987	997
NH_3 rock	1301	1343	1331	1301		1332
BH_3 def	1186		1216	1186		1216
NH_3 def	1608		1648	1608		1648
B-H str	2415		2418	2427		2432
N-H str	3386		3414	3386		3414

[a] str = stretch; def = deformation. [b] Original assignment in reference 5. [c] New assignment (if different from the original assignment). [d] The second valence force field calculation was performed by using PEFF and the new assignment.

Table 6.4: The calculated vibrational frequencies (cm^{-1}) for the two isotopomers of BH_3-NH_3 in the gas phase by using the new assignment.

D_3N-$^{11}BD_3$/D_3N-$^{10}BD_3$				D_3N-$^{11}BH_3$/D_3N-$^{10}BH_3$			
Mode[a]	Org.[b]	New[c]	2nd Cal.[d]	Mode[a]	Org.[b]	New[c]	2nd Cal.[d]
			A_1 Symmetry				
B-N str	931/956	466	471	B-N str	945/960	610	600/602
BD_3 def	818	931/956	932/955	BH_3 def	1031/1040		1033/1057
ND_3 def	1038	1006	993/996	ND_3 def	1100	1001	980/983
B-D str	1682		1695/1706	B-H str	2339		2333/2339
N-D str	2406		2402	N-D str	2397		2402
			E Symmetry				
BD_3 rock	466	818	754/761	BH_3 rock	610	945/960	965/967
ND_3 rock	1006	1038	1013/1016	ND_3 rock	1001	1010	1014/1022
BD_3 def	898		874/875	BH_3 def	1187		1152
ND_3 def	1179		1170	ND_3 def	1271		1272/1273
B-D str	1817/1837		1810/1830	B-H str	2414/2426		2417/2431
N-D str	2528		2514	N-D str	2528		2515

[a] str = stretch; def = deformation. [b] Original assignment in reference 5. [c] New assignment (if different from the original assignment). [d] The second valence force field calculation was performed by using PEFF and the new assignment.

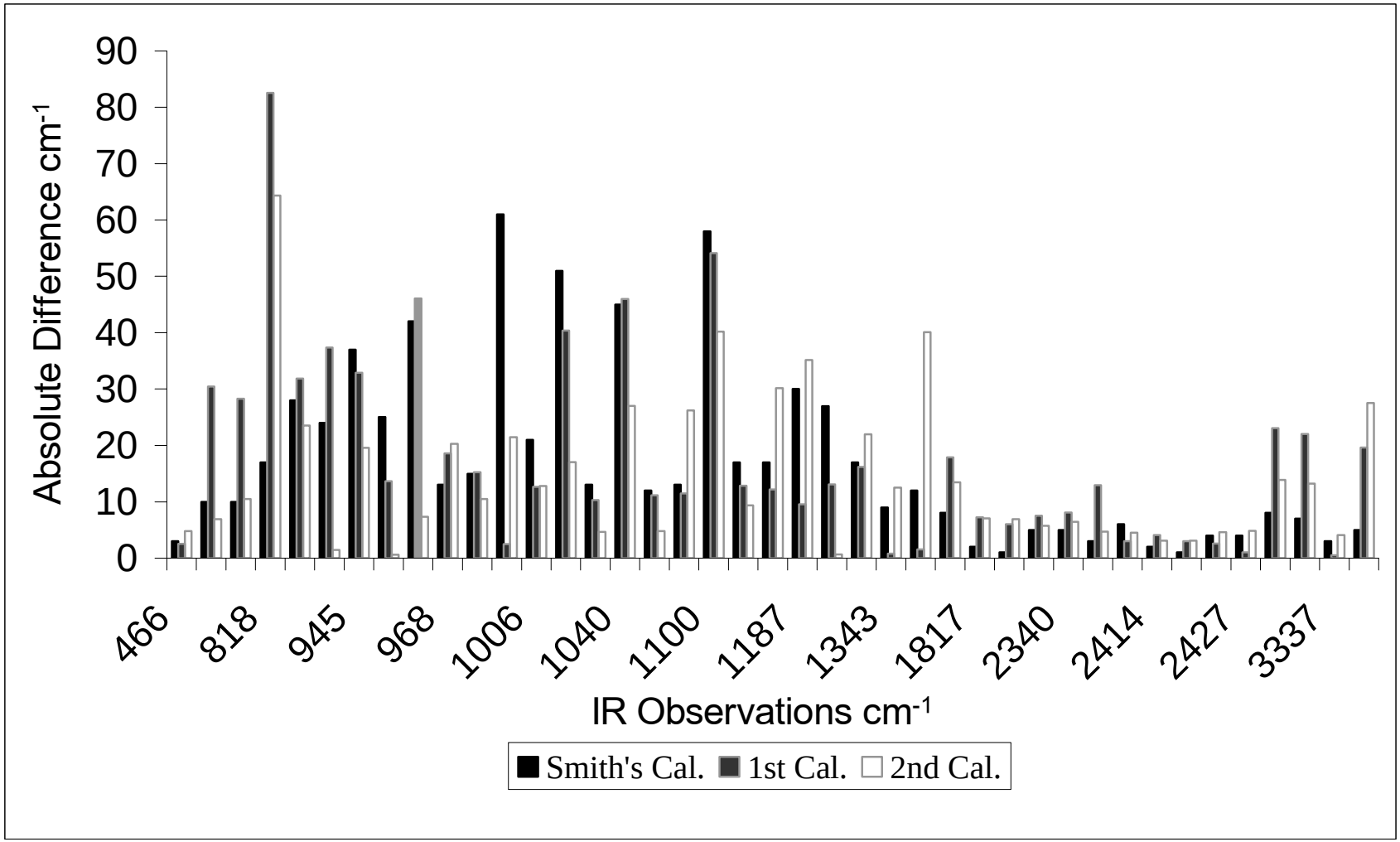

Figure 6.2: The absolute differences for the three different force field calculations of the H_3N-BH_3 experimental vibrational frequencies.

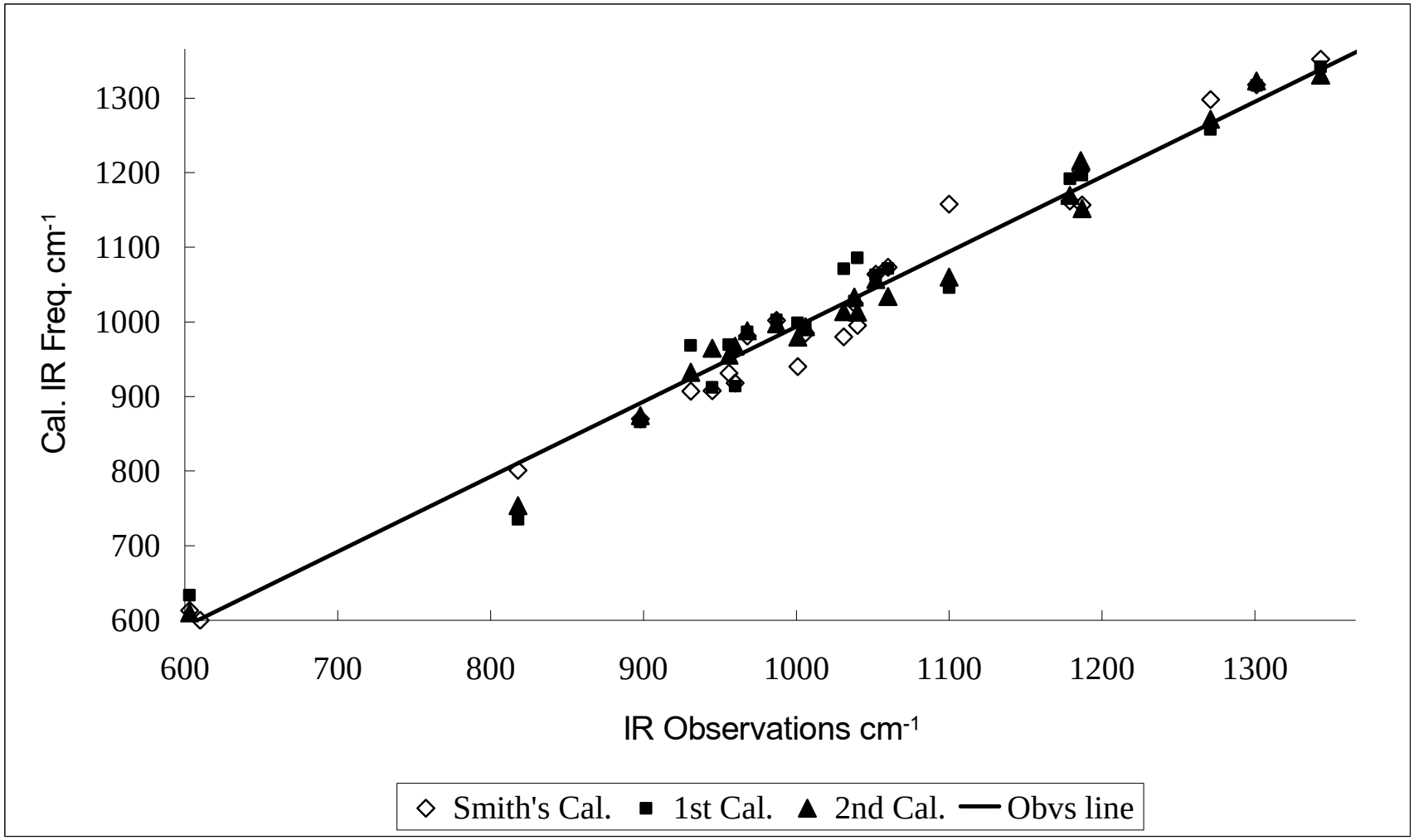

Figure 6.3: The deviations for the three different force field calculations of the H_3N-BH_3 experimental vibrational frequency in the range of 600 to 1300 cm^{-1}.

In the second calculation, for the H_3N-$^{11}BH_3$/H_3N-$^{10}BH_3$ species, the assignment of Dillen *et al.*[6] is used as a guide. The largest deviation between the new and the original assignment is for the B-N stretching frequency. The 603 cm^{-1} peak is assigned to be the B-N stretching mode, rather than the BH_3 rock. This implies that the 968/987 cm^{-1} peak should be the BH_3 rocking mode. The 1301 cm^{-1} peak is assigned as the symmetric NH_3 deformation mode and the 1343 cm^{-1} is assigned as the NH_3 rocking mode. For the D_3N-$^{11}BD_3$/D_3N-$^{10}BD_3$ species, the 466 cm^{-1} peak is assigned to be the B-N stretching mode and the 818 cm^{-1} peak is assigned to be the BD_3 rocking mode. Other small changes are that the 931/956 cm^{-1} peak is assigned as the symmetric BH_3 deformation mode; the 1006 cm^{-1} is assigned as the symmetric NH_3 deformation mode and the 1038 cm^{-1} band is assigned as the NH_3 rocking mode. This disagrees slightly with the new assignment of Dillen *et al.*[6]. They assigned the 466 cm^{-1} to the ND_3 rocking mode according to their calculation. The B-N stretching mode was assigned by them to be not observed. The 898/912 cm^{-1} band was assigned to be the symmetric BD_3 deformation mode; the 1006 cm^{-1} was assigned to be the symmetric ND_3 deformation mode; the 818 cm^{-1} was assigned as the asymmetric BD_3 deformation mode; the 870 cm^{-1} was assigned to be the BD_3 asymmetric deformation mode. For the D_3N-$^{11}BH_3$/D_3N-$^{10}BH_3$ species, this work assigns the 610 cm^{-1} peak as the B-N stretching mode, the 1001 cm^{-1} as the symmetric ND_3 deformation mode, the 945/960 cm^{-1} as the BH_3 rocking mode and the 1010 cm^{-1} as the ND_3 rocking mode. There is only one difference between the current assignment and the one by Dillen *et al.*[6] They assigned the ND_3 rocking to be not observed. Overall, this study agrees with the previous assignment.

The two Figures 6.2 and 6.3 show the deviations between the calculated and experimental H_3N-BH_3 wavenumbers. The major differences in assignments lie in the range 600 to 1300 cm^{-1}. For Figure 6.3, only that particularly range is shown. The biggest deviation is the 818 cm^{-1} peak. The calculation done by Smith *et al.*[5] gives an absolute difference of 17 cm^{-1}, our first calculation shows a much larger difference of 82.5 cm^{-1} and the second calculation decreases the difference to 64.3 cm^{-1}.

Table 6.5: The calculation deviations (cm^{-1}).

	Smith's Cal.[a]	1st Cal.[b]	2nd Cal.[c]
Root Mean Square Deviation	23.01	24.75	19.70
Mean Absolute Deviation	16.85	17.87	14.56

[a] Reference 5. [b] The first calculation was done by using PEFF and the assignment in reference 5. [c] The second calculation was done by using PEFF and the new assignment.

There are two types of deviations used to measure the differences between the values predicted by a model and the values observed, namely, **root mean square deviation (RMSD)** and **mean absolute deviation (MAD).** Smith *et al.*[5] used 20 symmetry force constants (10 A_1 and 10 E species force constants) in their valence force field. The complete frequency assignment was based on C_{3v} molecular symmetry. It has a RMSD of 23.01 cm^{-1} and a MAD of 16.85 cm^{-1}. The first calculation in this study uses less parameters, but it has more or less the same deviations as Smith *et al.*[5] have. The RMSD for this calculation is 24.75 cm^{-1} and the MAD is 17.87 cm^{-1}. These values are close to the ones Smith *et al.*[5] have. Bear in mind that the first calculation in this work uses six parameters less, the close RMSD and MAD show the condition (parameters + force field program) here should be close to the one Smith *et al.*[5] did their calculations in. In general, our second calculation in this study gives the best agreement with the experimental values. The second calculation, using the new assignment, brings the deviation as low as 19.70 cm^{-1} for the RMSD and 14.56 cm^{-1} for the MAD. This implies that the assignment proposed by Smith *et al.*[5] is incorrect. The 603 cm^{-1} peak in the infrared spectra of the matrix isolated H_3N-BH_3 obtained by Smith *et al.*[5] should be assigned as the B-N stretching mode.

6.4 Force Constants Analysis

Table 6.6: Force constants for H_3B-NH_3, D_3N-BD_3 and D_3N-BH_3.

Force constant[a]	1st Calculation[b]	2nd Calculation[c]
k_s B-N	771.37	411.48
k_s B-H	443.15	445.54
k_s N-H	909.51	912.76
k_b H-B-H	61.57	62.79
k_b H-N-H	61.49	77.38
k_b H-B-N	63.14	77.82
k_b H-N-B	139.34	131.94
k_{sb} H-B/H-B-N	23.30	18.01
k_{sb} H-N/H-N-B	72.12	56.77
k_{sb} N-B/N-B-H	60.70	-16.82
k_{sb} B-N/B-N-H	71.22	36.89
k_{bb} B-N-H/B-N-H	-25.27	-32.58
k_{bb} N-B-H/N-B-H	-2.30	-36.98
k_{btb} H-B-N/H-B-N-H/B-N-H	-30.05	20.90

[a] k_s = stretch interaction constant (kcal.mol^{-1}.Å^{-2}); k_b = bend interaction constant (kcal.mol^{-1}); k_{sb} = stretch-bend interaction constant (kcal.mol^{-1}.Å^{-1}); k_{bb} = bend-bend interaction constant (kcal.mol^{-1}); k_{btb} = bend-torsion-bend interaction constant (kcal.mol^{-1}). [b] The first calculation was done by using PEFF and the assignment in reference 5. [c] The second calculation was done by using PEFF and the new assignment.

These are two sets of force constants. The first set was obtained in the calculation using PEFF and the frequency assignment by Smith *et al.*[5] The second set was gained in the calculation using PEFF and the new frequency assignment. The force constants for the two calculations are shown in Table 6.6. The major difference between the two calculations is the assignment for the B-N stretching mode and hence the value of k_sB-N, which decreases by 359.89 to 411.48 kcal.mol^{-1}.Å^{-2}. The stretch-bend interaction constant N-B/N-B-H changes from 60.70 to -16.82 kcal.mol^{-1}.Å^{-1}; the stretch-bend interaction constant N-B/N-B-H shifts from 71.22 to 36.89 kcal.mol^{-1}.Å^{-1}; the bend-bend interaction constant N-B-H/N-B-H decreases from -2.30 to -36.98 kcal.mol^{-1}; the bend-torsion-bend interaction constant H-B-N/H-B-N-H/B-N-H increases from -30.05 to 20.90 kcal.mol^{-1}. Those constants all correlate with the B-N bond and they were expected to change dramatically as the results showed. The other force constants only differ slightly.

6.5 Conclusion

In this chapter, a valence force field approach was used to calculate the vibrational frequencies for H_3B-NH_3, D_3N-BD_3 and D_3N-BH_3. There are two sets of calculations. The first set of calculations used the same assignment as Smith *et al.*[5] The second set was carried out using a new assignment, and gives much smaller RSMD and MAD values. The results imply that the assignment proposed by Smith *et al.*[5] appears to be incorrect. The frequency for the B-N stretching mode should be around 600 cm^{-1}.

A clear, high resolution IR spectrum of the isolated H_3N-BH_3 will definitely prove the new assignment. I have made numerous attempts, but failed to obtain a single spectrum. There are some reasons. (i) The compound is very hygroscopic. (ii) The compound is explosive and could decompose when heated. (iii) The volatility of H_3N-BH_3 is very low. (iv) The NaCl window transmission range is only down to 500 cm^{-1}, which is on the edge of my study. (v) Some of the peaks overlap with CO_2 stretching and bending peaks.

Chapter Seven

Statistical Analysis

7.1 Introduction

Numerous complexes containing B-N dative bonds were selected from the CSD to perform a statistical analysis. The aim was to correlate B-N dative bond length with, for instance, electric field. Section 7.2 gives details of the calculations. The results and discussion are presented in section 7.3.

7.2 Calculations

There are in total about 597 B-N entries in the CSD[4] version 5.28 (November 2006). Most of them have bulky or disordered groups attached, and do not contain a dative bond. Only 67 of them were used to perform a statistical analysis. Their CSD identifiers are presented in table 7.1. The selection criterion is that the substituents attached to the B and N atoms must be simple groups (e.g. CH_3, CN, etc.) or single atoms (e.g. F, Cl, etc.). The aim of the statistical analysis is to find relationships between the B-N dative bond length and the crystal environment from a macroscopic point of view. A few simple calculations were used to calculate the crystal environment.

Before the calculations, the chemistry errors (missing double and resonant bonds, etc.) in the crystal structures were fixed. The X-ray diffraction (XRD) technique cannot determine the position of the H atoms properly, so the positions of the H atoms were optimized by using the Universal Force Field (UFF). The unit cell was rebuilt and the size of the crystal lattice was increased to 5×5×5. The Charge Equilibration (QEq)

method is designed to predict effective atomic charges in chemically inhomogeneous systems so that the long-range interactions between atoms can be properly captured with empirical force fields.[101-104] The QEq charges were calculated in the rebuilt crystal lattice. Every atom in the crystal cluster was treated as a point charge. All the calculations were done through a computer language called *Tool Command Language (Tcl)*[105] in the *Cerius*^{2} molecular simulation program[78]. The magnitude of the electric fields, potential energies and electric potentials at *the middle point*, *the B atom* and *the N atom* of each B-N dative bond in the unit cell was calculated by using Eq. (3.86), (3.87) and (3.88), respectively, as a summation of the individual contributions of the atoms in the crystal cluster. The angle between the electric field and the B-N bond was also indicated. As mentioned earlier (see page 78), all atoms in a 1.5 Å sphere with the selected point (*central point of the B-N bond*, *B atom*, or *N atom*) as a centre should be excluded when calculating electrostatic potential properties. In current calculations, all the atoms bonded to the B (or N) atoms were excluded when calculating electrostatic potential properties at that point. When calculating at the centre point of the B-N bond, only the B and N atoms were excluded.

Table 7.1: All the 67 crystal CSD Identifiers involved in the statistical analysis.

ABEMEZ	FUZREX	QAGPIX	TAMBCL	VIBZEL
ABEMID	IGEGIK	QIVWAT	TEAMBO	WAVPU
AZIBOR	JUXDAH	QUFVES	TMABBR	WAVQAM
BEMQUF	LAQDUC	RASQIM	TMABIO	WIKSOY
CACSEF	LEGFIM	RASQUY	TMAMBF10	WUCTAP
DABVUY	LENXAD	RASRAF	TOSYAB	XALJOK
EDABRO	LOKFAS	REDNUJ	TUHHEJ	XORRAX
FASJIT	LOYTAU	RENVUB	TUHHIN	YAMSAG
FIJHEX	NAXPEI	RIJHIB	TUHJEL	ZABDEL
FOHSOK	NAXPIM	RUYJIE	UHEQED	ZEQNEO
FOHVAZ	OCIBAD	SAGNIX	VELXUF	ZEQNIS
FOTMOQ	PUBHEZ	SAXGIH	VELYAM	ZIDJIF
FOTNEH	PUPHOX	SAXYUL	VIBYUA	ZZZVPE
FUYVUQ	PUVNEZ			

7.3 Results and Discussion

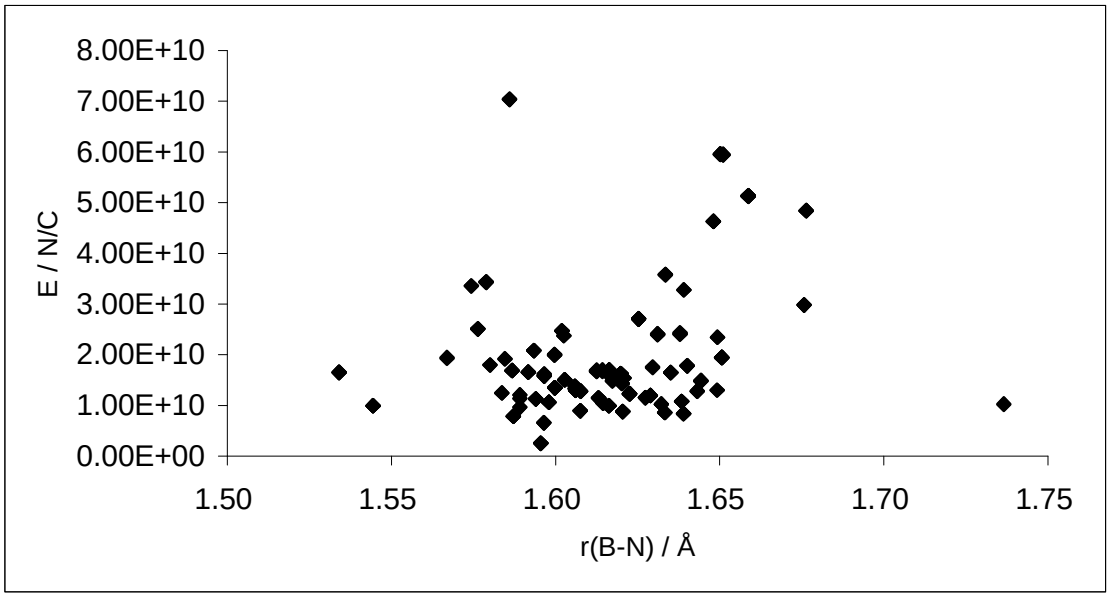

Figure 7.1: The experimental dative bond length in the selected B–N complexes, as a function of the self-generated crystal electric field at the mid-point of the B-N bond.

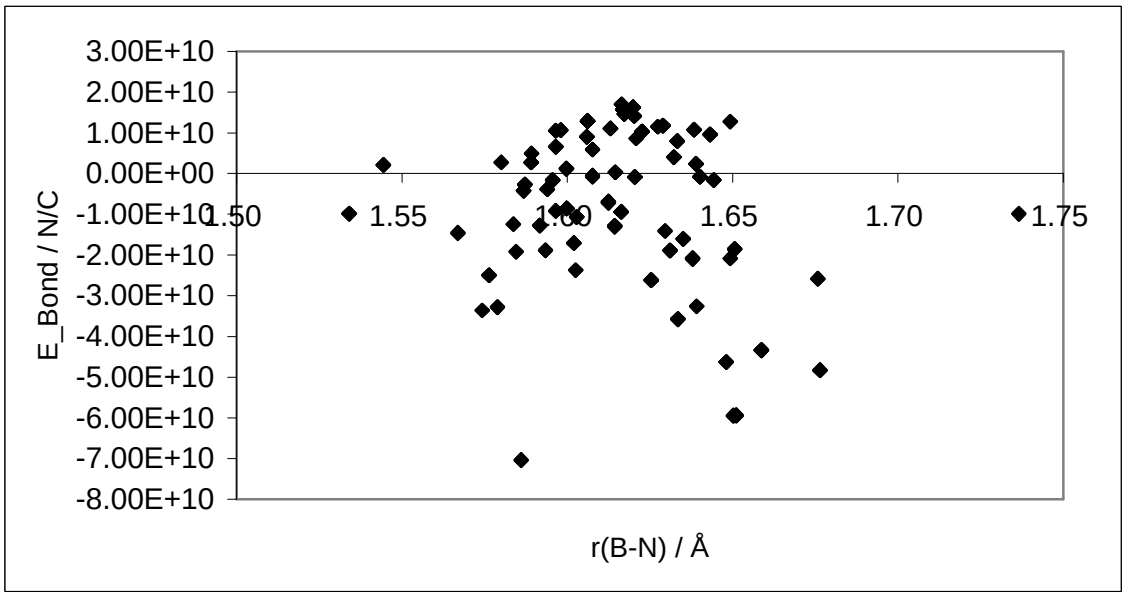

Figure 7.2: The experimental dative bond length in the selected B–N complexes, as a function of the component along the B-N bond for the self-generated crystal electric field at the mid-point of the B-N bond.

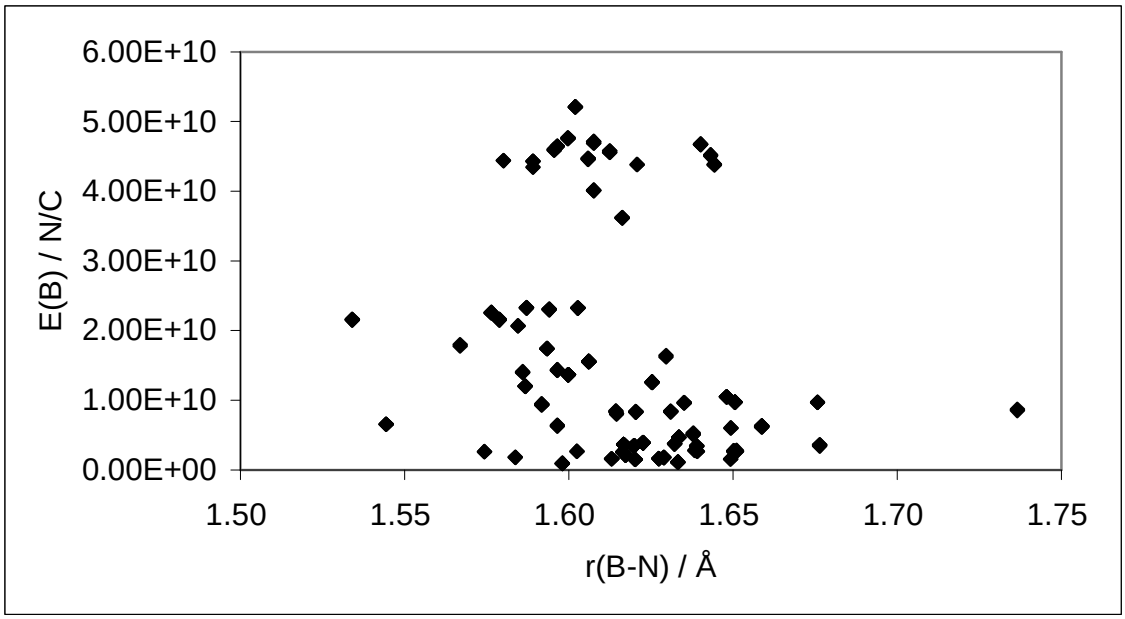

Figure 7.3: The experimental dative bond length in a selection of B–N complexes, as a function of the self-generated crystal electric field at the B atom.

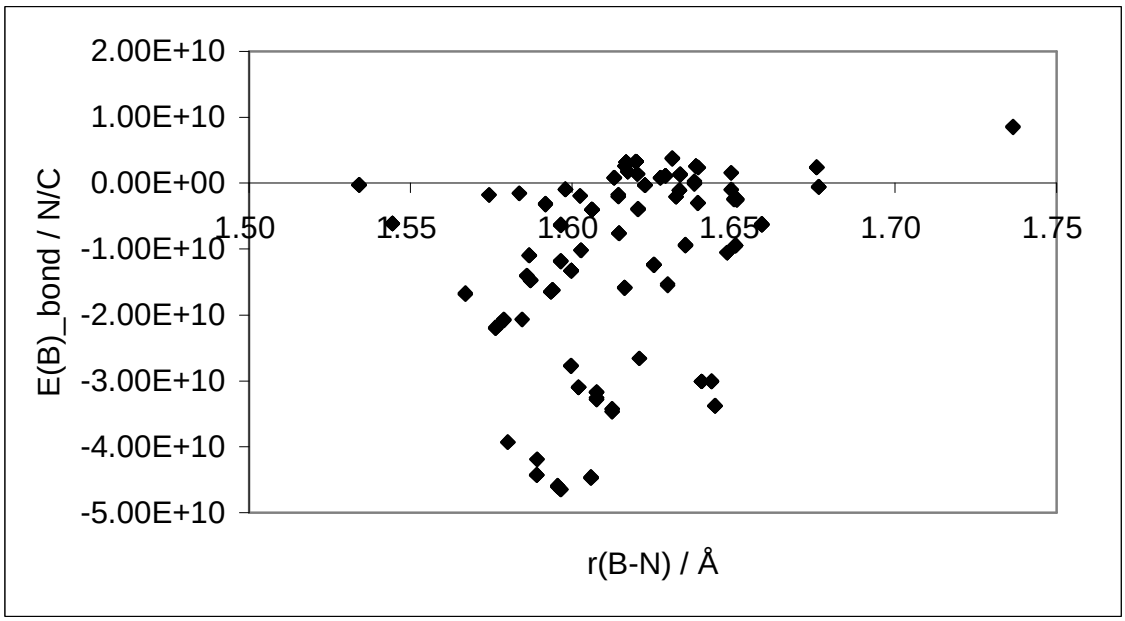

Figure 7.4: The experimental dative bond length in a selection of B–N complexes, as a function of the component along the B-N bond for the self-generated crystal electric field at the B atom.

All the substituents on the B and N atoms are simple and thus minimize intra-molecular interactions. Generally speaking, the physical properties of the B-N bond should be similar. The hypothesis is that if similar bonds have different bond lengths in the crystal phase, this may be due to the crystal self-generated electric field and the charges on the B and N atoms. The positively charged atoms would move along the direction of the electric field and the negatively charged atoms would move against the direction of the electric field. However, normally the B atom is positively charged and the N atom is negatively charged, thus the strength of the self-generated electric field would be a more important factor. The reason for measuring the electric field in the middle point of the B-N bond is that the electric field varies everywhere and the middle point is assumed to feel the average electric field. The size of each crystal lattice is 5×5×5. The molecules in the central unit cell experience both short-range and long-range interactions. Usually, there is more than one molecule in the unit cell and all of these molecules would have more or less the same crystal environment in the large crystal lattice.

The detailed results are shown in addendum B. The statistical graphs of the experimental dative bond lengths versus electric fields are presented in Figures 7.1-7.4. The electric fields in Figure 7.2 and 7.4 are the components of the electric fields at the central point of the corresponding B-N bond and B atom, respectively. It is difficult to find any trend and any relationships between other physical properties and the B-N bond length.

Chapter Eight

Conclusion

We have carried out a computational study on ten boron-nitrogen compounds containing a dative bond and three borane carbonyl complexes. The geometries of the isolated molecules were calculated at the HF, MP2 and DFT levels of theory. The molecules were found to be sensitive to the choice of the basis set. Furthermore, the B-CO complexes were found to be sensitive to electron correlation effects as well.

It was found that the intra-molecular van der Waals interactions affected the selected B-N complexes substantially and that the B-N bond changed almost 0.1 Å in the rotational analysis along the B-N bond. The B-N bond was much more sensitive to an external electric field with varying strength than the B-CO bond. There were large differences between the atomic charges calculated with common methods like NPA, CHelpG, MKS or Mulliken. The Mulliken charges were the most suitable ones to explain the B-N bond shortening from a classical perspective, and for the B-CO bond the NPA charges. The charges were best, especially on the boron atoms, varied considerably in the external field as well.

In the solid state calculations, the calculated bond lengths were close to the experimental values for Me_3N-BX_3 (X = Cl, Br, CN), $(CF_3)_3$B-CO and H_3N-B$(CF_3)_3$. Meanwhile, the B-CO bond only varied by about 0.02 Å from the gas phase to the solid state in the calculations, but there was a much larger difference for e.g. $(CF_3)_3$B-CO, 0.077 Å in the experimental data. For the B-N compounds, the central molecules were stabilized in the dimeric, trimeric, tetrameric and pentameric models. It was found that the short-range dipole-dipole interactions did not affect the B-CO bond. The shortening of the B-N dative bond in the solid state was correlated to the strength of the crystal field, which was

calculated classically from point charges. Unfortunately, large differences were noted between the "classical" and the "predicted" fields, the latter being obtained from the value that the external electric field should be to cause the same bond shortening in an isolated molecule compared to the HF crystal calculation. Furthermore, a statistical analysis of 67 crystal structures taken from the Cambridge Structural Database did not reveal a correlation between the length of the B-N bond and the crystal field calculated with QEq charges.

Finally, a valence force field approach was used to calculate the vibrational frequencies for $H_3B\text{-}NH_3$, $D_3N\text{-}BD_3$ and $D_3N\text{-}BH_3$. In this work, the B-N stretching mode was reassigned to the 603 cm^{-1} band rather than the peak observed at 968 cm^{-1}. It was shown that there is a much better fit of the vibrational spectrum, as evidenced by a smaller value of the RMSD and MAD values.

Future work should concentrate on trying to find a better way to calculate the self-generated electric field in the crystal lattice and find out why some of the selected complexes have a large difference between experimental and calculated bond distances.

Bibliography

[1] Hoard, J. L.; Geller, S.; Cashin, W. M. *Acta Crystallogr.* **1951**, *4*, 396.

[2] Legon, A. C.; Warner, H. E. *J. Chem. Soc., Chem. Commun.* **1991**, 1397.

[3] Jonas, V.; Frenking, G.; Reetz, M. T. *J. Am. Chem. Soc.* **1994**, *116*, 8741-8753.

[4] Allen, F. H. *Acta Cryst.* **2002,** *B58*, 380-388.

[5] Smith, J.; Seshadri, K. S.; White, D. *J. Mol. Spectrosc.* **1973**, *45*, 327-337.

[6] Dillen, J.; Verhoeven, P. *J. Phys. Chem. A* **2003**, *107*, 2570-2577.

[7] Atkins, P. W.; Berran, J. A. *General Chemistry;* Scientific American Books: New York, USA, **1992**.

[8] Pearson, R. G. *Chemical Hardness;* Wiley-VCH: Weinheim, Germany, **1997**.

[9] Drago, R. S. *Structure and Bonding* **1973**, *15*, 73.

[10] Haaland, A. *Angew. Chem. Int. Ed. Engl.* **1989**, *28*, 992.

[11] Bent, H. A. *Chem. Rev.* **1968**, *68*, 587.

[12] Reeve, S. W.; Burns, W. A.; Lovas, F. J.; Suenram, R. D.; Leopold, K. R. *J. Phys. Chem.* **1993**, *97*, 10630.

[13] Cotton, F. A.; Wilkinson, G. *Advanced Inorganic Chemistry;* John Wiley and Sons: New York, USA, fifth ed., **1988**.

[14] Muetterties, E. L. *The Chemistry of Boron and its Compounds;* Wiley: New York, USA, **1967**.

[15] Leopold, K. R. In *Advances in Molecular Structure Research*; Hargittai, M., Hargittai, I., Eds., Vol. 2; Jai Press: Greenwich, USA, **1996**.

[16] (a) Vogt, J.; Mez-Starck, B.; Vogt, N.; Hutter, W. *J. Mol. Struct.* **1999**, *485-486*, 249-254. (b) Vogt, J.; Vogt, N.; Kramer, R. *J. Chem. Inform. Comput. Sci.* **2003**, *43*, 357-361. (c) Vogt, J.; Vogt, N. *J. Mol. Struct.* **2004**, *695*, 237-241.

[17] Janda, K. C.; Bernstein, L. S.; Steed, J. M.; Novick, S. E.; Klemperer, W. *J. Am. Chem. Soc.* **1978**, *100*, 8074.

[18] Bruno, I. J.; Cole, J. C.; Edgington, P. R.; Kessler, M.; Macrae, C. F.; McCabe, P.; Pearson J.; Taylor, R. *Acta Cryst.* **2002**, *B58*, 389-397.

[19] Janda, K. C.; Bernstein, L. S.; Steed, J. M.; Novick, S. E.; Klemperer, W. *J. Am. Chem. Soc.* **1978**, *100*, 8074.

[20] Fujiang, D.; Fowler, P. W.; Legon, A. C. *J. Chem. Soc., Chem. Commun.* **1995**, 113.

[21] Klooster, W. T.; Koetzle, T. F.; Siegbahn, P. E. M.; Richardson, T. B.; Crabtree, R. H. *J. Am. Chem. Soc.* **1999**, *121*, 6337.

[22] Umeyama, H.; Morokuma, J. *J. Am. Chem. Soc.* **1976**, *98*, 7208-7220.

[23] Binkley, J. S.; Thorne, L. R. *J. Chem. Phys.* **1983**, *79*, 2932-2940.

[24] Bühl, M.; Steinke, T.; v. R. Schleyer, P.; Boese, R. *Angew. Chem., Int. Ed. Engl.* **1991**, *30*, 1160-1161.

[25] Jiao, H.; Schleyer, P. v. R. *J. Am. Chem. Soc.* **1994**, *116*, 7429-7430.

[26] Branchadell, V.; Sbai, A.; Oliva, A. *J. Phys. Chem.* **1995**, *99*, 6472-6476.

[27] Vijay, A.; Sathyanarayana, D. N. *Chem. Phys.* **1995**, *198*, 345-352.

[28] Leboeuf, M.; Russo, N.; Salahub, D. R.; Toscano, M. *J. Chem. Phys.* **1995**, *103*, 7408-7413.

[29] Skancke, A.; Skancke, P. N. *J. Phys. Chem.* **1996**, *100*, 15079-15082.

[30] Rablen, P. R. *J. Am. Chem. Soc.* **1997**, *119*, 8350-8360.

[31] Popelier, P. L. A. *J. Phys. Chem. A* **1998**, *102*, 1873-1878.

[32] Jagielska, A.; Moszyński; R.; Piela, L. *J. Chem. Phys.* **1999**, *110*, 947-954.

[33] Kulkarni, S. A. *J. Phys. Chem. A* **1999**, *103*, 9330-9335.

[34] Cremer, D.; Olsson, L.; Reichel, F.; Kraka, *E. Isr. J. Chem.* **1993**, *33*, 369.

[35] Hofmann, M.; Schleyer, P. v. R. *J. Am. Chem. Soc.* **1994**, *116*, 4947.

[36] Wong, M. W.; Wiberg, K. B.; Frisch, M. J. *J. Am. Chem. Soc.* **1991**, *113*, 4776.

[37] Wong, M. W.; Wiberg, K. B.; Frisch, M. J. *Ibid.* **1992**, *114*, 523.

[38] Jurgens, R.; Almlöf, J. *Chem. Phys. Lett.* **1991**, *176*, 263.

[39] Dvorak, M. A,; Ford, R. S.; Suenram, R. D.; Lovas, F. J.; Leopold, K. R. *Ibid.* **1992**, *114*, 108.

[40] Gilbert, T. M. *J. Phys. Chem. A* **2004**, *108*, 2550-2554.

[41] Venter, G. A. *PhD thesis*, University of Stellenbosch, **2003**.

[42] Burg, A. B.; Schlesinger, H. I. *J. Am. Chem. Soc.* **1937**, *59*, 780-787.

[43] *Gmelins Handbuch der Anorganischen Chemie, Borverbindungen, Teil 10;* 1980; 1st. Suppl. Volume 1., **1983**; 2nd. Suppl. Volume 1, **1987**; 3rd, Suppl. Volume 1, 1994; 4th Suppl. Volume la, and **1996**, ed.; Volume 1b 1; Springer-Verlag: Berlin, Heidelberg, New York, **1976**; Vol. 37.

[44] Finze, M.; Bernhardt E.; Terheiden, A.; Berkei, M.; Willner, H.; Christen, D.; Oberhammer, H.; Aubke, F. *J. Am. Chem. Soc.* **2002**, *124*, 15385-15398.

[45] Mackie, I. D.; Hinchley, S. L.; Robertson, H. E.; Rankin, D. W. H.; Pardoe, J. A. J.; Timms, P. L. *J. Chem. Soc. Dalton Trans.* **2002**, 4162-4167.

[46] Levine, I. N. *Quantum Chemistry;* Prentice-Hall: New Jersey, USA, fifth ed., **2000**.

[47] Szabo, A.; Ostlund, N. S. *Modern Quantum Chemistry;* Dover: New York, USA, **1996**.

[48] Jensen, F. *Introduction to Computational Chemistry;* John Wiley and Sons: Chichester, England, **1999**.

[49] Cramer, C. J. *Essentials of Computational Chemistry;* John Wiley and Sons: Chichester, England, **2002**.

[50] Dillen, J. *Understanding Chemistry with Theoretical Molecular Models: An introduction to some classical and quantum techniques of molecular modelling;* Stellenbosch University, Stellenbosch, RSA, **2006**.

[51] Schleyer, P.; Allinger, N; Clark, T; Gasteiger, J; Kollman, P; Schaefer, H; Schreiner, P. *Encyclopedia of Computational Chemistry;* John Wiley and Sons: Chichester, England, **1998**.

[52] Frisch, E.; Frisch, M. J.; Trucks, G. W. *Gaussian 03 User's Reference;* Gaussian Inc.: Pennsylvania, USA, **2003.**

[53] Thomas, L. H. *Proc. Camb. Phil. Soc.* **1927**, *23*, 542.

[54] Fermi, E. *Rend. Accad. Lincei* **1927**, *6*, 602.

[55] Slater, J. C. *Phys. Rev.* **1951**, *81*, 385.

[56] Bloch, F. *Z. Physik* **1929**, *57*, 545.

[57] Dirac, P. A. M. *Proc. Camb. Phil. Soc.* **1930**, *26*, 376.

[58] Hohenberg, P.; Kohn, W. *Phys. Rev. B* **1964**, *136*, 864.

[59] Kohn, W.; Sham, L. J. *Phys. Rev. A* **1965**, *140*, 1133.

[60] Becke, A. D. *J. Chem. Phys.* **1993**, *98*, 5648.

[61] Vosko, S. H.; Wilk, L.; Nusair, M. *Can. J. Phys.* **1980**, *58*, 1200.

[62] Perdew, J. P. *Phys. Rev. B* **1986**, *33*, 8822.

[63] Perdew, J. P.; Burke, K.; Wang, Y. *Phys. Rev. B* **1996**, *54*, 16533.

[64] Lee, C.; Yang, W.; Parr, R. G. *Phys. Rev. B* **1988**, *37*, 785.

[65] Stevens, P. J.; Devlin, J. F.; Chabalowski, C. F.; Frisch, M. J. *J. Phys. Chem.* **1994**, *98*, 11623.

[66] Mulliken, R. S. *J. Chem. Phys.* **1955**, *23*, 1833.

[67] Cox, S. R.; Williams, D. E. *J. Comput. Chem.* **1981**, *2*, 304.

[68] Chirlian, L. E.; Francl, M. M. *J. Comput. Chem.* **1987**, *8*, 894.

[69] Singh, U. C.; Kollman, P. A. *J. Comput. Chem.* **1984**, *5*, 129.

[70] Besler, B. H.; Mertz, Jr., K. M.; Kollman, P. A. *J. Comput. Chem.* **1990**, *11*, 431.

[71] Breneman, C. M.; Wiberg, K. B. *J. Comp. Chem.* **1990**, *11*, 361.

[72] Löwdin, P. O. *Phys. Rev.* **1955**, *97*, 1474.

[73] Weinhold, F. *J. Mol. Struct. (Theochem)* **1997**, *398*, 181.

[74] Weinhold, F. In *Encyclopdedia of Computational Chemistry*; v. R. Schleyer, P.; Allinger, N. L.; Clark, T.; Gasteiger, J.; Kollman, P. A.; Schaefer, III, H. F.; Schreiner, P. R.; Eds., Vol. 3; John Wiley and Sons: Chichester, UK, **1998**; page 1792.

[75] Reed, A. E.; Curtiss, L. A.; Weinhold, F. *Chem. Rev.* **1988**, *88*, 899.

[76] Bader, R. F. W. *Atoms in Molecules. A Quantum Theory;* Oxford University Press: New York, USA, **1990**.

[77] Popelier, P. *Atoms in Molecules. An Introduction;* Prentice Hall: Essex, UK, **2000**.

[78] Accelrys, Inc., *Cerius^2 molecular simulation program version 3.8;* Molecular Simulations Inc.: San Diego, USA, **1998**.

[79] Gaussian 98, Revision A.7. Frisch, M. J.; Trucks, G. W.; Schlegel, H. B.; Scuseria, G. E.; Robb, M. A.; Cheeseman, J. R.; Zakrzewski, V. G.; Montgomery, Jr., J. A.; Stratmann, R. E.; Burant, J. C.; Dapprich, S.; Millam, J. M.; Daniels, A. D.; Kudin, K. N.; Strain, M. C.; Farkas, O.; Tomasi, J.; Barone, V.; Cossi, M.; Cammi, R.; Mennucci, B.; Pomelli, C.; Adamo, C.; Clifford, S.; Ochterski, J.; Petersson, G. A.; Ayala, P. Y.; Cui, Q.; Morokuma, K.; Malick, D. K.; Rabuck, A.

D.; Raghavachari, K.; Foresman, J. B.; Cioslowski, J.; Ortiz, J. V.; Baboul, A. G.; Stefanov, B. B.; Liu, G.; Liashenko, A.; Piskorz, P.; Komaromi, I.; Gomperts, R.; Martin, R. L.; Fox, D. J.; Keith, T.; Al-Laham, M. A.; Peng, C. Y.; Nanayakkara, A.; Gonzalez, C.; Challacombe, M.; Gill, P. M. W.; Johnson, B.; Chen, W.; Wong, M. W.; Andres, J. L.; Gonzalez, C.; Head-Gordon, M.; Replogle, E. S.; .; Pople, J. A.; Gaussian, Inc.: Pittsburgh, PA, USA, **1998**.

[80] Gaussian 03, Revision B.05. Frisch, M. J.; Trucks, G. W.; Schlegel, H. B.; Scuseria, G. E.; Robb, M. A.; Cheeseman, J. R.; Montgomery, Jr., J. A.;Vreven, T.; Kudin, K. N.; Burant, J. C.; Millam, J. M.; Iyengar, S. S.; Tomasi, J.; Barone, V.; Mennucci, B.; Cossi, M.; Scalmani, G.; Rega, N.; Petersson, G. A.; Nakatsuji, H.; Hada, M.; Ehara, M.; Toyota, K.; Fukuda, R.; Hasegawa, J.; Ishida, M.; Nakajima, T.; Honda, Y.; Kitao, O.; Nakai, H.; Klene, M.; Li, X.; Knox, J. E.; Hratchian, H. P.; Cross, J. B.; Bakken, V.; Adamo, C.; Jaramillo, J.; Gomperts, R.; Stratmann, R. E.; Yazyev, O.; Austin, A. J.; Cammi, R.; Pomelli, C.; Ochterski, J. W.; Ayala, P. Y.; Morokuma, K.; Voth, G. A.; Salvador, P.; Dannenberg, J. J.; Zakrzewski, V. G.; Dapprich, S.; Daniels, A. D.; Strain, M. C.; Farkas, O.; Malick, D. K.; Rabuck, A. D.; Raghavachari, K.; Foresman, J. B.; Ortiz, J. V.; Cui, Q.; Baboul, A. G.; Clifford, S.; Cioslowski, J.; Stefanov, B. B.; Liu, G.; Liashenko, A.; Piskorz, P.; Komaromi, I.; Martin, R. L.; Fox, D. J.; Keith, T.; Al-Laham, M. A.; Peng, C. Y.; Nanayakkara, A.; Challacombe, M.; Gill, P. M. W.; Johnson, B.; Chen, W.; Wong, M. W.; Gonzalez, C.; Pople, J. A.; Gaussian, Inc.: Wallingford, CT, USA, **2004**.

[81] Cassoux, P.; Kuczkowski, R. L.; Serafini, A. *Inorg. Chem.* **1977**, *16*, 3005.

[82] Iijima, K.; Shibata, S *Bull. Chem. Soc. Japan* **1979**, *52*, 711.

[83] Iijima, K.; Shibata, S *Bull. Chem. Soc. Japan* **1980**, *53*, 1908.

[84] Cassoux, P.; Kuczkowski, R. L.; Bryan, P. S.; Taylor, R. C. *Inorg. Chem.* **1975**, *14*, 126.

[85] Iijima, K.; Adachi, N.; Shibata, S. *Bull. Chem. Soc. Japan* **1984**, *57*, 3269.

[86] Thorne, L. R.; Suenram, R. D.; Lovas, F. J. *J. Chem. Phys.* **1983**, *78*, 167.

[87] Boese, R.; Niederprum, N.; Blaser, D. *Molecules in Natural Science and Medicine;* **1991**, 103.

[88] Geller, S.; Hoard, J. L. *Acta Crystallogr.* **1951**, *4*, 399.

[89] Hess, H. *Acta Crystallogr., Sect. B: Struct. Crystallogr Cryst. Chem.* **1969**, *25*, 2338.

[90] Clippard, P. H.; Hanson, J. C.; Taylor, R. C. *J. Cryst. Mol. Struct.* **1971**, *1*, 363.

[91] Williams, D.; Pleune, B.; Kouvetakis, J.; Williams, M. D.; Anderson, R. A. *J. Am. Chem. Soc.* **2000**, *122*, 7735.

[92] Klooster, W. T.; Koetzle, T. F.; Siegbahn, P. E. M.; Richardson, T. B.; Crabtree R. H. *J. Am. Chem. Soc.* **1999**, *121*, 6337.

[93] Ansorge, A.; Brauer, D. J.; Burger, H.; Krumm, B.; Pawelke, G. *J. Organomet. Chem.* **1993**, *446*, 25.

[94] Brauer, D. J.; Burger, H.; Dorrenbach, F.; Krumm, B.; Pawelke, G.; Weuter W. *J. Organomet. Chem.* **1990**, *385*, 161.

[95] Taylor, R. C.; Cluff, C. L. *Nature* **1958**, *182*, 390-391.

[96] Taylor, R. C.; Schultz, D. R.; Emery, A. R. *J. Am. Chem. Soc.* **1958**, *80*, 27-30.

[97] Taylor, R. C. *Adv. Chem. Ser.* **1964**, *42*, 59-70.

[98] Sawodny, W.; Goubeau, J. *Z. Phys. Chem.* **1965**, *44*, 227-241.

[99] Dillen, J. L. M. *J. Comput. Chem.* **1992**, *13*, 257-267.

[100] Dillen, J. L. M. *QCPE Bull.* **1993**, *13*, 3, version 2.1(unpublished).

[101] Mortier, W. J.; van Genechten, K.; Gasteiger, J. *J. Am. Chem. Soc.* **1985**, *107*, 829-835.

[102] Rappé, A. K.; Goddard III, W. A. *J. Phys. Chem.* **1991**, *95*, 3358.

[103] Rick, S. W.; Stuart, S. J.; Berne, B. J. *J. Chem. Phys.* **1994**, *101*, 6141.

[104] Rick, S. W.; Stuart, S. J. *Rev. Comp. Chem.* **2002**, *18*, 89.

[105] Ousterhout, J. K. *TCL and the TK Toolkit*; Addison-Wesley: Reading, Massachusetts, USA, **1994**.